

Electro-spinning of Poly (ethylene-co-vinyl alcohol)  
(EVOH) Nanofibres for Medical Applications and  
its Mechanical Properties

A thesis submitted for the degree of Doctor of Philosophy

By

**Chao Xu**

School of Engineering and Design, Brunel University, London

September 2012

## **Acknowledgements**

First of all, I would like to express my gratitude to my supervisor, Dr. Bin Wang. His knowledge and logical thinking has been of immense value to me. Through his encouragement, sound advice, guidance and the access that he provided to the right resources and research collaborations, he helped me to successfully complete this work; without his help, I would have been lost.

I am also deeply grateful to my second supervisor, Professor Luiz Wrobel, who supported me in answering all my questions and set up the laboratory equipment.

My warm thanks also go to Professors Tianjian Lu and Zhimao Yang, Dr. Feng Xu, Mr. Peichun Lv, Mr. Heng Zhang and Dr. Xiaoyun Lu, who all helped me in the anti-bacteria tests and animal tests.

I would like also to thank Dr. Benjamin McCalla and Mr. Keith Withers for their kind help in setting up the laboratory, the mechanical property tests and the electro-spinning system.

Last but not least, my deepest gratitude goes to my beloved parents and my lovely wife Yang Yang, for their endless love, help and encouragement. To them I dedicate this thesis.

## **Publications of this research work**

### **Journal papers:**

Chao Xu, Feng Xu, Bin Wang and Tianjian Lu, Electrospinning of Poly(ethylene-co-vinyl alcohol) Nanofibres Encapsulated with Ag Nanoparticles for Skin Wound Healing, *Journal of Nanomaterials*, Vol. 11, Article ID 201834, pp.1-7  
doi:10.1155/2011/201834

Bin Wang, Chao Xu and Yanling Li, Tensile strength of electrospun Poly (ethylene-co-vinyl alcohol) nanofibre sheets, *Key Engineering Materials*, Vols. 535-536 (2013) pp 215-218

### **Conference paper:**

Bin Wang and Chao Xu, Mechanical strength of Poly (ethylene-co-vinyl alcohol) Nanofibre sheets under tensile loading, the 3<sup>rd</sup> Conference of ISPI, December 2011, Hong Kong.

## Abstract

Skin wound healing is an urgent problem in clinical treatment, in particular, with a military context. Although significant advances have been made in treating skin wounds, traditional methods face several challenges, *e.g.*, limited donor skin tissue for transplants and inflammation over the period of long term healing. To address these challenges, in this study we present a method to fabricate Poly (ethylene-co-vinyl alcohol) (EVOH) nanofibres encapsulated with the Ag nanoparticle, using the electro-spinning technique.

The manufacturing process of nanofibres by electro-spinning is the subject of the present research. Electro-spinning is a process which produces nanofibres through the electrically charged jet of a polymer solution. While the principle has long been understood, the process of forming them still remains difficult to control. In its simplest form, the technique consists of a pipette to hold the polymer solution, two electrodes and a DC voltage supply over a 10 KV range. The polymer dropping from the tip of the pipette is drawn into a jet which is electrically charged and spun into fine fibres by the electronic field. An appropriate combination of the control parameters, such as the charge voltage, density and viscosity of the polymer solution and the travel distance of the jet, etc. will lead to the production of fibres with diameters in the range of  $10^{-7-8}$  meters. The fibres can then be collected on the surface of a grounded target.

The fibres in this study were fabricated with controlled diameters (50 nm – 3  $\mu$ m) by regulating three main parameters, namely, a concentrated EVOH solution, the electric voltage and the distance between the injection needle tip (high voltage point) and the fibre collector. Ag was added to the nanofibres to offer long term anti-inflammation properties by the slow release of Ag nanoparticles through the gradual degradation of the EVOH nanofibre. The method developed here could lead to new dressing materials for the treatment of skin wounds.

The thin EVOH nanofibre sheets obtained from electro-spinning were tested in uniaxial tension for their mechanical properties, with a view to the possibilities of

using them as wound dressings. It was found that the sheets show a mild hardening behaviour with extensive elongation and necking before failure in multiple fractures at random locations. The failure is not simply fibre breakage. Due to the random orientation of the continuing fibres in the sheet, detachment, shear, straightening and twinning. etc., among the fibres all occur at the same time to different extents. The Young's modulus and the yield stress (at 0.4~0.5% proof strains) are predominately affected by the diameters of the fibres. The latter are largely insensitive to strain rate over the range tested.

## Table of contents

Acknowledgements.....	I
Publications.....	II
Abstract.....	III
List of Figures.....	VIII
List of Tables.....	XIV
Abbreviations.....	XV
1. Introduction.....	1
1.1 Background to nanotechnology and nanofibres .....	1
1.2 Aims and objectives.....	2
1.3 Scope of this thesis .....	4
2. Literature review .....	6
2.1 History and science of electro-spinning .....	6
2.1.1 The principle of electro-spinning and electrospray .....	13
2.1.2 Equipment and Technology .....	25
2.1.2.1. The electro-spinning instrument .....	25
2.1.2.2. The Spinneret .....	26
2.1.2.3. The Collector .....	27
2.1.2.4. Parameters effecting electro-spinning .....	28
2.1.2.5. Solution Parameters .....	28
2.1.2.6. Processing parameters .....	29
2.1.2.7. Ambient parameters .....	30
2.2 Wound dressing for burn injuries.....	31
2.3 Chapter summary .....	32
3. Electro-spinning of EVOH nanofibres.....	34
3.1 Polymer EVOH .....	34
3.2 EVOH solution.....	34

3.3 Electro-spinning system.....	35
3.3.1 Syringe section .....	35
3.3.2 High Voltage Power Supply .....	38
3.3.3 Housing Unit and safety measures for high voltage.....	39
3.4 Electro-spinning processes .....	40
3.4.1 Method of making parallel and web nanofibres .....	42
3.4.2 The method of producing tube fibres .....	44
3.5 Results for the inter-relations between fibre diameter and kV, distance, and density .....	45
3.6 Chapter summary .....	56
4. Mechanical properties of nanofibre mats.....	57
4.1 Introduction .....	57
4.2 Samples of EVOH nanofibre sheets.....	57
4.2.1 Introduction of 7.5%, 10% and 12.5% EVOH nanofibre sheets .....	57
4.2.2 The inter-relations between the diameters of 7.5%, 10% and 12.5% in EVOH nanofibres .....	58
4.2.3 Methods of making nanofibre sheet samples for mechanical property tests .	59
4.3 Uniaxial tensile tests .....	62
4.3.1 Process of uniaxial tensile tests .....	62
4.3.2 Results and discussions .....	65
4.4 Unloading and reloading tests .....	70
4.4.1 Purpose.....	70
4.4.2 Process of the unloading and reloading tests.....	71
4.4.3 Results and discussions .....	72
4.4.4 Repeated unloading and reloading for the Damage Parameter .....	75
4.5 Chapter summary .....	77
5. Fabrications of Ag, iodine and gentamicin EVOH nanofibres and Ag degradation test.....	78
5.1 Introduction .....	78
5.2 Fabrication of Ag EVOH nanofibres .....	79
5.2.1 Electro-spinning system and solutions .....	79

5.2.2 Ag and EVOH polymer solution.....	79
5.2.3 Electro-spinning process of producing Ag EVOH nanofibres, iodine and gentamicin EVOH nanofibre.....	79
5.2.4 Energy spectrum check of encapsulated Ag particles.....	84
5.3 Fibre degradation and the release of Ag particles.....	85
5.3.1 Introduction .....	85
5.3.2 Process of Ag release tests .....	85
5.3.3 Water and PBS release tests.....	86
5.3.4 Simulated sunlight and UV light release tests .....	87
5.3.5 Results of Ag particles release .....	89
5.4 Chapter summary .....	89
6. Anti-bacteria tests on and animal tests.....	91
6.1 Process of anti-bacteria tests .....	91
6.2 The choice of the virus used .....	93
6.3 Anti-bacterial tests on Ag, gentamicin and iodine.....	96
6.4 Anti-bacterial tests on different concentrations of Ag particles .....	98
6.5 Animal tests.....	100
6.5.1 The license, site and protocol of the animal test .....	100
6.5.2 The design, make and test of a burn machine.....	101
6.5.3 The process of animal testing.....	103
6.5.4 Results of the animal tests.....	107
6.6 Chapter summary .....	108
7. Conclusions and future work .....	109
7.1 Conclusions .....	109
7.2 Future work .....	111
Appendices.....	113
Bibliography .....	129

## List of figures

Figure 2.1a Schematic diagram showing the fibre formation dynamics during electrospinning ( <a href="http://en.wikipedia.org/wiki/Electrospinning">http://en.wikipedia.org/wiki/Electrospinning</a> , 2012). .....	15
Figure 2.1b Taylor Cone in 5 mm range [Taylor,G.1969, Wan et al., 2004].....	16
Figure 2.2 A 2 strips collector.....	18
Figure 2.3 A 4-strip collector for web fibres (fibre diameter between 1 to 3 micro meters) used in the present research work. Fibres are collected diagonally between neighbouring strips forming a cobweb-like texture. The white dots are droplets produced during electro-spinning.....	19
Figure 2.4 A to J The process of formation of a Taylor Cone and a stable jet [ Carney, L .et al., 2001, Zeleny, J .1917, Juraschek, R .et al.1998].....	22
Figure 2.5 Taylor cone computational model.....	23
Figure 2.6 Dropjet model in the static field.....	23
Figure 2.7 A and b. the mathematic model of the dropjet during the electro-spinning process.....	25
Figure 3.1 Reflux setup for making EVOH solution [Li D., Wang Y., Xia Y., 2003].....	35
Figure 3.2 Original needle and high voltage point .....	36
Figure 3.3 Mode of the first design .....	36
Figure 3.4 Needle with power supply and solution supply .....	37
Figure 3.5 Pump (Masterflex, 77120-52) with polymer solution .....	38
Figure 3.6 A Spellman CZE1000R, 0-30 kV high power supply.....	39
Figure 3.7 House Unit .....	40

Figure 3.8 Basic design for Electro-spinning .....	41
Figure 3.9 The thinnest fibre that was made in our lab – 59nano-meters.....	42
Figure 3.10 Parallel fibres with a box collector .....	43
Figure 3.11 Web fibres with 4 strips Aluminium .....	44
Figure 3.12 .A basic setup to produce tube fibre; B and C are images of Tube fibres taken by TEM .....	44
Figure 3.13 The relationship between weight per cent and fibre diameter when 20 kV and 25 cm from the needle to the collector are applied .....	46
Figure 3.14 The relationship between distance from the needle to the collector and fibre diameter when 20 kV and 10 wt% are applied .....	47
Figure 3.15 The relationship between voltage and fibre diameter when 25 cm from needle to the collector and 10 wt% are applied .....	48
Figure 3.16 An SEM image of EVOH nanofibres with temperature control.....	49
Figure 3.17 An SEM image of EVOH nanofibres without temperature control .....	50
Figure 3.18 The method of measuring the diameters of EVOH nanofibres by means of an SEM.....	51
Figure 3.19 The method of measuring the diameters of EVOH nanofibre by means of an SEM (continued).....	52
Figure 3.20 Effect of the distance on fibre diameters when the solution density is 7.5% (wt) and the voltage is 20 kV.....	53
Figure 3.21 Effect of the voltage on the diameters of the fibre when the solution density is 7.5% (wt) and the needle-tip-to-collector distance is 30 cm.....	54
Figure 3.22 Effect of the solution density on diameters of the fibre when the voltage is 20kV and the tip-to-collector distance is 30 cm.....	55

Figure 4.1 The fibre sheets were collected on two aluminum foil strips with some biased orientation across the gaps .....	60
Figure 4.2 A coupon sample after being cut .....	61
Figure 4.3a Image of a nanofibre sample of 10% EVOH fibre sheets on the Instron machine.....	62
Figure 4.3b Image of a torn nanofibre sample of 10% EVOH) fibre sheets on the Instron machine.....	63
Figure 4.3c The strain-stress curve in the tensile extension test of a 10% EVOH nanofibre sample.....	63
Figure 4.4 The original report from the Instron 8500.....	64
Figure 4.5a The average strain-stress curve of 7.5% EVOH nanofibre sheets in response to different loading speeds .....	65
Figure 4.5b The average strain-stress curve of 10% EVOH nanofibre sheets in response to different loading speeds.....	66
Figure 4.5c The average strain-stress curve of 12.5% EVOH nanofibre sheets in response to different loading speeds.....	67
Figure 4.6a Average strain-stress curve of 3 different EVOH nanofibre sheets(7.5%, 10% and 12.5%) at 2mm/min loading speed .....	68
Figure 4.6b Average strain-stress curve of 3 different EVOH nanofibre sheets(7.5%, 10% and 12.5%) at 5mm/min loading speed.....	68
Figure 4.6c Average strain-stress curve of 3 different EVOH nanofibre sheets(7.5%, 10% and 12.5%) at 10mm/min loading speed.....	69
Figure 4.6d Average strain-stress curve of 3 different EVOH nanofibre sheets (7.5%, 10% and 12.5%) at 20mm/min loading speed.....	69
Figure 4.7 SEM image on the fractured edge of a 10% EVOH nanofibre after the tensile test .....	71
Figure 4.8 Yield stress at 0.4% proof strain and moduli.....	71

Figure 4.9 Yield stresses of the samples under different strain rates.....	72
Figure 4.10a Moduli E, E <sub>y</sub> and K <sub>p</sub> vs strain rate. (a) Sample A .....	73
Figure 4.10b Moduli E, E <sub>y</sub> and K <sub>p</sub> vs strain rate. (b) Sample B .....	73
Figure 4.10c Moduli E, E <sub>y</sub> and K <sub>p</sub> vs. strain rate. (c) Sample C.....	74
Figure 4.11 Repeated unloading and reloading test on Sample B at a strain rate of 1.11x10 <sup>-3</sup> .....	75
Figure 4.12 Damage parameter in terms of the plastic strain .....	76
Figure 5.1 An SEM image of 7.5% Ag EVOH nanofibres (0.04g AgNO <sub>3</sub> added to 10 ml 7.5% EVOH polymer solution) .....	81
Figure 5.2 An SEM image of Ag particles attached to and imbedded in EVOH nanofibres (0.15g AgNO <sub>3</sub> was added to 10 ml 10% EVOH polymer solution).....	82
Figure 5.3 A TEM image of Ag EVOH nanofibre.....	83
Figure 5.4 A TEM image of a single fibre of Ag EVOH nanofibre .....	83
Figure 5.5 Energy spectrum using an SEM for the encapsulated Ag particles.....	84
Figure 5.6 The results of the energy spectrum using an SEM for the encapsulated Ag particles .....	85
Figure 5.7 Degradation of the EVOH nanofibre in a PBS solution (note: three data points for a straight line is not enough; more data should be added.) .....	86
Figure 5.8 (a) Original fine fibre sample before exposure to UV light, (b) fibre sample after 72 h continuous exposure to UV light, (c) SEM image of EVOH fibre after 24 h UV degradation test, (d) SEM image of EVOH fibre after 72 h UV degradation test.....	87
Figure 5.9 UV degradation test of nanofibres .....	88

Figure 5.10 The release speed of Ag nanoparticles exposed to UV light .....	89
Figure 6.1 Anti-bacterial tests at 37oC with 10 mm x 10 mm square shapedEVOH nanofibre samples impregnated with Ag nanoparticles.....	91
Figure 6.2 Anti-bacterial tests at 37oC with EVOH nanofibre samples impregnated with circular Ag nanoparticlesof 10 mm diameter.....	92
Figure 6.3 Staphylococcus aureus [ <a href="http://www.picsearch.com/pictures/Science/Bacteri">http://www.picsearch.com/pictures/Science/Bacteri</a> , 2010].....	93
Figure 6.4 An image of Staphylococcus aureus [ <a href="http://www.picsearch.com/pictures/Science/Bacteri">http://www.picsearch.com/pictures/Science/Bacteri</a> , 2010] .....	94
Figure 6.5 Bacteria test after 6 hours of incubation at 37°C, for EVOH nanofibres encapsulated with (a) no agent, (b) gentamicin, (c) Ag nanoparticle, (d) iodine.....	96
Figure 6.6 Average diameter of the bacterial loop for: EVOH nanofibre containing: 1) no agent; 2. Gentamicin; 3. Ag nanoparticles; and 4. iodine.....	97
Figure 6.7 An image of EVOH fibre without Ag, iodine and gentamicin in the bacterial test.....	98
Figure 6.8 An image of one set of cultures in a test for Bacteriostatic Loop measurement.....	99
Figure 6.9 Averaged measurement of the Bacterial Loop diameter vs. Ag concentration (wt/10ml).....	99
Figure 6.10a The burn machine .....	101
Figure 6.10b The touching point of a burn machine for making level 3 skin burn wounds .....	102
Figure 6.11a The skin burn wounds were produced at a temperature of 150°C applied for 60 seconds.....	103
Figure 6.11b The skin burn wound covered EVOH nanofibrescontaining Ag nanoparticles.....	104

Figure 6.11c Skin burn wounds covered in different materials: A- Traditional cotton dressing with Vaseline; B- EVOH nanofibre with Ag; C- Normal bandage only; D- EVOH nanofibres without Ag .....	105
Figure 6.11d The burn wound areas enswathed by normal bandage .....	106
Figure 6.12a A skin burn wound covered by EVOH nanofibres containing Ag nanoparticles after 72 hours .....	107
Figure 6.12b A skin burn wound covered by traditional material after 72 hours.....	107
Figure 7.1 Sample holder for the Tension mode .....	113
Figure 7.2a DMA creep test on 7.5% EVOH nanofibre sheets from 20 °C to 60 °C .....	114
Figure 7.2b DMA creep test on 10% EVOH nanofibre sheets from 20 oC to 60 oC.....	115
Figure 7.2c DMA creep test on 12.5% EVOH nanofibre sheets from 20 oC to 60 oC.....	116
Figure 7.3 Sample holder for the Tension mode.....	117
Figure 7.4a Displacement – temperature curve of 7.5% sample under 0.1N constant tensile load.....	118
Figure 7.4b Displacement – temperature curve of 10% sample under 0.1N constant tensile load.....	118
Figure 7.4c Displacement – temperature curve of 12.5% sample under 0.1N constant tensile load.....	119

## List of tables

Table 1 Comparison of processing techniques for obtaining nanofibres .....	9
Table 2 Advantages and disadvantages of various processing techniques. (Ramakrishna, 2004).....	10
Table 3 Effect of processing method, material and solvent on nanofibre dimension. (Ramakrishna, 2004) .....	11
Table 4 Effect of electro-spinning method, with the material and solvent. on the nanofibre dimensions. (Ramakrishna, 2004).....	11
Table 5 Description of sample A(7.5% EVOH nanofibre sheet) B (10% EVOH nanofibre sheet) and C (12.5% EVOH nanofibre sheet).....	58
Table 6 The thicknesses of 7.5%, 10% and 12.5% EVOH nanofibre sheet samples.....	59

## Abbreviations

Nanofibres – Fibres with diameters measured in around nanometers

Electro-spinning – An electrical process to create nanofibres

HVU – High Voltage Unit

VDU – Visual Display Unit

SEM – Scanning Electron Microscope

LED – Light Emitting Diode

RJ11 – A standard phone cable containing 4 individual wires

F – Farad: SI unit of electrical resistance

A – Area of nanofibre sheet

Ag – Silver substance

AgNO<sub>3</sub> - Silver nitrate

EVOH - Poly (ethylene-co-vinyl alcohol)

PVA – Polyvinyl acetate

PVP – Poly (vinylpyrrolidone)

RBC – Red blood cell

m – Mass of the membrane

M – Molecular weight of the polymer

PBS – Phosphate buffered saline

PCL – Polycaprolactone

PEO-PPO-PEO – The triblock poly(ethylene oxide) and poly(propylene oxide) based system

Pico – PA prefix meaning one trillionth ( $1/1,000,000,000,000$  or  $10^{-12}$ )

Nano – Prefix meaning one billionth ( $1/1000,000,000$  or  $10^{-9}$ )

# 1. Introduction

## 1.1 Background to nanotechnology and nanofibres

Since the invention of the term ‘nanotechnology’ by K. Eric Drexler in his book “Engines of Creation”, the field of nanotechnology has been a hotly debated topic in both academia and industry. Although the positional manipulation of xenon atoms on a nickel substrate in 1990 was hailed by some as the “first unequivocal” experiment in nanofabrication, it should be borne in mind that the growth of nanowires and nano-rods by the vapor-liquid-solid method was reported at the beginning of the 1960s and the spontaneous growth of nanowires came in the 1950s. The scientific know-how of gold nanoparticle synthesis was, in fact, performed by Faraday in 1841. Perhaps the medieval stained-glass makers can be called the first nanotechnologists, since they prescribed varying amounts of gold to modify colours. Unbeknown to these stained-glass makers, these tiny gold spheres, which absorbed and reflected sunlight in different frequencies, will forever be part of the history of size effects in nano-scale objects.

The manufacture of nanofibres has the potential to confer significant economic benefits. Some economic and business reports state that by 2015 the nano-medical materials field may be worth around \$18 billion [Ramakrishna Seeram., 2004, Ken Herbert.,2005, Robert Zufan., 2005]. The United States appears to be investing the most money into nanotechnology at the moment. In 2005, the direct funding of this technology by the U.S. Government was around \$1.2 billion [K. Herbert., 2005, T.J Rudd., 2005] with the greater part of this amount coming from three bodies (the U.S. National Science Foundation, the U.S. Department of Defense and the U.S. Department of Energy)[Robert Zufan., 2005, Ken Herbert, 2005]. This figure shows a rise in funding of over \$1 billion dollars in 8 years. The same report estimated that in 2006 this amount would fall to just over \$1 billion, but this is still a very substantial amount and should be considered as a mark of the industry moving to self sustainability rather than a public lack of confidence in the technology. There are various areas the funding of which is dedicated to including nano-materials and devices, nano-manufacturing and

various applications[T. James Rudd,2005, J.H. Lee et al.,2003, W. He, et al., 2005].

Skin wounds are a significant health problem, which negatively affect the lives of millions of people worldwide, involving huge costs to society [Xu F. et al., 2010, Zhou, L., 2008, Choinière M. et al., 1990].In the U.S.A., more than 1.25 million people every year suffer burns[Brigham PA. et al., 1996, Sheridan, R. L., 2003,Yu B.-H.1999] and 6.5 million people have chronic skin ulcers caused by pressure, venous stasis or diabetes mellitus [Calif, I., 1997]. Although skin wound healing has become an increasingly mature topic of study in clinics and academia [Xu F. et al 2009, Xu F. et al., 2009], only few breakthroughs in skin wound therapies, mainly due to the limited capacity to mitigate the loss of body fluid and inflammation, in particularly when large areas of skin are damaged.

The present research aims, by the extensive potential benefit and application of nano-fibres, to achieve multiple targets, with medical applications as the main expected outcome.

## **1.2 Aims and objectives**

As the title of this thesis implies, the aim of the study is to provide a new dressing material for the healing of skin wounds, in particular for skin burn healing and battle ground rescue; the fabrication of this material would use electro-spinning techniques. For interest, we provide various possible biomedical applications of nanofibres to aid skin wound healing by means of their unique mechanical properties.

This study is mainly based on experimental methodology and also includes both the experimental techniques and a theoretical understanding of the electro-spinning process.

The first objective is to produce nano-fibres using an electro-spinning machine. This will be a milestone for the project. The successful production of the fibre will allow us to investigate various control parameters in manipulating the

properties and features of the fibres. Such a capacity is necessary to customise fibres for different applications in a build-up of capacity. The work includes diameter and orientation control as well as a trial of tube production. Extensive SEM examinations should be carried out to quantify the produced fibres.

The second objective of the study is to present the mechanical properties as revealed by such tests as uniaxial tensile tests and viscoelastic tests, etc. To test the potential of the EVOH nanofibre sheets for use in dressing applications, the material will be subjected to stretching, tearing, cutting and other types of mechanical loading. Only the findings of the tensile tests on thin sheets made of nanofibres in random directions are discussed here.

The third objective is to examine the potential medical applications of the fibres as a possible wound dressing. More details will be given in later chapters on this aspect. It will be treated in two parts: making the fibres capable of killing germs; and giving the results of animal tests to verify the effectiveness of the fibres. The second part also includes an optimisation study on the range of diameters most suitable for such an application.

To achieve the germ killing capacity, silver (Ag) particles, as an approved agent for suppressing infection, was added to the polymer solution in order to form the fibres. Culture tests were carried out in a biological laboratory (at a collaborative institution) to evaluate the density of the silver particles needed to achieve the nominal level of suppression capacity. Once this was completed, the fibres were tested on animals in collaboration with a university hospital which holds an approved license for animal testing. The tests were under the instruction of surgeons/specialists in burn treatment.

To summarize, the objectives of this research are: 1. To produce the nano-fibres using the electro-spinning machine. 2. To examine the potential medical applications of the fibres as possible wound dressing. 3. To harness the germ killing capacity of Ag nanoparticle EVOH nanofibres. 4. To qualify the release speed of the Ag nanoparticles. 5. To discover a new dressing material by electro-spinning EVOH nanofibres and Ag nanoparticles and validate it via animal tests.

### **1.3 Scope of this thesis**

This thesis can be split into four main parts, with a conclusion: the first part extends from Chapters 1 to Chapter 3 and deals with the background to and principles of electro-spinning. The next part, Chapter 4 presents the mechanical properties of nanofibre mats. The third part, Chapter 5, focuses on the method of producing Ag-nano-particle EVOH nanofibres and Ag release speed tests. The final part, Chapters 6 and 7, presents the anti-bacterial tests and animal tests, before drawing some conclusions.

Chapter 1 covers some basic aspects of electro-spinning process and principles. Chapter 2 contains the literature review of electro-spinning technology, which covers its history and key developments.

The process of electro-spinning is dealt with in Chapter 3; to carry out this process, the polymer solution parameters (such as viscosity, surface tension, etc.), the parameters of the electro-spinning process (such as voltage, tip-to-collector distance etc.) and the ambient conditions (e.g., temperature) are considered. In addition, issues of the uniformity, productivity, patterning and the creation of various types of nanofibre are outlined, in view of their importance in the specific applications.

Chapter 4 shows the mechanical properties of the EVOH nanofibre sheets. To test the potential use of EVOH nanofibre sheets for wound dressing applications, the material will be subjected to stretching, tearing, cutting and other types of mechanical loading. Only the findings of the tensile extension tests on thin sheets made of nanofibres in random direction are discussed in Chapter 4 here, together with the viscoelastic tests using the Dynamic Mechanical Analyzer (DMA).

Chapter 5 concerns the electro-spinning methods and process of making Ag nanoparticle EVOH nanofibre and iodine and gentamicin EVOH nanofibre. The release speed of the Ag nanoparticles in EVOH nanofibres is assessed by testing the degradation properties of EVOH nanofibres. In this study, the degradation

tests were performed in different conditions, such as with water, PBS, sunlight and UV light.

Chapter 6 shows the process and results of anti-bacterial tests and animal tests. The bacteriostatic abilities of Ag, iodine and gentamicin EVOH nanofibre were tested and the results explain the reason for finally choosing silver as the substance for this new dressing material for skin wounds. In addition, the bacteriostatic abilities of Ag nanoparticle EVOH nanofibres in different Ag concentrations were tested. Animal tests were performed by using a burn machine with young pigs. Chapter 7 provides the conclusion of this thesis and also suggests future subjects for research.

## 2. Literature review

### 2.1 History and science of electro-spinning

Electro-spinning descends from the technique of electro-spraying. The first recorded observation of the deformation of liquid droplets under the influence of an electric field was that reported by William Gilbert in the 17<sup>th</sup> century [Gilbert, 1628]. He observed that when a sufficiently electrically charged amber was brought close to a water droplet on a dry surface, the drop was drawn towards the amber in a cone shape and water droplets were lifted off the tip of the cone. The events since Gilbert's observation of this phenomenon leading to modern electro-spinning are summarized in 1749 also demonstrated the disintegration of a water jet under the influence of an electric field [Nollet, 1749].

The first theoretical work related to electro-spinning was reported by Rayleigh [Rayleigh, 1882]. He calculated the limiting charge at which an isolated drop of water of a certain radius became unstable. Thereafter, Joseph Larmor in 1898 explained the excitation of a dielectric liquid under the influence of an electrical charge [Larmor, 1898]. In 1902, the first patents on electro-spinning were granted to Morton and Cooley. J.F.Cooley's setup [Cooley, 1902] demonstrated the use of a rotating collector and auxiliary electrodes, while Morton showed how needled and needleless forms of electro-spinning could be carried out [Morton, 1902]. However, it was not possible to exploit this method due to the lack of technology to supply power at high voltage. Further experimental work on electro-spinning was done by John Zeleny between 1914 and 1917; at this time he designed the needle/capillary apparatus which enabled him to study electrical discharges from liquid points [Zeleny, 1914].

The foundation for today's electro-spinning technology was based on the patents of Formhals between 1934 and 1944, for which he gained recognition as the father of present day electro-spinning [Formhals, 1934, Formhals, 1938a, Formhals, 1938b, Formhals, 1939b, Formhals, 1939a]. He developed a variety of innovative electro-spinning setups with different spinneret and collector

configurations, some of which are still used widely today. Meanwhile, in 1936, Norton had demonstrated the melt-electro-spinning of polymers [Norton, 1936].

The first industrial scale production of electro-spun membranes was undertaken in 1939 by Natalie Rozenblum and Igor Petryanov-Sokov, who developed cellulose acetate based nano-fibrous meshes as filters inserted in gas masks for military use in the former USSR [Filatov, 1977]. The filters were popularised as ‘Petryanov filters’. It was only in 1981 that the commercial production of electrospun products for a variety of filtration applications was achieved; the successful firm was an American company called Donaldson. Finally the commercial manufacture of electro-spinning equipment for industrial production and academic research was achieved in 2006, by Elmarco Liberec, a Czech company [Jirsak et al., 2005].

Listed below are the main events in the history of electro-spinning in order of their chronology:

In 1638 • Gilbert, W made the first recorded observation of electro-spraying; showing the typical conical shape induced on a water droplet under the influence of an electrically charged piece of amber.

In 1749 • Nollet A demonstrated the disintegration of water jet when it was charged.

In 1882 • Rayleigh L calculated the limiting charge at which an isolated drop of certain radius became unstable – the first theoretical work related to electro-spinning.

In 1898 • Larmor, J explained the excitation of dielectric liquid under the influence of an electrical charge.

In 1902 • Cooley, JF patented an electro-spinning setup, used auxiliary electrodes to direct electro-spinning jet on to a rotating collector.

In 1902 • Morton WJ, patented the electro-spinning method, used needle as well as needleless forms of electro-spinning.

In 1917 • Zeleny, J designed the needle/capillary apparatus to study electrical discharges from liquid points.

In 1936 • Norton developed melt polymer electro-spinning

In 1939 • Rozenblum ND and Petryanov-Sokolov,I led the first industrial facility to produce electrospun fibrous materials for military gas masks, called ‘Petryanov filters’

In 1944 • Formhals, A, recognised as the father of present-day electro-spinning technology, made innovative setups, with and without spinneret, multiple spinnerets, parallel electrodes to produce aligned fibres.

In 1960 • Landau and Lifshitz modelled charge density – surface wave instability for conductive liquids, laying the foundation for the generalized theoretical modelling of electro-spinning

In 1969 • Taylor GI, published his theory underpinning electro-spinning; the characteristic droplet shape is named the ‘Taylor cone’ to honour his contribution

In 1967 • Mathews, wrote on the mass loss and distortion of freely falling water drops in an electric field, in which he gave the results of his experimental analysis

In 1981 • Donaldson Co. Inc., introduced the first commercial products containing electrospun nanofibres

In 1990 • Renneker and Rutledge were responsible for spinning a wide spectrum of polymers and popularized the term ‘electro-spinning’

In 2000 • A boom in research, theoretical modeling and applications, establishing the science of electro-spinning

In 2006 • Elmarco Liberec, began the first commercial manufacture of electro-spinning equipment for industries and academia

To make fine fibres, many ways are available to choose from, chosen such as drawing, phase separation, template synthesis, self-assembly and electro-spinning.

In this study, was chosen. Successful electro-spinning depends on the five factors shown below:

1. A suitable solvent should be available for dissolving the polymer.
2. The vapour pressure of the solvent should be suitable so that it evaporates quickly enough for the fibre to maintain its integrity when it reaches the target but not too quickly to allow the fibre to harden before it reaches the nanometer range.
3. The viscosity and surface tension of the solvent must neither be too large to prevent the jet from forming nor be too small to allow the polymer solution to drain freely from the pipette.
4. The high power supply should be adequate to overcome the viscosity and surface tension of the polymer solution to form and sustain the jet from the pipette.
5. The gap between the pipette and grounded surface should be so small as to create sparks between the electrodes but should be large enough for the solvent to evaporate in time for fibres to form.

Below is a table comparing the properties of the various processes for making fine fibres.

Table1. Comparison of processing techniques for obtaining nanofibres.

[Ramakrishna, 2004]

Process	Technological advance	Can the process be scaled?	Repeatability	Convenient to process?	Control on fibre dimensions
Drawing	Laboratory	No	Yes	Yes	No
Template Synthesis	Laboratory	No	Yes	Yes	Yes
Phase Separation	Laboratory	No	Yes	Yes	No
Self-Assembly	Laboratory	No	Yes	No	No
Electro-spinning	Laboratory (with potential for	Yes	Yes	Yes	Yes

	industrial processing)				
--	------------------------	--	--	--	--

Table2. Advantages and disadvantages of various processing techniques.

[Ramakrishna, 2004]

Process	Advantages	Disadvantages
Drawing	Minimum equipment requirement.	Discontinuous process
Template Synthesis	Fibres of different diameters can be easily achieved by using different templates	Complex process
Phase Separation	Minimum equipment requirement. Process can directly fabricate a nanofibre matrix. Batch-to-batch consistency is achieved easily. Mechanical properties of the matrix can be tailored by adjusting polymer concentration.	Limited to specific polymers
Self-Assembly	Good for obtaining smaller nanofibres.	Complex process
Electro-spinning	Cost effective. Long, continuous nanofibres can be produced.	Jet instability for some polymer materials

Table3. Effect of processing method, material and solvent on nanofibre dimension.

[Ramakrishna, 2004]

Process	Material	Solvent	Fibre diameter	Fibre length
Drawing	Sodium Citrate	Chloroauric acid	2 nm to 100 nm	10 microns to mms
Template Synthesis	Polyacrylonitrile	Dimethylformamide	100nm to 200 nm	10 microns
Phase Separation	PLLA	Tetrahydrofuran	50 nm to 500 nm	Up to 20 to 30 microns
Self-Assembly	PEMA core – PS shell	Tetrahydrofuran	100 nm	20 microns
	PECMA middle layer – PS corona	Tetrahydrofuran	100 nm	20 microns
	PS core – P4VP corona	Chloroform	25 nm – 30 nm	Up to 1 micron
	Peptide	Chloroform	7 – 8 nm	Several microns

Table 4. Effect of electro-spinning method, with the material and solvent. on the nanofibre dimensions. [Ramakrishna, 2004]

Process	Material	Solvent	Fibre diameter	Fibre length
Electro-spinning	EVOH	Water and propanol-2	50 nm – several microns	Several cms to several meters
Electro-spinning	Nylon 6-pollyimide	Formic acid	50 nm – several microns	Several cms to several meters

Electro-spinning	Polyaniline	Sulphuric acid	50 nm – several microns	Several cms to several meters
Electro-spinning	PLLA	Chloroform	50 nm – several microns	Several cms to several meters
Electro-spinning	PEO	water	50 nm – several microns	Several cms to several meters
Electro-spinning	PMMA	Toluene	50 nm – several microns	Several cms to several meters
Electro-spinning	PU	Dimethylformamide	50 nm – several microns	Several cms to several meters

Tables 1, 2 and 3 show comparisons of the various issues relating to these processing methods and lists some of the polymers that can be converted into nanofibres. Overall, we found that the electro-spinning method fits all the requirements in this study. Finally, Table 4 shows the effect of the method of electro-spinning with different materials and solvents on the size of the nanofibres produced.

### **2.1.1 The principle of electro-spinning and electrospray**

To understand the electro-spinning process, it is helpful first to look at the mechanism of the production of polymer fibres. The production of conventional fibres of large diameter involves the drawing out of molten polymer through a die. The resultant stretched polymer cools and dries to form individual strands of fibre. Similarly, electro-spinning also involves the drawing out of liquid, in the form of either molten polymer or polymer solution. However, unlike the conventional drawing method where there is an external mechanical force which pushes the molten polymer through a die, electro-spinning makes use of electric charges which are applied to the fluid jet to provide a stretching force to a collector, where there is a possible gradient. When a sufficiently high voltage is applied, a jet of polymer solution will erupt from a polymer solution droplet. The polymer chain entanglements within the solution will prevent the electro-spinning jet from breaking up. While the polymer solution used in both conventional fibre production methods cools and solidifies to yield fibre in the atmosphere, the electro-spinning of polymer solutions relies on the evaporation of the solvent for the polymer to solidify and form a fibre.

Electro-spinning uses a high voltage supply to stretch a polymer solution jet which comes out from a metal needle with a small diameter. The name comes from the physical response of the polymer as it passes through a high voltage electrical field. The polymer jet is forced to spin around in circles as it moves to the ground of the electric field. The process is very quick but may have more serious safety issues than other manufacturing methods because of the high voltages needed. The voltages are in the order of tens of kilovolts. Despite this disadvantage, this method is highly efficient and not expensive.

Electro-spinning technology was patented more than 100 years ago by J.F. Cooley in February 1902 and W.J. Morton in July 1902 [Cooley, 1902]. In 1914 John Zeleny published work on the behaviour of fluid droplets at the end of metal capillaries. His effort was the first attempt to mathematically model the behavior of fluids under electrostatic forces [Zeleny,1914]. Between 1964 and 1969 Sir Geoffrey Ingram Taylor produced the underlying theory with regard to electro-spinning Taylor's work contributed to electro-spinning by mathematically

modeling the shape of the cone formed by the fluid droplet under the effect of an electrical field; this characteristic droplet shape is now known as the Taylor cone [Taylor, G., 1964, Taylor, G., 1965, Taylor, G.,1969] ( see Figure 2.1b).

Electrospinning is a non-woven fibre spinning technology that allows spinning of fibres diameter ranging from 2 nm to 10s of  $\mu\text{m}$  Bhardwaj and Kundu, 2010). It is different from the conventional dry or wet spinning technologies, in that it generates submicron and nanometer size fibres, and does not require high temperatures or specialized solution chemistries, In addition it also allows spinning of large and complex molecules, as well as combinations of compatible or incompatible polymer solutions.

The principle behind electrospinning is the use of electric charge to create a charged jet of polymer solution. When sufficiently large voltage (+ or -) is applied, electrostatic repulsion of the charged moieties in the polymer solution repel to counteract surface tension resulting in the stretching of the droplet forming a cone shape known as Taylor cone. From the tip of the Taylor cone, a stream of liquid ejects and if the viscosity and the electrical resistivity of the polymer solution are sufficient, the stream does not break up. During the flow, as the solvent dries, the mode of current flow in the jet is said to change from ohmic to convective flow causing it to bend, whip and accelerate towards the grounded collector. The process, as illustrated, involves the formation of Taylor cone and jet, followed by the travel of jet along a straight line during the ohmic flow and then starts bending during the convective flow. The bending during the convective flow of charges within the electrospinning jet is attributed to the mutual repulsive force between the electric charges carried by the jet [Reneker et al., 2000]. The bending and acceleration stretches the fibre resulting in the thinner fibres observed with non-woven fibres spun using electrospinning.

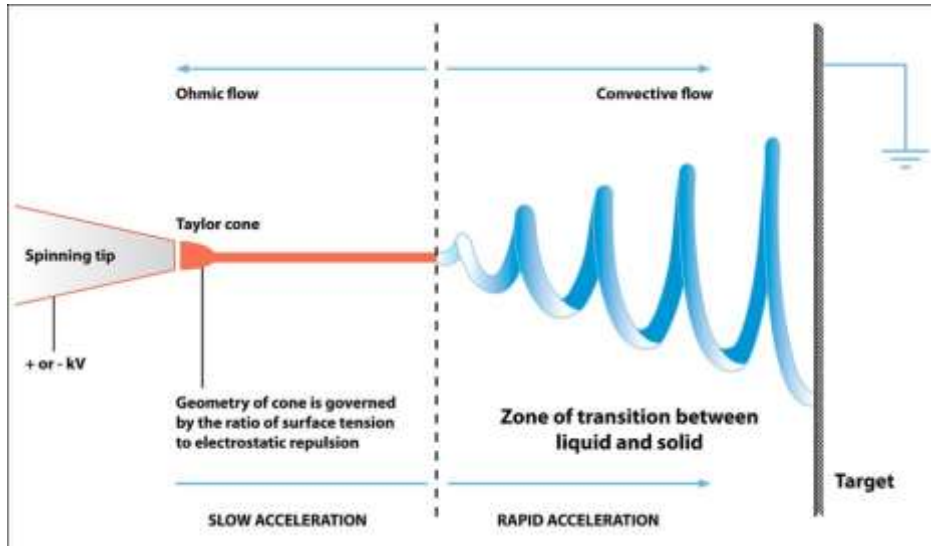


Figure 2.1a Schematic diagram showing the fibre formation dynamics during electrospinning [<http://en.wikipedia.org/wiki/Electrospinning>, 2012].

In real-time, the bending instability of the jet appears to naked eye or conventional photography as the single stream of polymer solution splitting into multitude of jets in a cone shape. However, using high speed photography, Shin et al. demonstrated that it is essentially a single fibre that bends and whips rapidly to give the illusion of splitting and multiple jets [Shin et al., 2001].

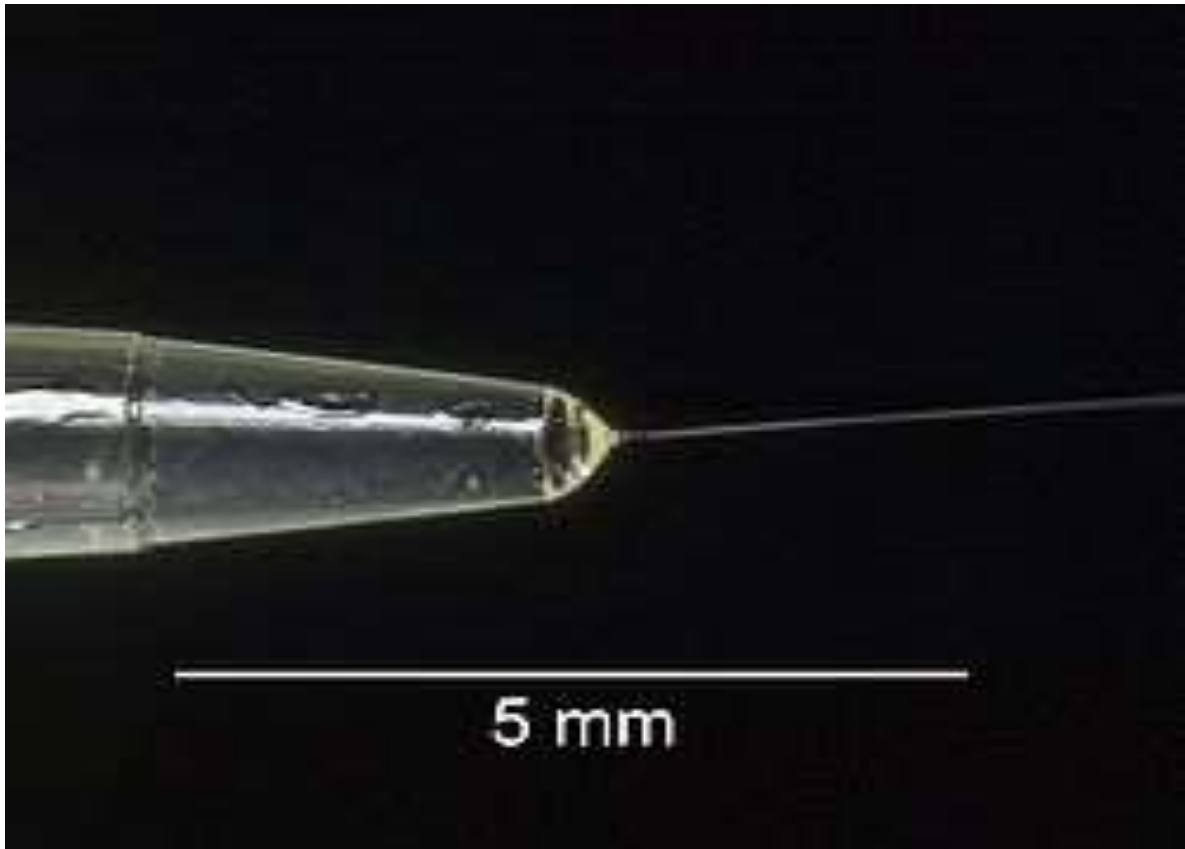


Figure 2.1b Taylor Cone in 5 mm range [Taylor,G.1969, Wan et al., 2004]

When a very small droplet of electrically charged solution is exposed to a static field, the shape of the solution starts to be deformed from its original shape under surface tension alone [Huang Z. et al., 2003, Li D. et al., 2003, Ko, F. et al., 2003, Wan, Y.Q. et al., 2004]. As the voltage is increased the effect of the static field becomes more pronounced and as it approaches the exerting of a similar degree of force on the droplet as that of the surface tension there starts to form a cone shape with convex sides and a rounded tip. This approaches the shape of a straight Generatrix (cone) with a whole angle degree width of  $98.6^\circ$  [SubbianT. et al., 2005]. When a specific threshold voltage has been reached the slightly rounded tip inverts and emits a small jet of the solution. This is called a cone-jet and marks the beginning of the electro-spinning process. It is generally found that, in order to achieve a stable cone-jet, a slightly higher voltage than the threshold value must be provided. As the voltage is increased further, other modes of droplet disintegration are found. The term Taylor Cone [Morton,W.J. 1902] can also specifically refer to the theoretical limit of a perfect cone of exactly the

predicted angle or generally refer to the approximately conical portion of a cone-jet after the electro-spinning process has started.

There are the three major pieces of equipment which are essential to the electro-spinning process; first of all, a high voltage unit is needed, which should be able to provide up to 20 or 30 kV, namely, to provide enough energy to spin the solution from the needle. This unit and the effects of the voltage on the fluid will be explained in the last part of this section.

The second one is the collector; this needs to be connected to the ground. In theory, it does not matter whether it is connected to positive or negative. However, in practice and in the interests of safety, the collectors normally connected to the negative. What makes the jet circulate between needle and collector is the presence of several forces inside the static field such as the Coulomb force and the Lorentz force. When the polymer solution comes out of the needle, it has already taken a positive charge and also the field is positive. Hence, as soon as the drops of liquid fall into the static field they push each other. At this point, the jet starts to spin and it becomes thinner and thinner. In theory if the voltages and distance could be increased very greatly then very thin fibres, down to tens of nanometers, could be spun.



Figure 2.2 a 2 strips collector

Figure 2.2 shows a variation of the plate method for collecting fibres. This particular example uses 2strips, both of which are made of conductive materials. The method is that lines of fibres form a bridge across the gap between the strips. They do this because of the circulating (whipping) jet that is formed. Depending on the place where the falling jet lands, for instance, the jet could be collected on the left strip first. In this case, the further jet will fall across the gap and land on the right strip (Figure 2.3). This will yield two thick sections of fibres clumped together on each strip with single strands over the gap to connect them. Once

these are produced they can be laid on top of each other to form a web (Figure 2.3). Fibres of different types can be obtained from changing collectors. For our applications (involving parallel fibres and web fibres), it is quite suitable to use the collectors which are shown in Figure 2.2 and Figure 2.3.

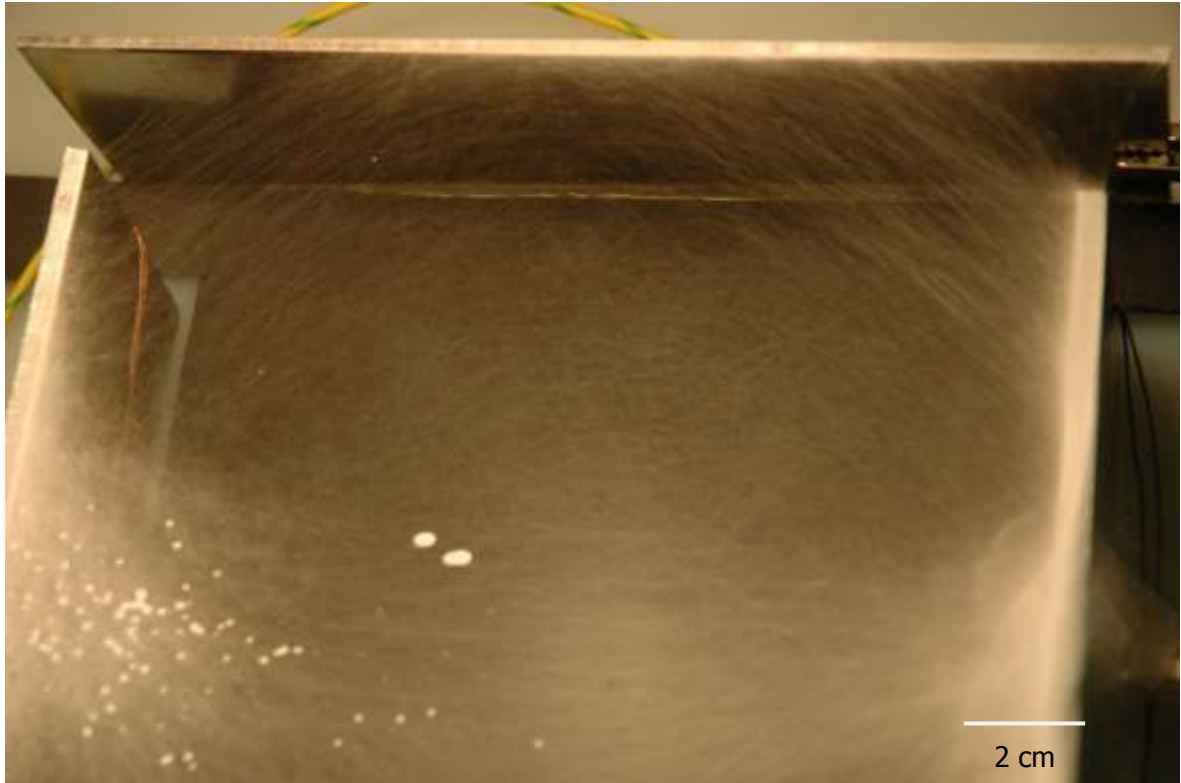
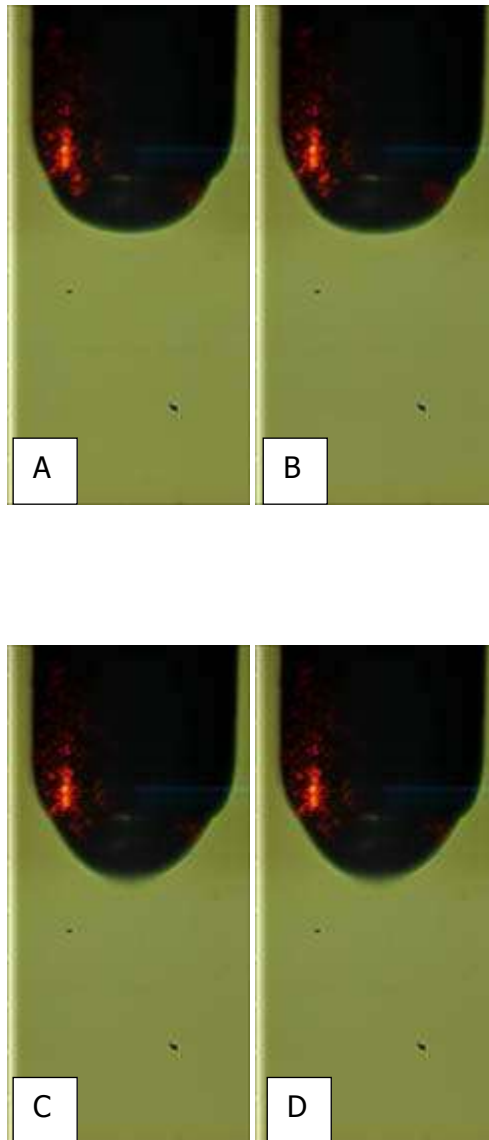
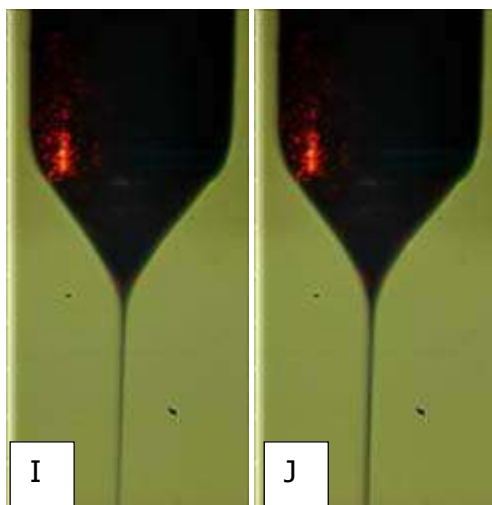
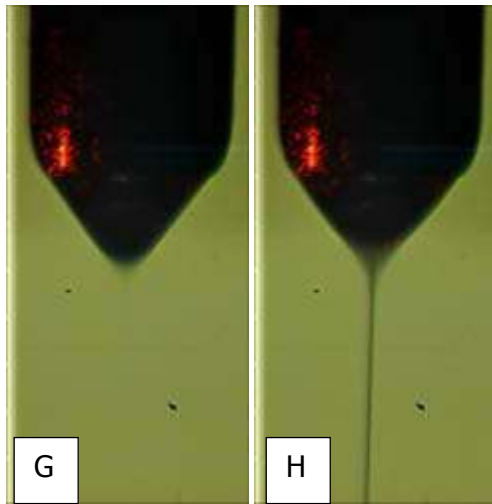
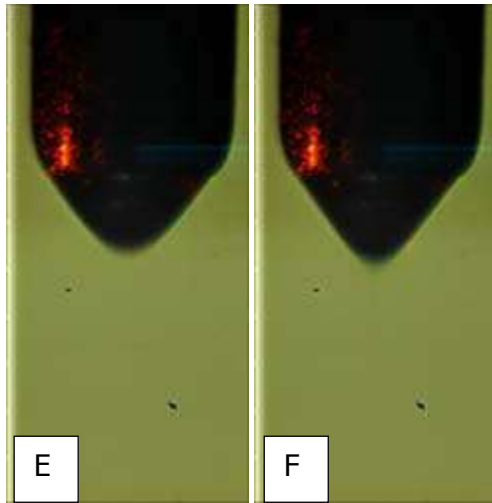


Figure 2.3 a 4-strip collector for web fibres (fibre diameter between 1 to 3 micrometers) used in the present research work. Fibres are collected diagonally between neighbouring strips forming a cobweb-like texture. The white dots are droplets produced during electro-spinning

The final section is the syringe section. This section is again very important to the overall process. The syringe holds the polymer solution and has to be finely controlled to deliver the correct amount of solution. The needle of the syringe is connected to the high voltage supply to set up the electric field with the collector. The control of the fluid has to be uniformly correct. If too much fluid is pumped, only large fibres will be obtained which do not solidify properly; this will leave a large amount of fluid on the collector which will prevent any extracted fibres from being collected. If not enough fluid is pumped, the growth of the fibre will not be sustainable and either fragments or drops will be produced. Ideally, with the right amount of fluid a Taylor cone will be formed at the end of the needle of the same

size throughout the process [Yarin,A.L. et al., 2001, G.C. Rutledge et al., 2001]. The fibre extends outwards from this cone due to the electric field; this cone is thus vital to the functioning of the process [Kirichenko,V.N. et al., 1986,Ganan-Calvo,A.M. 1997]. The development of the Taylor cone and finally the jet are shown (as the dark shape) in Figure 2.4A-J, below





Figures 2.4 A to J The process of formation of the Taylor Cone and a stable jet  
 [Carney, L. et al., 2001, Zeleny, J. 1917, Juraschek, R. et al., 1998]

The cone develops due to the building up of the electric field. At this stage, the droplet should not be pushed at all. The fluid of which this droplet is made will have a specific surface tension and the voltage needs to be built up gradually. Slowly, as the droplet gets bigger with a more abundant supply of the liquid, it stretches out into a cone shape. This is because the ions in the solution become more and more charged and increase the tension in the droplet. The polymer solution must be conductive for the charge to build up. Baumgarten demonstrated that the radius of the jet is inversely proportional to the cube root of the conductivity of the solution [Baumgarten, P.K. 1971, Shin, Y.M. et al., 2001]. Proof of the importance of conductivity on the final fibre has also been shown by adding ionic salts to the polymer solution [Zong, X.H. et al., 2002]. Eventually this cone will “break” at the point when the charge in it becomes higher than the surface tension can bear and a stream of fluid will stretch out of the tip of the cone [Baumgarten, P. K. 1971, G. I. Taylor, 1964]. This is all the effect of the electrical field between the cone and the collector, which will make the stream head toward the collector. This phenomenon allows us to have a horizontal or vertical set-up. The properties of the jet are also controlled by the voltage. Recent advances in picture technology have shown that the true behaviour of the jet is a whipping motion, which in turn has allowed for the development of the new collecting techniques.

In summary, Taylor cone can directly effect the process of electro-spinning. In 1965 Taylor published equation 1-1 which explained how the small dropjet being influenced in the static field.

$$h = \frac{\left[ \frac{\rho Q^3}{2\pi^2 I E_\infty} \right]^{1/4}}{z^{1/4}} \quad (1-1)$$

In Eq.(1-1), h is the wideness of the dropjet, Q is the charge density, I is the current on the top of the Taylor cone, ρ is the solution density, E is the voltage of the field [Taylor, 1965].

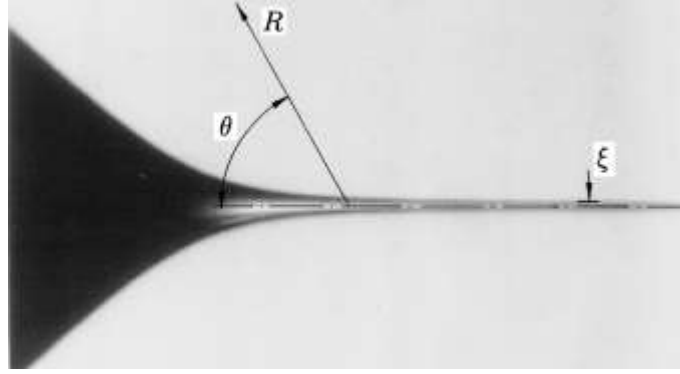


Figure 2.5 Taylor cone computational model

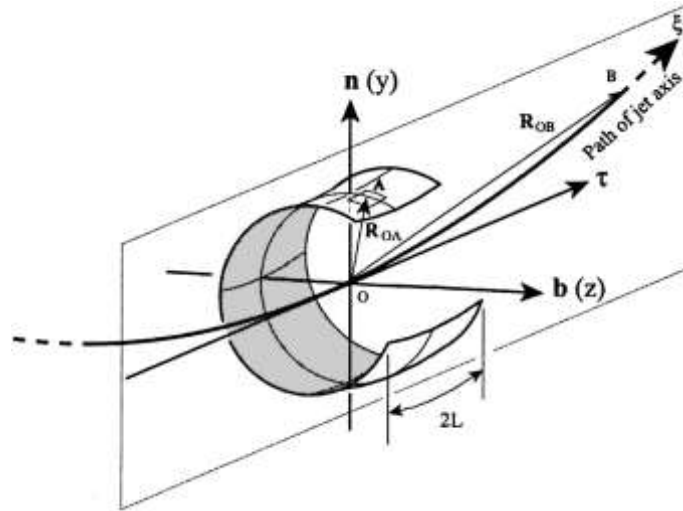


Figure 2.6 Dropjet model in the static field

Equation 1-2 shows the load-carrying capability of a small dropjet in the static field as Figure 2.6 shown.

$$dF = |k|nd\xi \left[ \pi a \sigma - e^2 \ln \frac{L}{a} \right] \quad (1-2)$$

In equation Eq. (1-2),  $k$  is the curvature,  $\sigma$  is the surface tension factor.

Due to the size of the dropjet is tiny, therefore, air resistance is necessary to be discussed, equations (1-3) to (1-8) are describing the effective of air resistance in the electro-spinning process [Ramakrishna, 2004].

$$\lambda f = \lambda_0 f_0 \quad (1-3)$$

$$\rho\lambda_0 f_0 \frac{\partial V}{\partial t} = \tau \frac{\partial P}{\partial s} + \lambda |k| P n - \rho g \lambda_0 f_0 k + \lambda |k| \times \left( \pi a \sigma - e^2 \ln \frac{L}{a} \right) n - \lambda e \frac{U_0}{h} k \quad (1-4)$$

In equation 1-3 and 1-4,  $\lambda$  is the extension ratio,  $f$  is the cross section area.

$$\frac{\partial \sigma_{\tau\tau}}{\partial t} = G \frac{1}{\lambda} \frac{\partial \lambda}{\partial t} - \frac{G}{\mu} \sigma_{\tau\tau} \quad (1-5)$$

$$\frac{1}{\lambda} \frac{\partial \lambda}{\partial t} = \frac{X_{,s} u_{,s} + Y_{,s} v_{,s} + Z_{,s} w_{,s}}{\lambda^2} \quad (1-6)$$

$$P = \frac{\lambda_0 f_0}{\lambda} \sigma_{\tau\tau} \quad (1-7)$$

The formula derivation from 1-3 to 1-8, the equation 1-8 eventually shows the extension ratio of the droplet in the static field during the electro-spinning process [Ramakrishna, 2004].

$$\gamma_* = \frac{\left[ e_0^2 \ln(L/a_0) \pi a_0 - \sigma \right]^{2/3}}{(3\mu\rho a_0^4)^{1/3}} \quad (1-8)$$

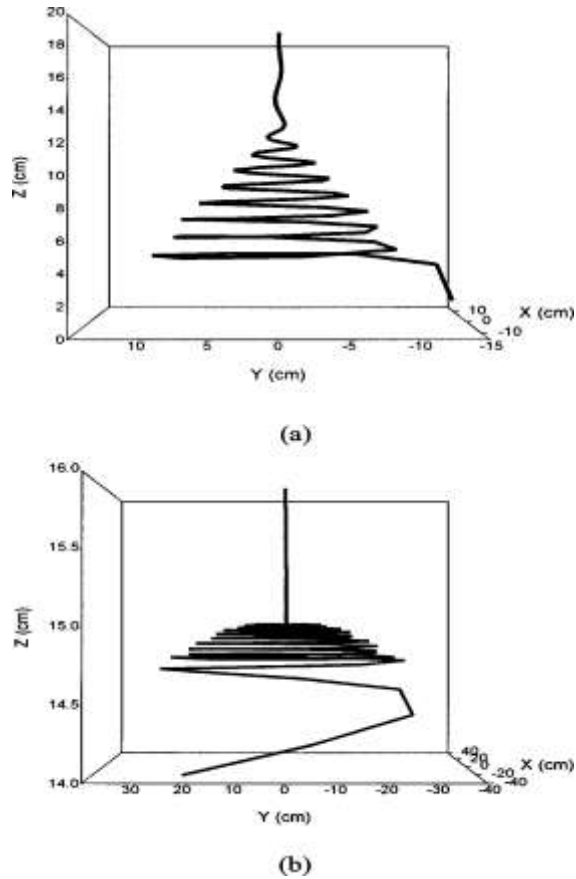


Figure 2.7 a and b. the mathematic model of the dropjet during the electro-spinning process [Ramakrishna, 2004].

Figure 2.7a shows the mathematic model of electro-spinning in the static field with considering the solution volatilization. Figure 2.7b shows the mathematic model of electro-spinning in the static field without considering the solution volatilization. In our study, first of all, the polymer solution was required to be heat till 80 °C, secondly, some of the tests were completed in the open area, therefore, Figure 2.7a is suitable for this study.

## 2.1.2 Equipment and Technology

### 2.1.2.1. The electro-spinning instrument

The equipment needed for electro-spinning is simple in construction and consists of a high voltage power source, a syringe pump with tubing to transport the solution from the syringe to the spinneret and a conducting collector. The

spinneret and collector are opposite each other in alignment and together they are usually oriented either horizontally or vertically. Any variations in the equipment are primarily concerned with the spinneret and the collector.

#### **2.1.2.2. The Spinneret**

The construction of the Spinneret allows greater versatility in the nano-fibre structures. They can be single or multiple and needle-type or needleless configurations [Teo and Ramakrishna, 2006]. Typical electro-spinning setups are equipped with a single blunt ended needle for spinning single polymer fibres. To introduce a composite fibre structure, either coaxial or dual-capillary (side-by-side), spinnerets are used. The former produce core-shell and the latter side-by-side fused fibre structures, respectively. An additional advantage of using coaxial spinnerets is that incompatible or non-electro-spinnable polymer solutions can be combined to obtain fibres [Teo and Ramakrishna, 2006]. For example, a non-electro-spinnable polymer solution can be extruded in the inner capillary, while the spinnable solution extruded in the outer capillary. Thus the inner solution is contained by the outer solution, resulting in a core fibre. The shell can then be dissolved to obtain the fibres of the non-electrospinnable solution. This method can also produce hollow fibres by dissolving the core fibre. Overall the coaxial fibre has a reinforcing core polymer fibre encapsulated by a shell of a different polymer, while the side-by-side fused composite fibres have two different polymers side-by-side. The permutations and combinations of the two polymers can be used to engineer membranes for a variety of applications, in particular in the emerging field of tissue engineering. In addition, the coaxial spinnerets can further be modified to incorporate, for example, three concentric polymer fibres, or a large fibre reinforced with three different polymer fibres within its composite structure.

Needleless electro-spinning through an orifice in the flat base of a tube is another method, often used for melt-spinning. In this, the pure polymer is melted by heating and the molten polymer is injected through the orifice.

From the perspective of industrial production, an inherent limitation of electro-spinning is that the volume of fibrous meshes or structures produced per

unit time is much less than that obtained using conventional spinning technologies. To increase productivity, multiple parallel spinnerets (needleless or needle-based) are used.

One concern raised by electro-spinning which uses needle-based or needleless spinnerets is the clogging of the spinneret; this usually occurs when the solvent used is highly volatile. To avoid clogging, pointed tip or spike structures are often used.

### **2.1.2.3. The Collector**

In a basic configuration, the spinneret needle is aligned perpendicular to a static grounded flat plate (the collector). During electro-spinning, the seamless fibre is collected as a sheet, typically on top of the flat plate collector. The resulting sheet has random fibre orientation. However, the orientation, 3D architecture and properties of the electrospun structures can be varied either by influencing the electric field between the spinneret and the collector or by rotating the collector in the field of electro-spinning. A wide variety of collector configurations used in research were collated and offered as schematic representations by Teo and Ramakrishna as illustrated in 2006 [Teo and Ramakrishna, 2006 ].

An important collector configuration is the use of a rotating drum in the field of electro-spinning. When the speed of rotation matches the speed of the accelerating electrospun fibre, the fibres are primarily aligned along the circumference of the drum. A few thousands of rpm, e.g. 4500 rpm, for the rotating drum is needed for fibres to align [Matthews et al., 2002]. A low rotation speed, e.g. around 500 rpm, allows the orientation of the fibres to be randomised. When the rotation speed crosses the speed of accelerating electrospun jet, the fibre breaks, thus, disrupting its seamless nature. Increasing the speed of rotation is also reported to influence the mechanical properties of the fibres, e.g. by inducing better alignment of the polymer crystals in the fibres [Kim et al., 2004]. In addition, the use of an alternating-current (AC) high voltage supply instead of the traditional direct-current (DC) high voltage supply for charging the

electro-spinning solution is reported to induce a better alignment of the fibres [Kessick et al., 2004].

The presence of a conducting object in the field of electro-spinning significantly influences the nature of the fibre deposition. The use of rings can control the area in which the fibres are deposited. Similarly, a sharp pin in the centre of a drum can focus the fibre deposition towards the pin. In addition, significant research has gone into the alignment of fibres. Parallel electrodes are used to exert a pulling force towards the electrodes, thus aligning the fibres perpendicular to these electrodes. Similarly, knife edge electrodes also induce highly aligned fibres along the length of the knife edge. Wire drum and wires wound around a drum have also been used for generating aligned fibres. Furthermore, special ways of patterning the fibres was also achieved using collector configurations. The former configuration was used to induce fibre structures which were twisted or shaped like springs, while the latter allowed the deposition of aligned fibres which were perpendicular to each other. For a comprehensive review of the advantages and disadvantages of the different collector configurations, the reader may refer the review by Teo and Ramakrishana (Teo and Ramakrishana, 2006).

#### **2.1.2.4. Parameters effecting electro-spinning**

The electro-spinning of fibres and their resulting morphology and diameter are all affected by the solution (its viscosity, elasticity, conductivity and surface tension), processing (the solution flow rate, applied electric potential and the spinneret and collector) and ambient conditions (temperature and humidity) and excellent surveys of their effects on electro-spinning are available in the literature [Ramakrishana et al., 2005a, Huang et al., 2003, Tan et al., 2005, Li and Xia, 2004, Lukas et al., 2009, Theron et al., 2004].

#### **2.1.2.5. Solution Parameters**

The ability of a polymer to be electro-spun depends on its solution viscosity and electrical resistivity. If the viscosity is too low, the cohesiveness between the polymer chains (surface tension) is too low to hold together the jet of fluid

emerging from the Taylor cone. Similarly, if the solution is too conductive, the repulsive forces between the polymer molecules cause the fluid jet to breakdown, forming droplets. With increasing viscosity and electrical resistivity, the breaking up of the jet into droplets makes a transition to the formation of a beads-on-string fibre structure before proper fibres, according to Shenoy et al. (2005). A further increase in viscosity results in increases in the diameter of the fibre diameter until a maximum viscosity beyond which the Taylor cone becomes too big, causing the jet to become unstable [Megelski et al., 2002, Jarusuwannapoom et al., 2005, Demir et al., 2002, Deitzel et al., 2001a]. Thus, for a given polymer, there exists a range of solution viscosity in which proper fibres can form. This range varies for any given polymer, depending on the solvent that it is dissolved in, and it varies also for different polymers [Huang et al., 2003].

The solution parameters not only determine the electrospinning ability of a polymer, but also affect its morphology and diameter. The higher the conductivity of the solution is, the higher is the number of charges carried by the electro-spinning jet. Thus, the higher the charged content, the higher the stretching of the jet, yielding thinner fibres. This aspect has been exploited by the introduction of ionic salts to adjust solution conductivity in order to decrease the diameter of the electrospun fibres [Zong et al., 2002, Son et al., 2004]. Similarly, for making highly conducting polymer solutions electrospinnable, less conductive polymers are added as fillers. Furthermore, the volatility of the dissolving solvent is another dominant factor that affects the formation of nanostructures by influencing the surface tension of the polymer solution [Megelski et al., 2002]. Reducing the surface tension has been correlated with the formation of smooth and thicker fibres [Fong et al., 1999, Zeng et al., 2003]. In addition, mixtures of solvents can also be used to tune the surface tension of the polymer solution, thus tailoring the morphology and diameter of the electrospun fibres.

#### **2.1.2.6. Processing parameters**

The next essential group of parameters that affects the structure of electrospun fibres are the electro-spinning process variables, namely, the voltage applied, the feed rate and the distance between the spinneret and the collector. In most cases, a higher voltage causes greater stretching of the solution due to larger

coulombic forces within the jet and a stronger electric field, thus reducing the fibre diameter [Buchko et al., 1999, Lee et al., 2004a, Megelski et al., 2002]. However, the higher voltage can also shorten the flight time of the electro-spinning jet, providing less time for the fibre to stretch before it reaches the collector [Demir et al., 2002]. Furthermore, higher voltages are also associated with a greater tendency to form beads, due to the greater instability of the jet [Demir et al., 2002, Deitzel et al., 2001a, Deitzel et al., 2001b, Zong et al., 2002]. The contrasting effects of the applied voltage is often primarily due to the influence of other process variables. For instance, with increasing applied voltage, an appropriate increase in the polymer solution feed rate is needed to ensure the formation of the Taylor cone.

Furthermore, increasing the flow rate increases the amount of polymer in the electro-spinning jet, thus increasing the fibre diameters. The increased volume of the jet is also associated with inadequate solvent evaporation, leading to a fusion of fibres at contact points between the electrospun fibres [Rutledge et al., 2001]. Therefore, a lower feed rate is more desirable for bead-free fibre manufacture, because the solvent has more time to evaporate giving more time for the fibre to stretch [Zhang et al., 2009].

The distance between the spinneret and the collector has a significant influence on the strength and distribution of the electric field. The shorter this distance is, the stronger is the electric field and vice versa. Typically, an intermediate optimum distance is needed so as to allow sufficient stretching of the fibre, as well as sufficient evaporation of the solvent.

#### **2.1.2.7. Ambient parameters**

In most reported studies, the ambient parameters, namely, temperature, humidity and air circulation, are not controlled. However, they can induce significant variations in fibre morphology and diameter and can sometimes interfere with the electro-spinning process. A higher temperature increases the rate of solvent evaporation as well as reducing the viscosity of the polymer solution. Thus, morphological imperfections such as the formation of beads or curly fibres are enhanced when the temperature is increased, through speeding up the

electro-spinning process [Demir et al., 2002]. Conversely, the lower viscosity induced by increasing temperature means that higher columbic forces further stretch the solution, yielding fibre of small diameter [Mit-uppatham et al., 2004].

The effect of humidity on the average fibre diameter is correlated to the variation in chemical and molecular interactions, as well as the rate of solvent evaporation. For water insoluble polymers such as cellulos acetate (CA), the average diameter increases with increased relative humidity (RH), while for water soluble polymers such as poly (vinylpyrrolidone) (PVP), an opposite trend is shown [De Vrieze et al., 2009]. Furthermore, when the humidity was increased by 50%, the formation of circular pores on the surface of the fibre was reported for electrospun polysulfone fibres [Casper et al., 2004].

The air circulation within the chamber can impair the electro-spinning process, in particular when the volatility of the solvent is high. The fast evaporation of the volatile solvent often leads to the clogging of the spinneret during electro-spinning. Saturation of the atmosphere around the spinneret with the solvent vapour helps to avoid this problem.

## **2.2 Wound dressing for burn injuries**

Wound dressing materials have been used for many hundreds of years and many varieties of wound dressing materials have appeared in human history. At first, the dressing materials were used simply to protect the wound surface and insulate this surface from the environment. With other developments of civilization in human history, new wound dressing materials have been produced, which are intended not only to protect the surface of the wound from being damaged once more and insulating it from its surroundings, but also, to exploit the anti-bacterial abilities of certain dressings, which have been very considerably increased. Indeed, some of the new dressing materials can reduce the time of cicatrization by using a growth factor.

Over the past thirty years, clinicians as caregivers have been exposed to a plethora of new and advanced wound dressings. The moist wound care revolution began in the 1970s with the introduction of film and hydrocolloid dressings and today these are the traditional types of dressings in the advanced categories.

Wound-healing science has progressed significantly over the same period, as a result of intense clinical and scientific research before such products are introduced. Today, the clinician must take into account moist wound healing, occlusion, cost effectiveness, wound bed preparation and MMP activity, to name but a few of the many concepts in wound care that have flourished as a result of technology and product advancement. However, in addition, such advancement is sometimes discussed in terms of its adoption in different parts of the world. The largest single markets of the world are generally the United States of America and Europe; this is because the development of both practice and technology generally begins there [Queen D. et al., 2004, Chang H. et al 1996, Horncastle J., 1995].

Compared with the traditional bandage types of dressing materials, the family of moist dressing materials may have marked advantages such as reducing the healing speed of the surface of a wound, etc. However, moist dressing materials not only help wound surfaces to recover, but also help the viruses to grow. In the present research, we produced Ag-nanoparticle EVOH nanofibres which can do no more than restrain the bacteria and viruses on the skin wounds surface. In addition, however, the Ag nanoparticle EVOH nanofibres are suitable for use on the battlefield [Chaby G. et al., 1995, Lo SF. et al., 2009].

### **2.3 Chapter summary**

This chapter mainly covers 4 parts, firstly, the background and main events recorded in the electro-spinning history since this phenomenon was firstly observed in 16 century. Secondly, the understandings of electro-spinning process, dropjet formation and theory of Taylor Cone formation have been discussed.

The parameters which affect the electro-spinning process have been discussed, such as solution parameters - viscosity and electrical resistivity etc., the processing parameters (voltage, distance and flow speed etc.) and ambient parameters, namely, temperature, humidity and air circulation.

Finally, a brief introduction about wound dressing materials and burn injuries was made. This part covers the disadvantages of the traditional wound dressing materials, from this point of view a new dressing material – EVOH nanofibre is necessary to be manufactured, this will lead us to the final purpose of this study.

### 3. Electro-spinning of EVOH nanofibres

#### 3.1 Polymer EVOH

The most suitable material and its solution are the first things to decide in order to obtain a given nanofibre. EVOH (poly (ethylene-co-vinyl alcohol)((CH<sub>2</sub>CH<sub>2</sub>)<sub>x</sub> [CH<sub>2</sub>CH (OH)]<sub>y</sub>) has been used in this study. The main reason for choosing it is that it is compatible with the biological activity that leads to its gradual absorption by the human body. Anhydrous polymer electrolyte membranes with a cross-linked structure have been prepared on the basis of a poly(vinyl alcohol-co-ethylene) (PVA-co-PE) copolymer. The PVA units of the copolymer served to induce thermal cross-linking with 4, 5-imidazole dicarboxylic acid (IDA) via esterification, while PE units controlled the membrane swelling and the mechanical properties of the films. Upon doping with phosphoric acid (PA, H<sub>3</sub>PO<sub>4</sub>) to form imidazole-PA complexes, the proton conductivity of the membranes continuously increased with the increasing PA content. As a result, proton conductivity reached 0.01 S/cm at 100 °C under anhydrous conditions. X-ray diffraction analysis revealed that both the *d*-spacing and the crystalline peak of the membranes were reduced upon the introduction of IDA/PA due to the cross-linking effect. The PVA-co-PE/IDA/PA membranes exhibited good mechanical properties, e.g., 150 MPa of Young's modulus, as determined by a universal testing machine. Thermal gravimetric analysis also revealed that the thermal stability of the membranes was increased up to 200 °C on the introduction of IDA/PA [El-Refaie Kenawya, 2003].

#### 3.2 EVOH solution

To make the EVOH polymer solution, we used water heated to 80°C with a reflux setup, as shown in Figure 3.1, below.

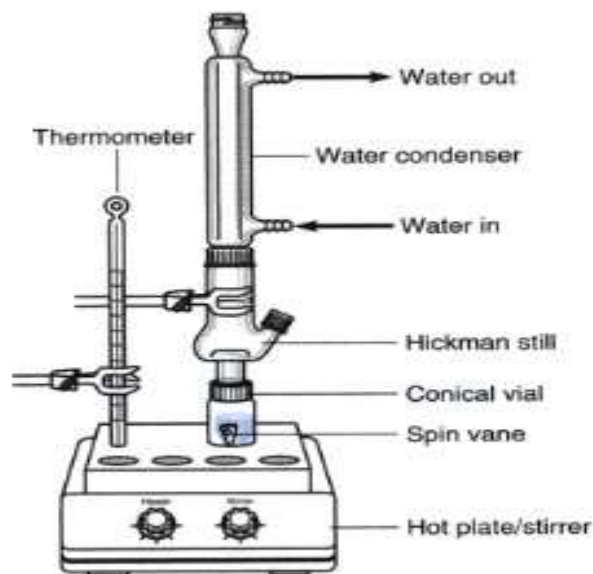


Figure 3.1 Reflux setup for making EVOH solution [Li D., Wang Y., Xia Y., 2003]

It normally takes around 2 or 3 hours, to form a polymer solution. The solvent used to dissolve EVOH is 80% propan-2 and 20% water. As the polymer solution must be conductive for its jet to form in the static electrical field, water is added partly to act as the conductive agent and partly to adjust the density of the solution.

### 3.3 Electro-spinning system

#### 3.3.1 Syringe section

The original syringe section went through many different designs. First the clasp was ruled out, as it was too delicate. There was a chance that it might break, an event which would have created many problems. Some solution might have leaked out and the apparatus could have damaged the casing, subjecting the person conducting the experiment to an electrical charge.

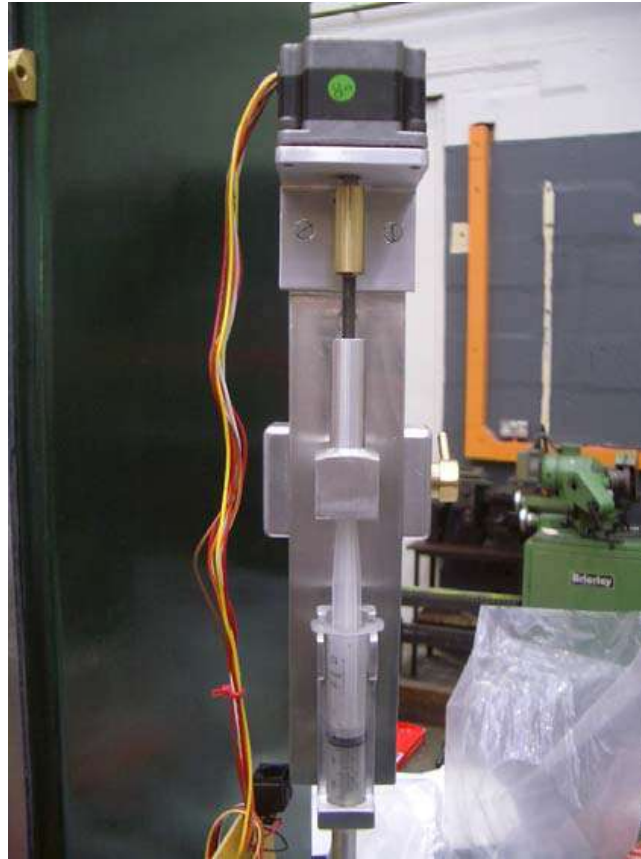


Figure 3.2 Original needle and high voltage point

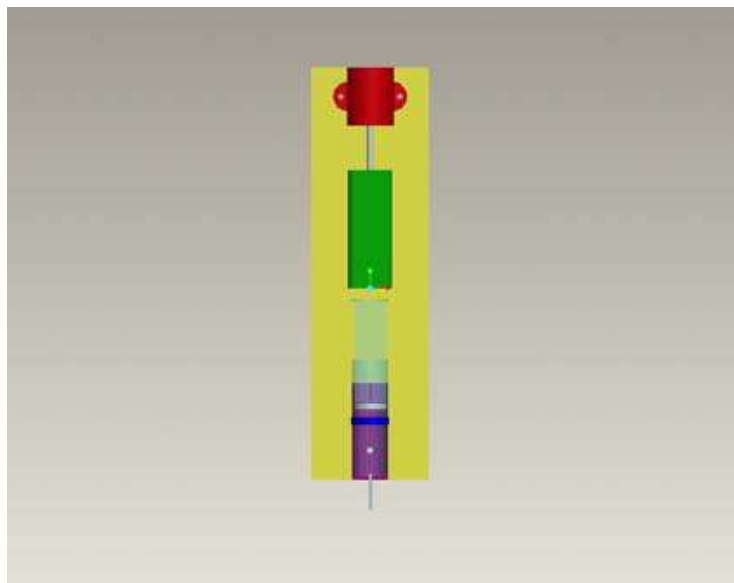


Figure 3.3 Model of the first design

After the first design change, a second problem arose due to the high voltage. A 25kV load can pass through 1 inch of air. The needle was too close to the back plate to be safe. Since it was thought that the 30kV might be transmitted to the stand. Not only would this have stopped the experiment from working but it could

have been very dangerous as a spark of electricity would have been produced which might have charged other parts of the set-up. However, all parts of the set-up were grounded for the sake of safety, had any charge been there. To avoid this problem, a third design was produced, which is shown in Figure 3.3.



Figure 3.4 Needle with power supply and solution supply

When the third design was made (see Figure 3.4) of the syringe section, it was found to avoid the first and second problems and it was also very helpful in controlling the structure of the nanofibres. The solution was planned to go to the needle through the grey tube (shown in Figure 3.4 on the right). The pressure which pushes the solution to the needle was supplied by a pump (Figure 3.5). It transferred the EVOH polymer solution to the high voltage point through a tube of silicon. Moreover, this arrangement allowed the speed to be controlled.



Figure 3.5 Pump (Masterflex, 77120-52) with polymer solution

### 3.3.2 High Voltage Power Supply

A safety precaution was built in when the high-power supply was purchased (Figure 3.6). This was to choose a supply with a built in current controller was purchased. The main danger with electricity is the current. A high current is capable of causing the most damage. As we were using a high voltage supply, we would in any case have set it at a low current, but with a built in controller we could set it as low as possible to avoid any severe danger. It was still a great risk, however, that someone would be given an electric shock from the supply. To prevent the transmission of any shocks the supply was also fitted with a discharger. This rids the unit of any charge and makes it safe for human contact. This facility however still has the slight disadvantage that the unit takes 15 seconds to discharge. It is important that operators are made aware of this delay before they operate the equipment.



Figure 3.6 A Spellman CZE1000R, 0-30 kV high power supply

### 3.3.3 Housing Unit and safety measures for high voltage

The housing unit containing the electro-spinning setup had to incorporate certain safety features due to the risk entailed by the high voltage used in the fabrication process. When the machine is fully charged, there should be no open access to it during its operation. A locking mechanism is installed on the door of the housing with two micro switches which will only be connected when the door is closed. Once the door is opened, the first switch will cut the power and second one will discharge any voltage within the set-up. The discharge switch is not actually necessary, in that the charger has automatic discharge functions once the power is turned off. However, it is regarded as a good way of increasing the safety factor in a laboratory environment.

After adding two mini switches and fixing the discharge capacity, holes were drilled on the side plates of the housing unit (Figure 3.7), to allow the fibre collectors to be placed at different distances from the tip of the needle. The distance is a controlling parameter of fabrication which affects the formation and

quality of the fibres, in particularly their final diameter. A changeable distance control is a necessity.



Figure 3.7 House Unit

### **3.4 Electro-spinning processes**

When a polymer jet is injected from the Taylor cone, it starts to circulate at the force of the electric field. These stretch the jet to a decreasing diameter. The dynamic motion in the space also accelerates the evaporation of dissolving agent propanol-2 and water. The fibre is tried out when it reaches the collector and accumulates into layers of randomly oriented fibres. After introducing the separated parts of our electro-spinning system, the system was assembled as shown in Figure 3.8. This would create normal nanofibres by the typical method, a method which was achieved in the present study.

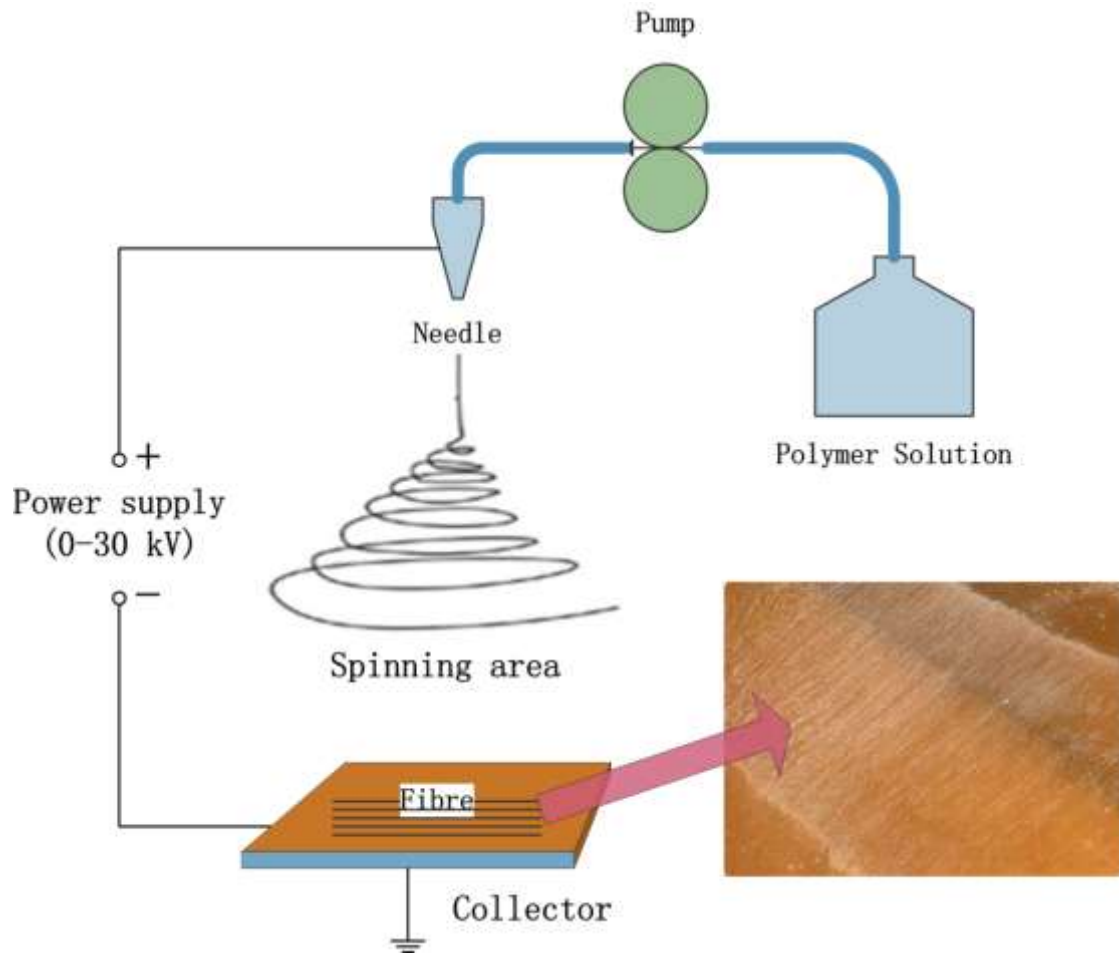


Figure 3.8 Basic design for Electro-spinning

From a piece of equipment of the design shown in Figure 3.8, nanofibres of many different diameters were made in our lab, the thinnest being around 60 nanometers (Figure 3.9). To make the thinnest EVOH fibres, a 4.5 wt% polymer solution was chosen with 25kV and the distance was set at 28 cm from the high voltage point down to the collector.

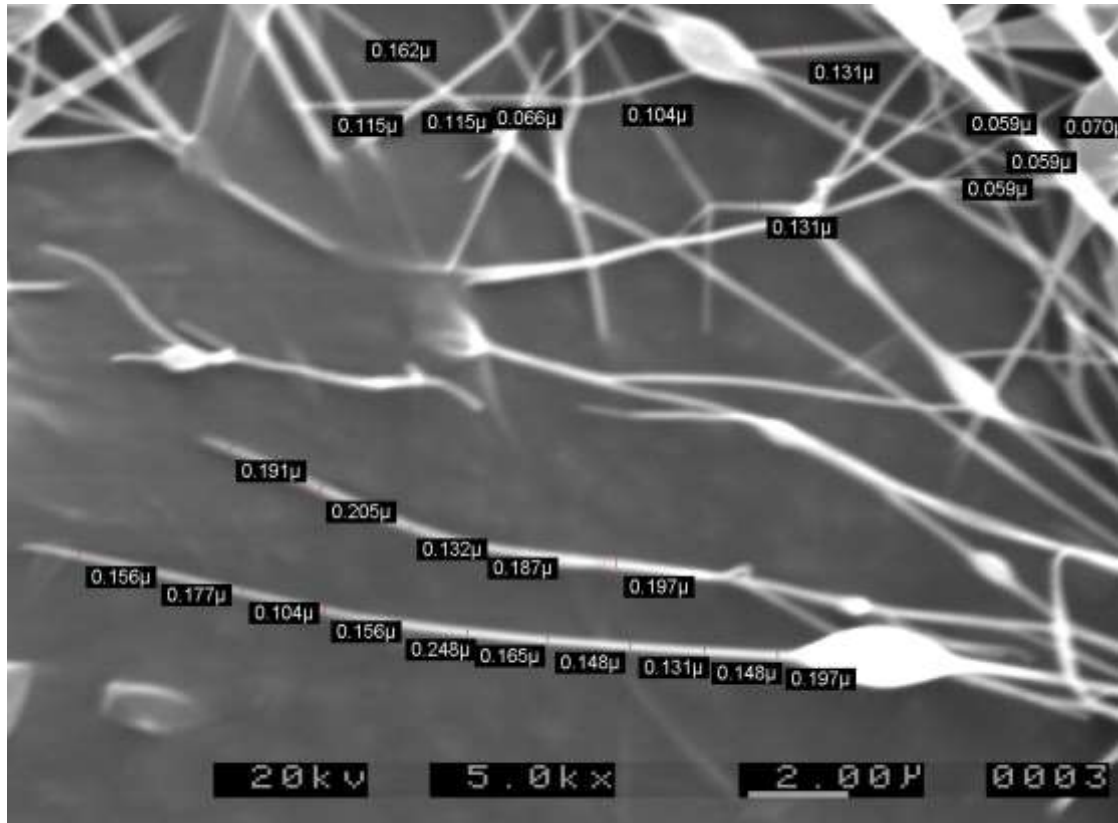


Figure 3.9 The thinnest fibre that was made in our lab – 59nano-meters

### 3.4.1 Method of making parallel and web nanofibres

The main purpose in making parallel and web nanofibres was to produce biological scaffolding. The first stage of making this scaffolding was to produce parallel fibres. This was successfully carried out in the lab. The key point in producing parallel fibres is the collector. In other words, in order to control the direction of the fibre, different collectors needed to be used. Figure 3.10 shows an example of a box collector. In our lab it is mainly used for making parallel fibres; the volume of the box collector is 25 cm x 25 cm x 25 cm. We put the needle on the top of the box in order to produce fibres which could be collected in the corner, as shown in Figure 3.10. The materials on the walls of the box collector can be changed to other metals for controlling the direction of the fibre.

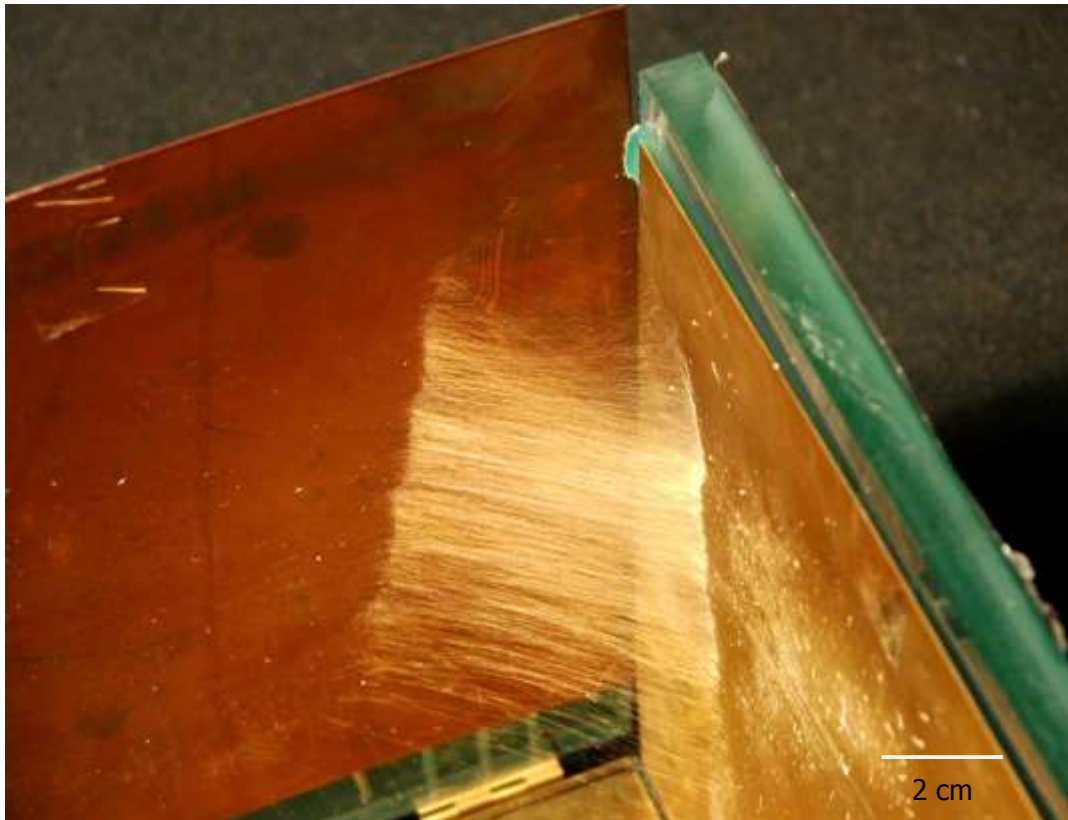


Figure 3.10 Parallel fibres with a box collector

The theory of making web fibres is quite similar to that of producing parallel fibres: the main idea is to change the structure of the collector (Figure 3.10). First, before charging, to make a four strip collector (Figure 3.11), we chose two of the four strips from which we could obtain parallel fibres which were opposite the direction to be grounded. Then we changed to two other strips and broke the first previous two collectors with grounded. After this action stage we could get twice the number of parallel fibres all crossing one another. This is basically how we made the web fibres in our lab.

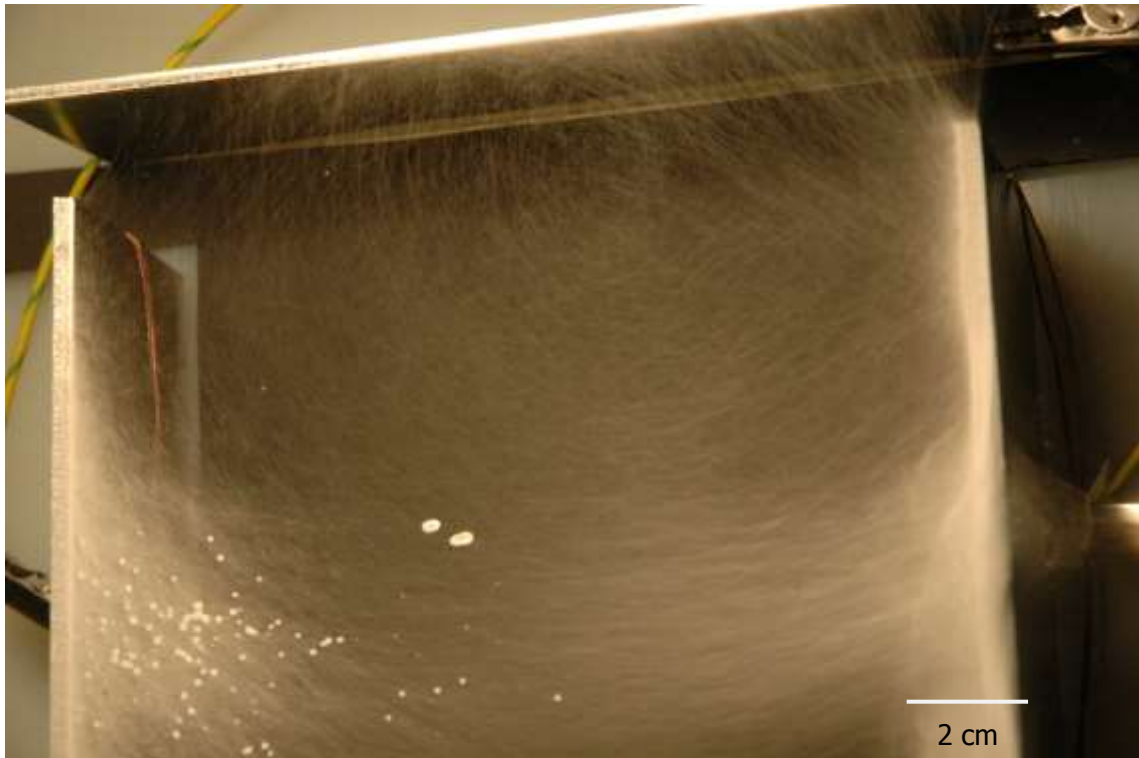


Figure 3.11 Web fibres with 4 strips Aluminium

### 3.4.2 The method of producing tube fibres

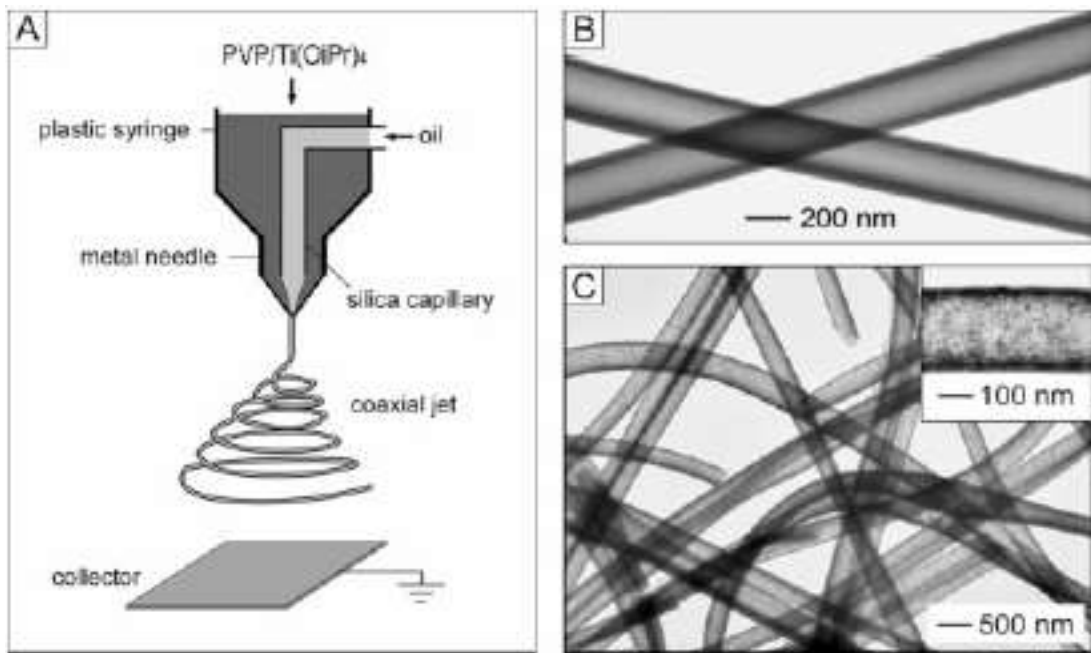


Figure 3.12 A basic setup to produce tube fibre, B and C are images of the tube fibres taken by TEM

In some research organizations which have made tube fibres, the researchers chose mainly PVP and PAN as their raw materials. However, the purpose of our research made it impossible to use materials which were not approved as biocompatible with our wound dressing applications. EVOH, an approved biocompatible polymer was chosen for our study. The most difficult feature of EVOH tube fibre is that when the temperature goes down the EVOH in the solution starts to separate out. The idea of producing tube fibre is to change the needle part to a plastic syringe and silica capillary part, as shown in Figure 3.12A. If some thin oil is put into the metal needle then after the normal spinning process, tube fibre can finally be obtained, as shown in Figure 3.12 B and C.

### **3.5 Results for the inter-relations between fibre diameter and kV, distance, and density**

Here, we first discovered the inter-relationship between the diameter and the liquid density, the distance (between needle and collector) and the changing voltages during the process of making random EVOH nanofibres. Figures 3.9, 3.10 and 3.11 show the relationship between  $D$  (the diameter of the nanofibres) and  $\rho$  (the consistency of the EVOH polymer solution),  $h$  (the distance between the needle and the collector),  $V$  (the voltages using to produce nanofibres), in line with the results of our experiments.

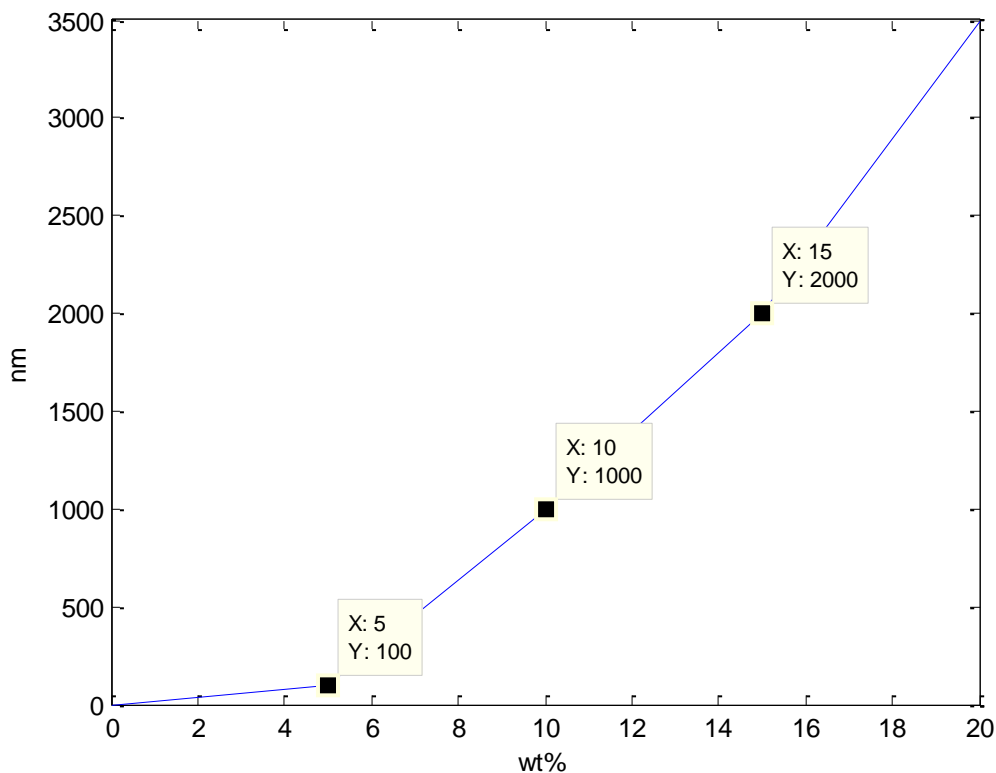


Figure 3.13 The relationship between the weight percentage and the diameter of the fibre when the variables of 20 kV and 25 cm from the needle to the collector are applied

When 20 kV is applied to the system and the distance from the outlet of the needle to the collector is set at 25 cm, the fibre diameter is shown to vary with the consistency of the solution (Figure 3.13). The diameter of the fibre is most affected by the consistency of the polymer solution (see Figure 3.13); once the weight percent in the solution is increased, the diameters will tend to increase rapidly. As mentioned above, the lowest consistency which has been successfully used in our lab in the course of this study is 4.5%. Consistencies of 0 to 4.5% have been tried more than once in our machine, but they did not work very well; The reason for this may have been that the polymer solutions were too thin. Some new materials and solvents are due to be tested and it is very much hoped that better results in this rangemay be obtained in the coming year.

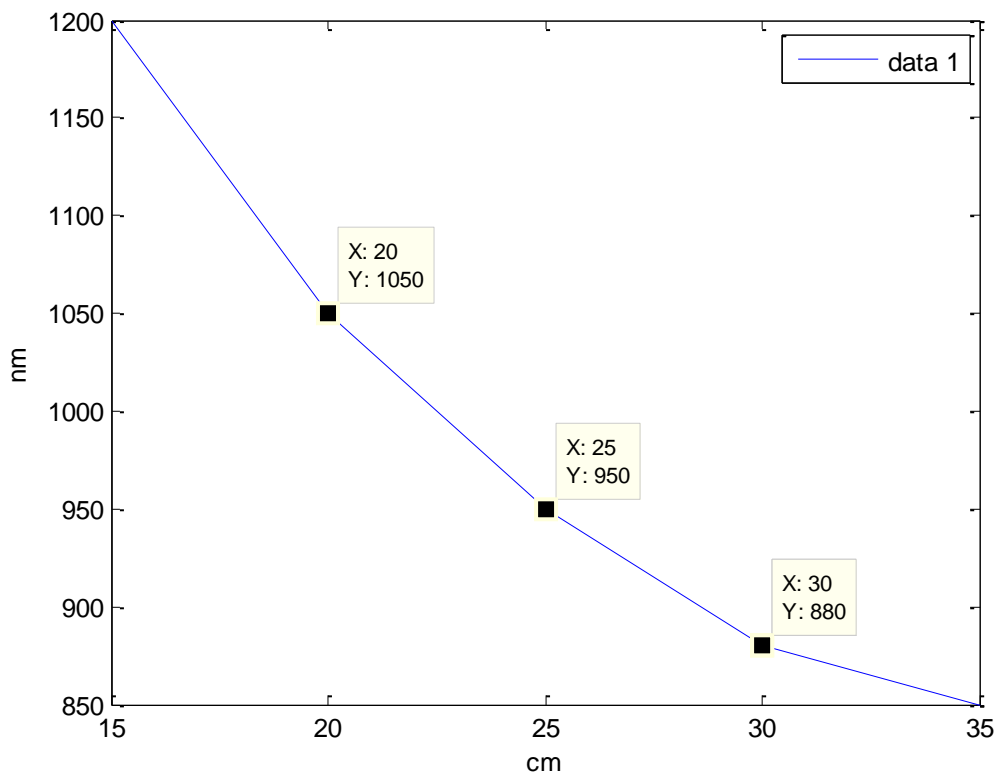


Figure 3.14 The relationship between the distance from the needle to the collector and the fibre diameter when 20 kV and 10 wt% are applied

Figure 3.14 shows how the diameters of nanofibres are influenced by H (the distance from the needle tip to the collector) when 10% weight percentage and 20 kV are used. When H is increased, the diameter of the fibre will go down. This is because the spinning material stays in the electric field for a longer time, and therefore the force exerted by the electric charge on the spinning material is greater, thus increasing the extent to which the material becomes deformed. The overall stretch of the fibre material is greater when the circulation is prolonged, leading finally to a smaller diameter for the fibre

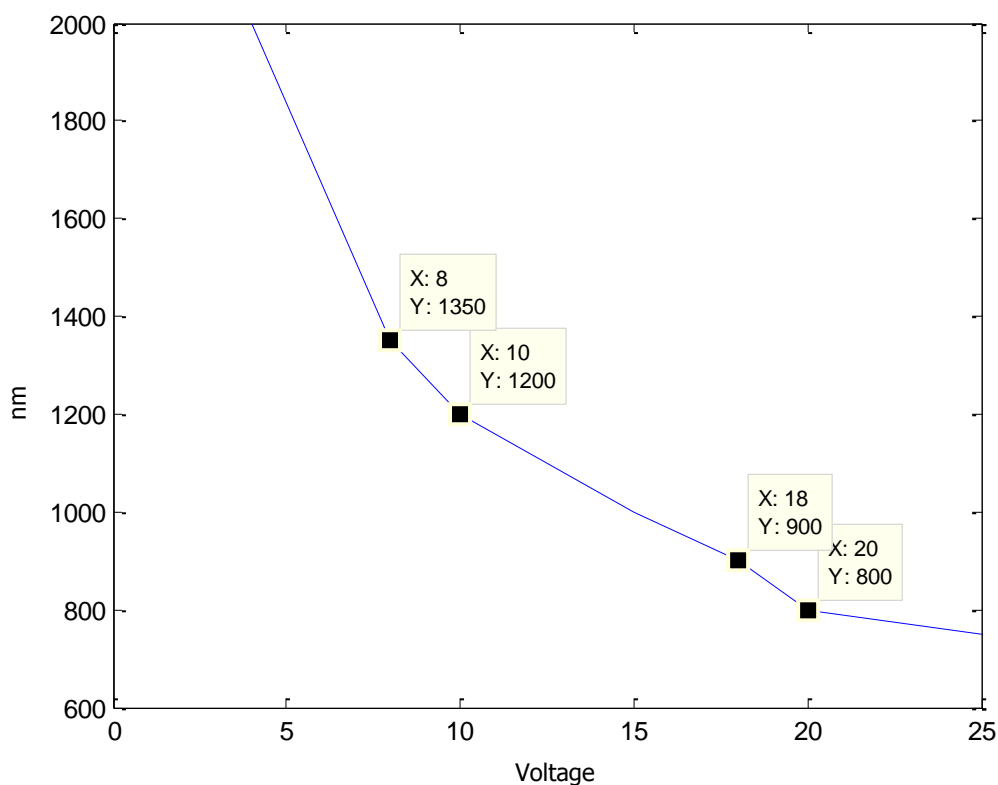


Figure 3.15 The relationship between voltage and fibre diameter when 25 cm from the needle to the collector and 10 wt% are applied

Figure 3.15 shows that different voltages influence the diameter of fibres. Voltages in the range of 5 kV to 30 kV were used in our lab. Usually, the range from 0 to 10 kV is not chosen because with this range there is not enough electrical power to make the EVOH polymer solution jet spin in the static field. Equally, anything over 30 kV is not chosen, because it will supply too much power in the field. The high power static field will break the fibres into fragments, thus in the end preventing continuous fibres from accumulating obtained on the collector.

EVOH is thermally sensitive and this may affect the electro-spinning process. To check the effect of temperature, we used the SEM to assess the morphology of the nanofibres fabricated with and without temperature control during their fabrication. The temperature of the solution was controlled either at a constant 80 °C or allowed to cool down naturally from 80 °C to room temperature during the spinning process. Comparison of Figure 3.16 shows that the quality of the fibres

deteriorates when the temperature of the solution is allowed to fall (Figure 3.17), *i.e.*, the fibres become sticky and viscous and form clusters with larger and more uneven diameters. Figure 3.16 also shows the greater inter-fibre space which is beneficial for regulating the degree of moisture.

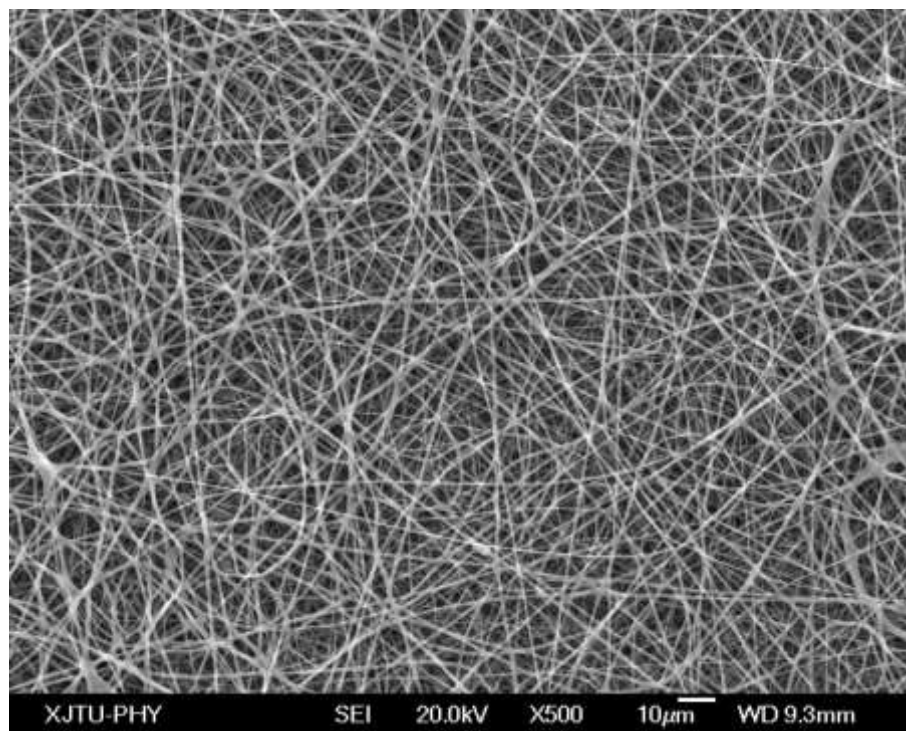


Figure 3.16 An SEM image of EVOH nanofibres with temperature control.

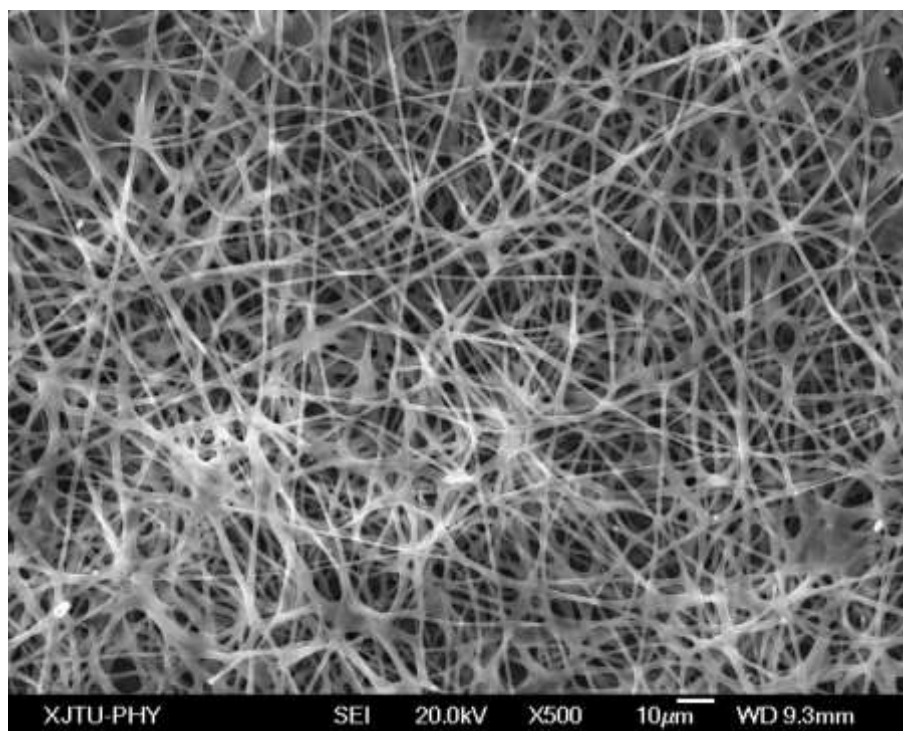


Figure 3.17 An SEM image of EVOH nanofibres without temperature control.

For a pure liquid system, the surface tension of the liquid is prone to decrease as the temperature increases. When the temperature is raised, the equilibrium between the surface tension and the vapour pressure decreases. At a critical point, the interface between the liquid and the gas disappears [Clark (1938)]. From the molecular point of view, at a higher temperature, the liquid molecules gain more energy and start to move more rapidly around the space. As a result, the fast moving molecules do not bound together as strongly as do the molecules in a cooler liquid. With the reduction of the bonding between the molecules, the surface tension drops. The effect of temperature on the surface tension for pure liquids may be different from the effect for mixtures. For a mix of methane and nonane, the surface tension actually increases as the temperature rises except at the lowest pressure. At a lower temperature, methane is more soluble than nonane and the effect of the liquid mixture composition is more pronounced than temperature is in determining the surface tension [Deam and Maddox (1997)].

After previous measurements of the diameter of the fibre, the inter-relations of fibre diameter with voltage, solution density and distance needed to be measured again, because the temperature control was not applied on the previous occasion of the electro-spinning process. This may have caused the amount of

error to increase. Moreover, the collector was changed to a 2 strip copper collector, with a view to letting the EVOH nanofibres hang in the air, since they were not fully dry immediately after the electro-spinning process. When EVOH nanofibres touch a flat collector it can cause their shape to be modified. In other words, when the diameters of the EVOH nanofibre are being measured using the SEM, only 2D images can be provided, and this of course increases the amount of error.

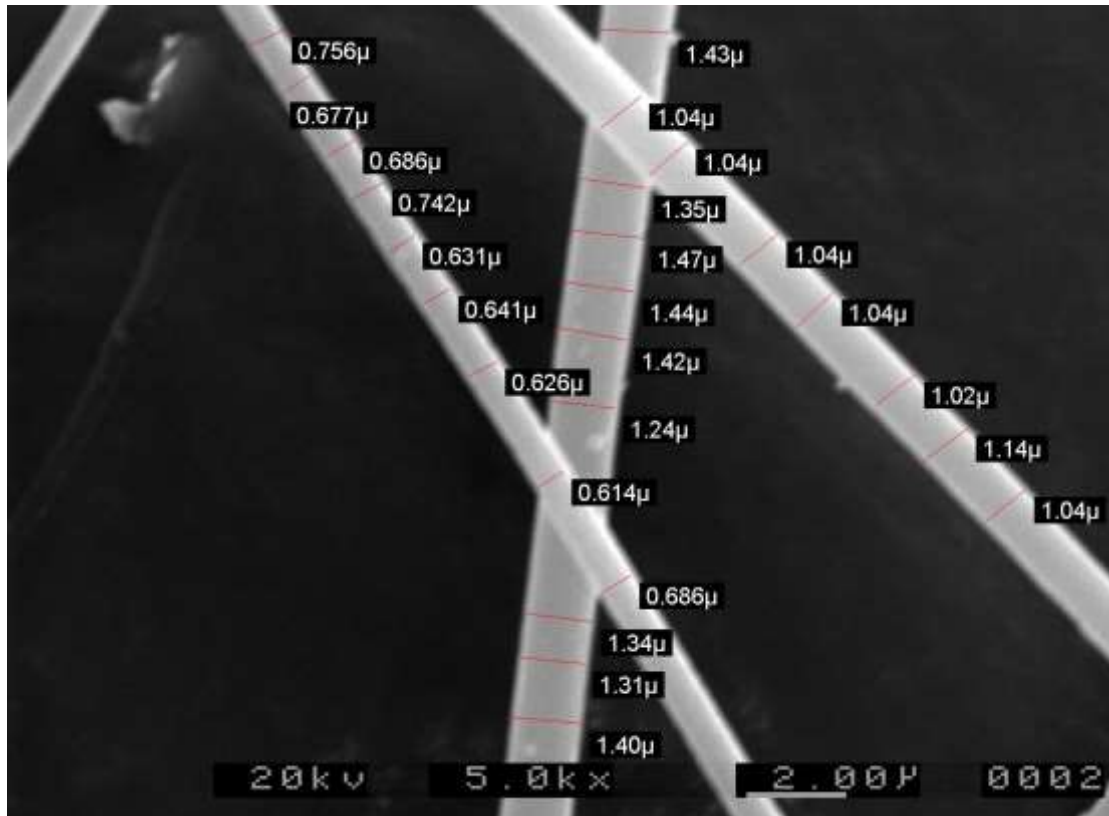


Figure 3.18 The method of measuring the diameters of EVOH nanofibres by means of an SEM

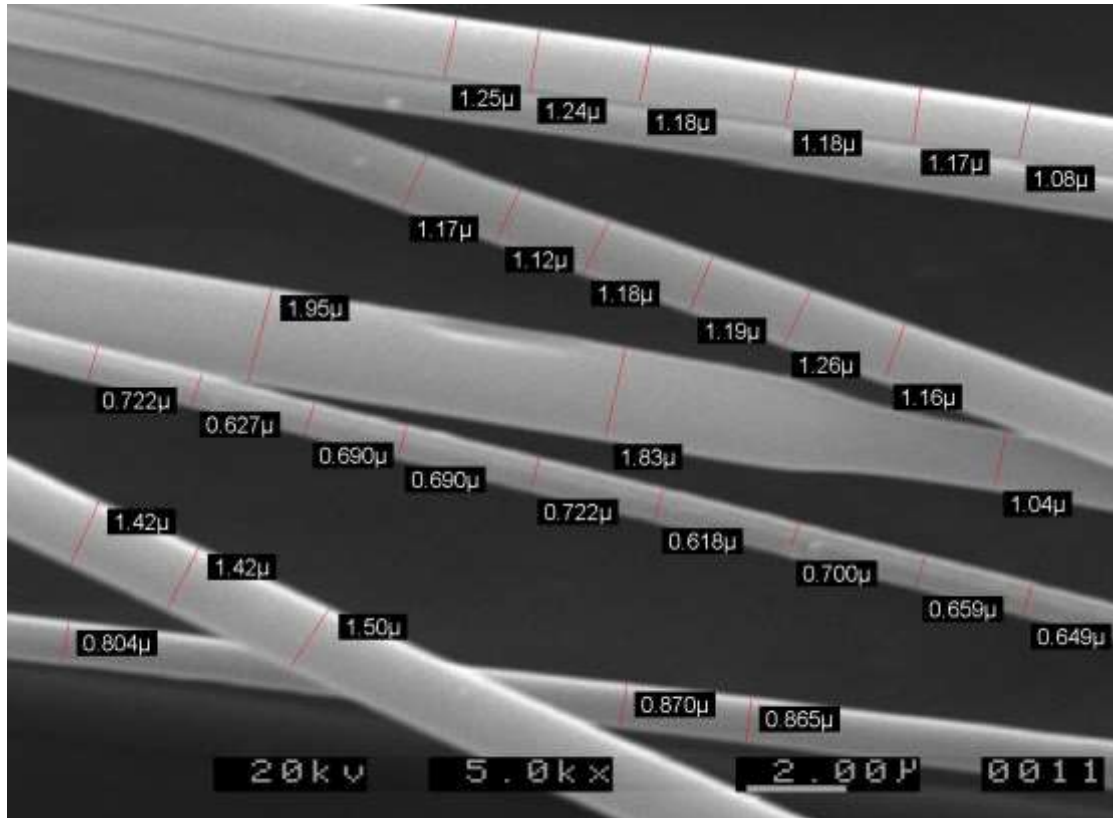


Figure 3.19 The method of measuring the diameters of EVOH nanofibre by means of an SEM (continued)

All the fibre samples were mounted on a copper stub and sputter-coated with gold for energy spectrum analysis in the SEM. Each sample was divided into 12 parts in order to measure its diameter. We used 12 uniform size conductive tapes (3x3 mm<sup>2</sup>) to make 12 fibre samples directly from each experiment in different areas. All the diameters of the 12 samples were measured under the SEM (Figure. 3.18 and 3.19) along each fibre. Due to the variation of fibre diameters, around 1000 measurements in total were carried out for statistical evaluation.

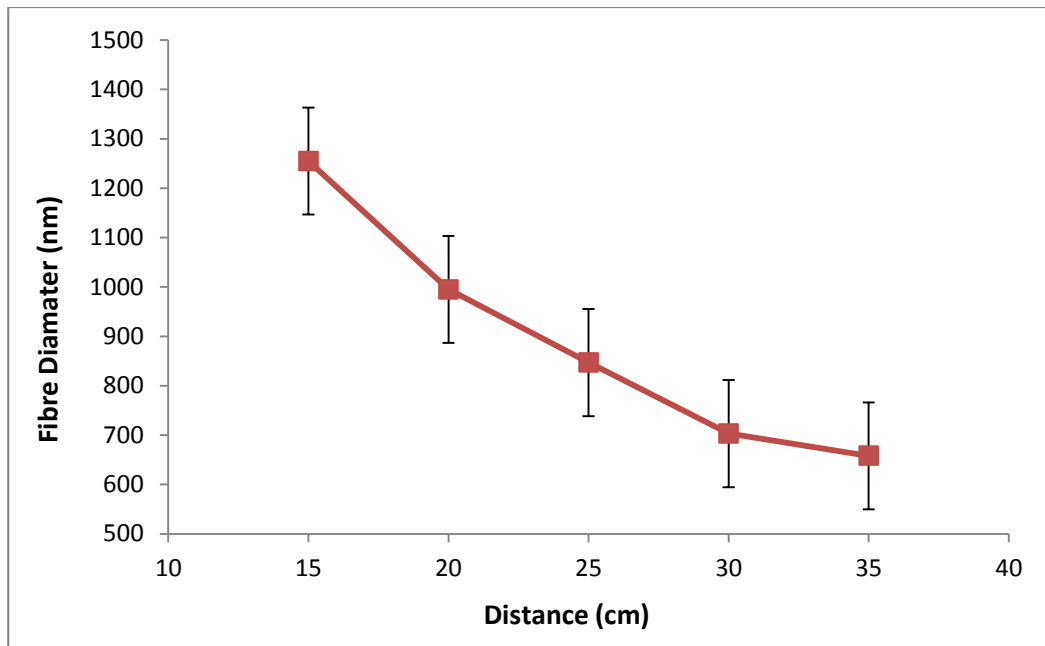


Figure 3.20 Effect of the distance on fibre diameters when the solution density is 7.5% (wt) and the voltage is 20 kV

Figure 3.20 shows the results of 5 tip-to-collector distances of 15, 20, 25, 30 and 35cm, respectively. 20kV field voltage and 7.5wt% solution density were used. We observed no significant effect of the distance on the fibre diameter. Nevertheless, the distance provided the necessary space for fibres to stretch and dry out before reaching the collector. Without this, the fibres would stick together to form clusters. In our tests, this occurred when the distance was reduced to 10 cm. At the opposite extreme, when the distance was increased to 40cm, the fibres could not be collected at all, due to being spun too violently.

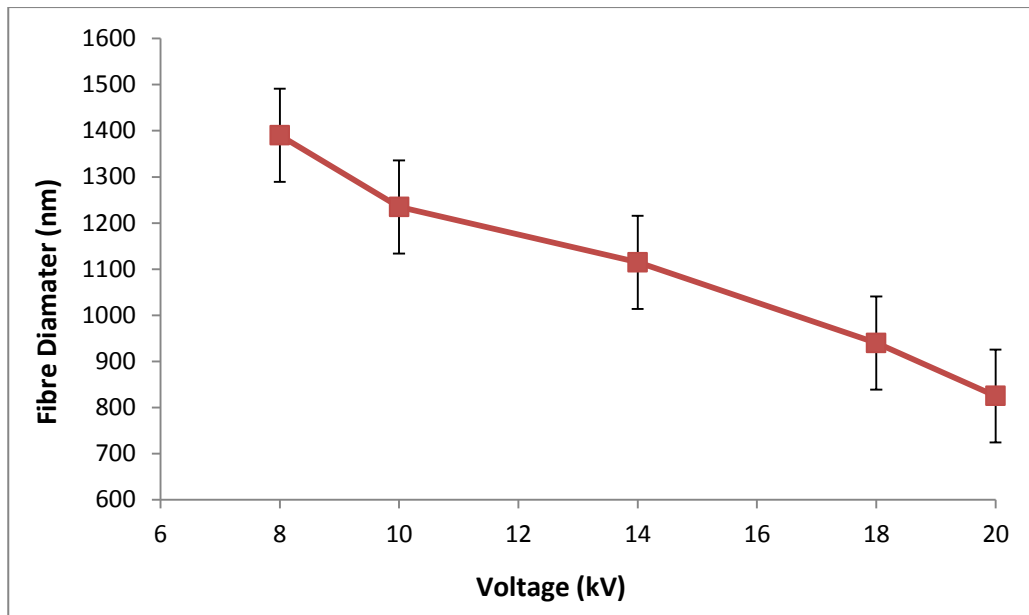


Figure 3.21 Effect of the voltage on the diameters of the fibre when the solution density is 7.5% (wt) and the needle-tip-to-collector distance is 30 cm

Figure 3.21 shows the effect of voltage for the cases with a constant solution density at 7.5% and a tip-to-collector distance of 30 cm. We observed that the most suitable voltage range was from 10 to 20 kV. At a lower voltage (<10kV) there is not enough power to drive the EVOH jet through the electric field to form nanofibres, while at a higher value (>20kV), the solution jet is broken by too strong a stretching force from by the electrical field such that no continuing fibres can be formed.

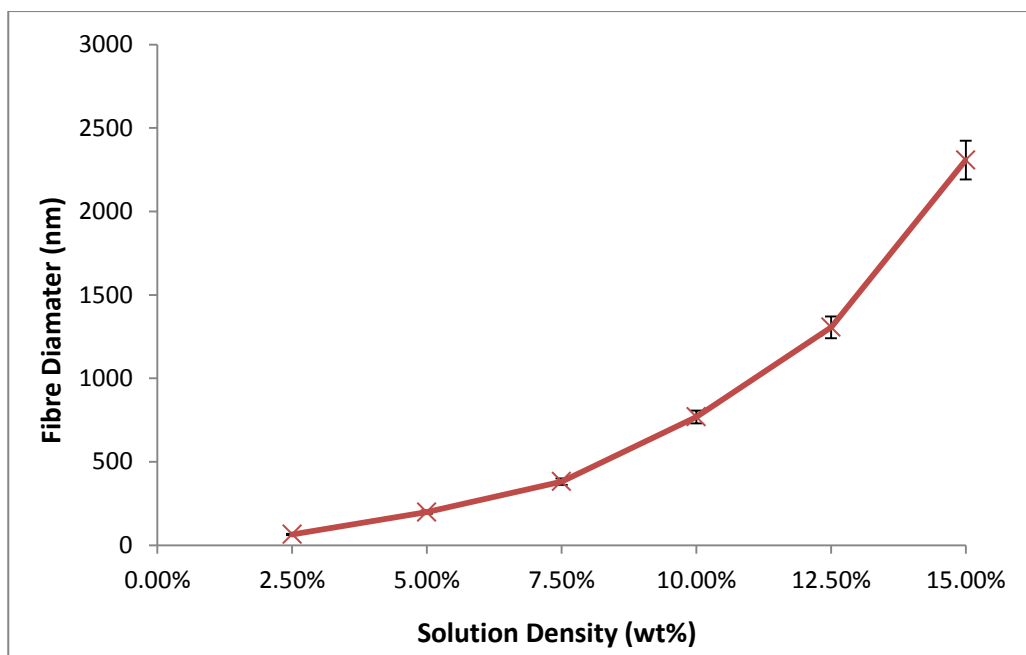


Figure 3.22 Effect of the solution density on diameters of the fibre when the voltage is 20kV and the tip-to-collector distance is 30 cm

Figure 3.22 shows the results of 6 different values of solution density at 2.5, 5.0, 7.5, 10, 12.5 and 15.0 wt%, respectively. The voltage was kept at 20kV and the tip-to-collector distance was 30cm. It is clearly shown that the diameter of the fibre increases rapidly as the density of the solution increased. The increased density leads to a higher viscosity which makes it more difficult to stretch the jet into finer fibres and also makes the solution more prone to form a “blockage” at the needle tip. We also noted that the diameter of the fibre can be influenced by the environmental temperature and level of humidity. Higher temperatures and low humidity are found to lead to the formation of finer fibres, though we were not able to quantify this. An effort to raise the temperature in the spinning space led to the circulation of air and resulted in severe disturbance to collection of fibre. Thus, all our results were obtained in ambient environmental conditions.

Electro-spinning is a straightforward approach to fabricating highly fibrous and porous EVOH materials for medical applications. In this part, we have described how we fabricated EVOH nanofibre. The results of the fibre characterization show that the nanofibre size can be controlled by regulating the EVOH solution concentration, the voltage and the distance of the electric field.

### **3.6 Chapter summary**

In this part, electrospun EVOH nanofibres having micro- and nano- scaled diameters were successfully prepared by using the electrospinning technology. Fibre diameters in the electrospun membranes are significantly influenced by the electrospinning conditions, namely, solution (solvents and solution concentration), processing (applied voltage, spinneret tip to collector distance etc.) and ambient parameters. The typical influence of the different solution and processing parameters on fibre structure and porosity was further reiterated by our study results with a commercial EVOH. More importantly, the solvent compositions, solution concentrations, flow rates, applied voltages, and distances to collector were identified for preparing electrospinning of EVOH nanofibre sheet having desired fibre diameter. Moreover, the system and equipments for electro-spinning EVOH nanofibre membranes were described in this chapter. The method of measuring the diameters of EVOH nanofibres by means of an SEM was presented.

## **4. Mechanical properties of nanofibre mats**

### **4.1 Introduction**

Electro-spinning is a well-known, but not necessarily well established method to fabricate fibres at the submicron level. The qualities of fibres, in terms of their size (diameter), quality and orientation, very much depend on the material used as well as the set-up of the fabrication apparatus. Often, a trial and error effort is required to achieve a continuous production of fibres of the desired dimensions. In the part of the research surveyed in this chapter, the EVOH nanofibre sheets of a controlled size were fabricated (having diameters in the range of 60 nm – 3  $\mu$ m) by regulating three main electro-spinning parameters, namely, the concentration of the EVOH solution, the distance and voltage of the static electrical field needed for the fibre to be produced. For the potential use for dressing applications, the material was to be subjected to stretching, tearing, cutting and other types of mechanical loading. Only the findings of the tensile extension tests are discussed here. The tests were made on thin sheets made of nanofibres arranged in random directions.

Dressings are normally applied in sheet formats of various thicknesses. The collectors therefore were designed to produce nanofibre sheets. The thickness of the sheets thus obtained was controlled by the length of time spent on their fabrication and also by the fibre diameters and injection speed of the solution. Once the sheet was completely dried, coupon samples were cut into rectangles whose long sides were 25mm to 40mm in length. Tests were conducted on a screw-driven universal test machine (Instron 8500) using a load cell of 1N nominal accuracy. The crosshead extension was used to calculate the engineering stress-strain curve.

### **4.2 Samples of EVOH nanofibre sheets**

#### **4.2.1 Introduction of 7.5%, 10% and 12.5% EVOH nanofibre sheets**

Samples were fabricated using solutions with densities of 7.5%, 10% and 12.5%. The specifications for EVOH fabrication parameters are: tip to collector

distance 20cm, voltage at 15kV and flow speed 2.0 ml/hr. As mentioned in the previous chapter, distance and voltage during the electro-spinning process can both influence the diameter of EVOH nanofibres, but the density of the solution is the most decisive of them all in making EVOH nanofibre sheets.

#### 4.2.2 The inter-relations between the diameters of 7.5%, 10% and 12.5% in EVOH nanofibres

The inter-relations between the diameter of an EVOH nanofibre and the distance, the voltage and the solution density were discussed in Chapter 3. In this chapter, the measured diameters of the samples obtained are given in Table 5. The dry densities of the fibre sheets are yet to be quantified. Figures 4.4a and 4.4b give the images of 7.5% EVOH nanofibre samples before and after the extension test. Figure 4.4c is the strain-stress curve from a tensile unloading test which uses 7.5% EVOH nanofibre; this can give us the Young's modulus and yield stress, etc.

Table 5. Description of sample A(7.5% EVOH nanofibre sheet) B (10% EVOH nanofibre sheet) and C (12.5% EVOH nanofibre sheet).

Sample	Fabrication parameters	Fibre diameter range
A	7.5% EVOH solution, voltage 15kV, tip to collector distance 20cm	400 - 900nm
B	10% EVOH solution, voltage 15kV, tip to collector distance 20cm	800 – 1500nm
C	12.5% EVOH solution, voltage 15kV, tip to collector distance 20cm	1300 – 2000nm

### 4.2.3 Methods of making nanofibre sheet samples for mechanical property tests

After qualifying the diameters of the nanofibre sheets for mechanical property tests, the thicknesses of the samples were also measured. The method of measuring the thickness can be divided into 3 steps. First, aluminum foil was used to cover the whole EVOH sample on both sides. Second, an electronic micrometer was used to clamp and measure the sample 20 times in different parts. The third step was to deduct the thickness of the aluminum foil and obtain the average value from the 20 measurements recorded.

Table 6. The thicknesses of 7.5%, 10% and 12.5% EVOH nanofibre sheet samples

Samples	Average value EVOH nanofibre sheets thickness
7.5% EVOH nanofibres (Sample A)	0.009mm
10% EVOH nanofibres (Sample B)	0.011mm
12.5% EVOH nanofibres (Sample C)	0.013mm



Figure 4.1 The fibre sheets were collected on two aluminum foil strips with some biased orientation across the gaps



Figure 4.2 A coupon sample after being cut

The sheet was completely dried as shown in Figure 4.1 and coupon samples were cut into rectangles whose long sides measured 25mm to 30mm(Figure 4.2). The sample shown in Figure 4.2, which is a 7.5% EVOH nanofibre sample, was made by a 2 strip copper collector (Figure 2.2). We set up the gap distance as 25mm due to the fact that the screw-driven universal test machine which was being used requires all the samples to be 25mm in length with 1kN load cell.

Figure 4.2 shows a coupon sample when it had been cut ready for the tests on its mechanical properties. We used aluminum foil to wrap around the top and bottom ends of the EVOH samples; this was done to make sure that the load cell on the Instron 8500 could not come into direct contact with the EVOH sample. If

they were to touch the sample would not break in the middle, which might cause more errors.

### **4.3 Uniaxial tensile tests**

#### **4.3.1 Process of uniaxial tensile tests**

Samples were tested at four different loading speeds, namely, 2mm per minute, 5 mm per minute, 10 mm per minute and 20 mm per minute. The tested samples were 7.5%, 10% and 12.5% EVOH nanofibre sheet samples.

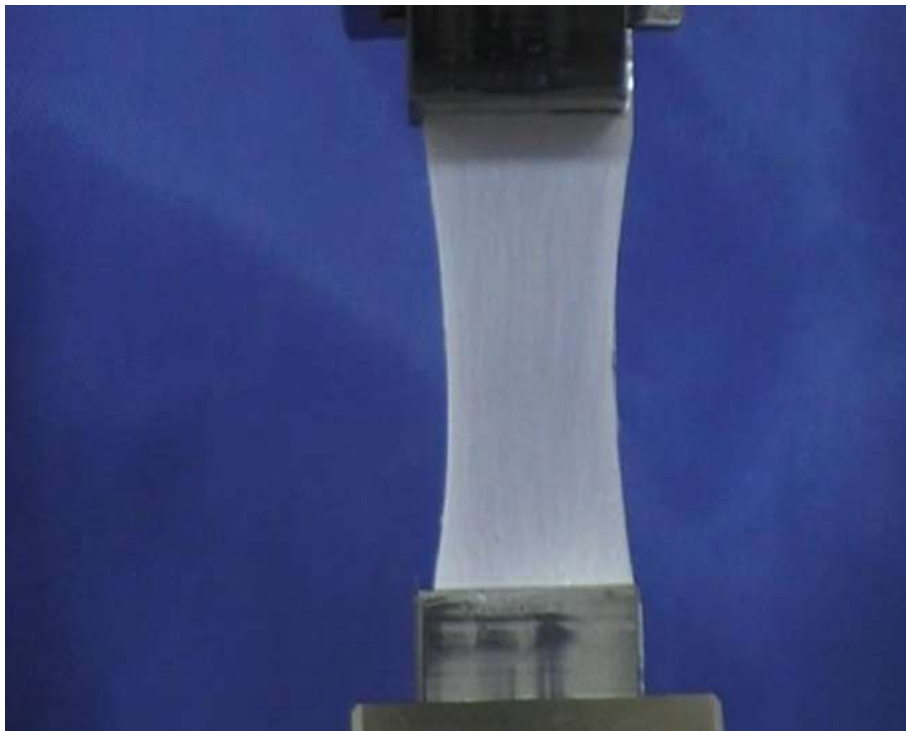


Figure 4.3a Image of a nanofibre sample of 10% EVOH fibre sheets on the Instron machine



Figure 4.3b Image of a torn nanofibre sample of 10% EVOH) fibre sheets on the Instron machine

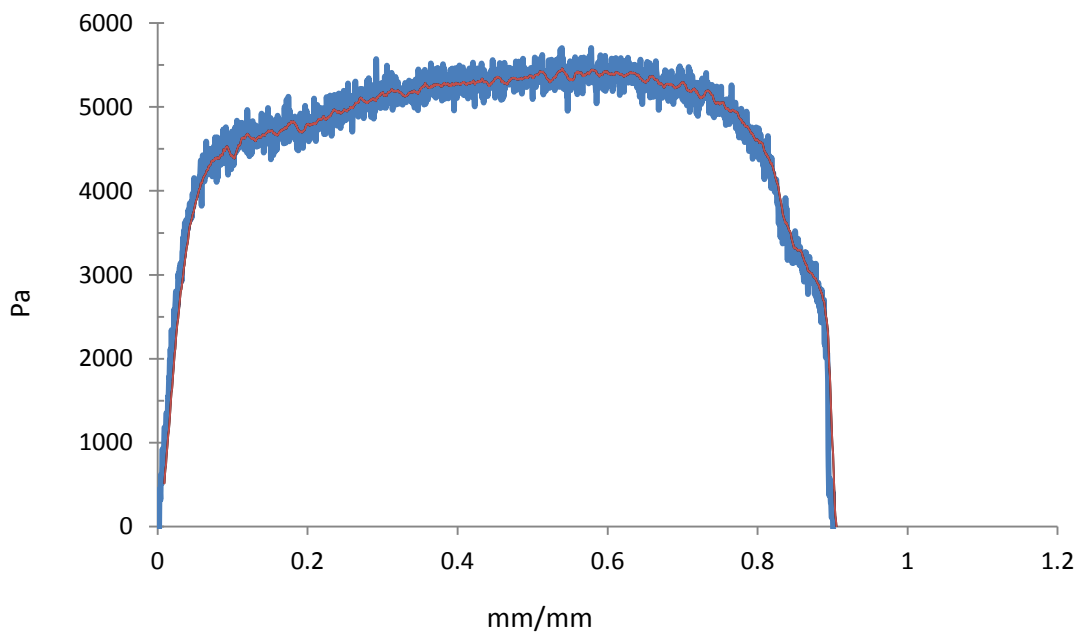


Figure 4.3c The strain-stress curve in the tensile extension test of a 10% EVOH nanofibre sample

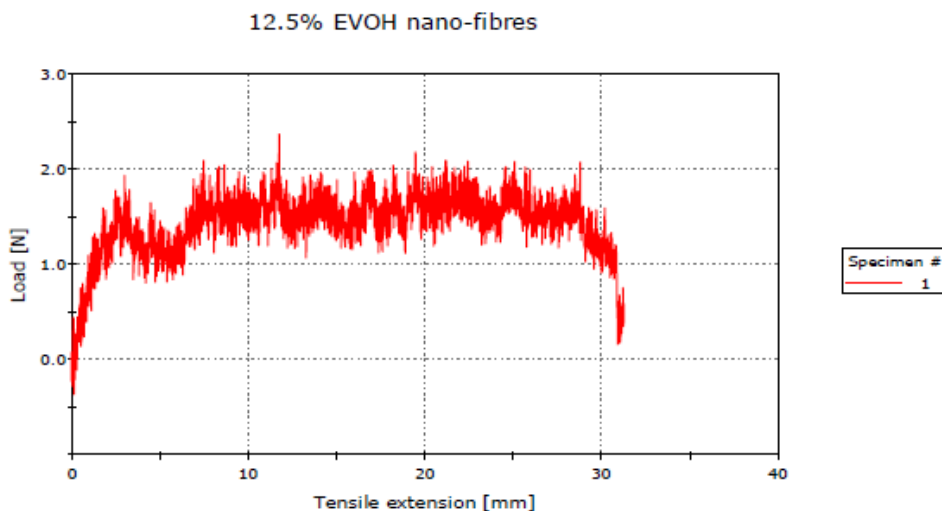
The 1kN load cell with an accuracy of 0.1N was used to carry out the tests. Figure 4.3a shows an EVOH nanofibre sheet sample on the Instron 8500, of which the necking has just appeared. Figure 4.3b gives an image of a torn EVOH nanofibre sheet sample, showing the failure mode in tearing (the stretching, sliding and breaking of the fibre). Figure 4.3c shows a typical engineering stress strain curve of a 10% EVOH nanofibre sheet sample, which is characterized by a linear elastic response, followed by a moderate hardening in an extended plateau stage before fracture and failure. It shows a typical pattern of a torn textile with uneven broken and unbroken fibres. Note that the texture of the sheet is of random unwoven fibres over a range of different diameters.

**Brunel University**  
**School of Engineering and Design**  
Structures and Materials Laboratory

**Nanofibre sheets**

**Test Parameters**

General: Last test date	01 February 2012
General: Last test time	15:19:38
General: System of units	SI
Test: Rate 1	5.00000 mm/min
Sample notes: Sample description	Nanofibre sheets
Sample notes: Sample note 1	Folded once
Specimen properties: Length	30.00000 mm
Specimen properties: Width	23.00000 mm
Specimen properties: Thickness	0.00800 mm



	Maximum Load [N]	Tensile extension at Maximum Load [mm]	Tensile stress at Maximum Load [MPa]	Tensile strain (Extension) at Maximum Load [mm/mm]
1	2.37112	11.74173	12.88651	0.39139

Figure 4.4 The original report from the Instron 8500

Figure 4.4 shows the original report which was obtained automatically from the tensile extension machine – an Instron 8500 –as soon as the test was completed. This report can provide all the test parameters such as strain rate, sample length, width and thickness, etc. In addition, the maximum load, tensile extension at maximum load, tensile stress at maximum load and tensile strain at maximum load were provided at the same time.

### 4.3.2 Results and discussions

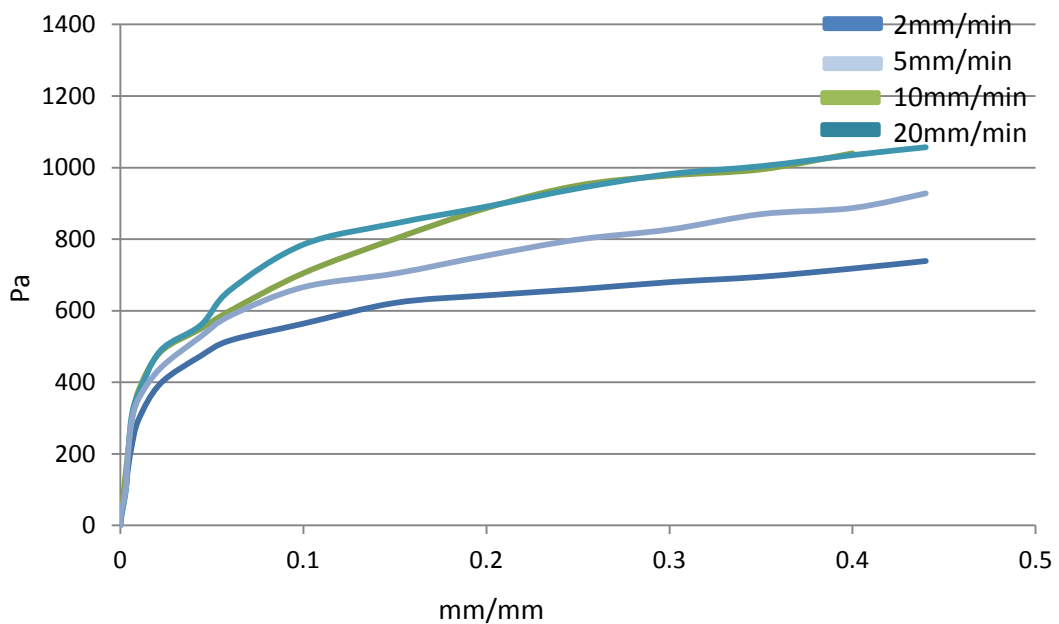


Figure 4.5a The average strain-stress curve of 7.5% EVOH nanofibre sheets in response to different loading speeds

Figure 4.5a shows the strain-stress curve of 7.5% EVOH nanofibre sheets adopting 2 mm/min, 5 mm/min, 10 mm/min and 20 mm/min loading speeds. The data of this strain-stress curve were obtained from the original data shown in Figure 4.3c. The strain-stress curve in Figure 4.3c is the original data but the curve is not smooth because of the noise, etc. We used a moving average to smooth out the original data. Figure 4.5a was obtained by using 20 per moving average. Figure 4.5a clearly shows that, even though the loading speed was changed, the

trend lines were not obviously influenced by an increase in the loading speed. Moreover, the Young's modulus (E) and yield stress are obviously very close. In fact, 100 mm/min and 200 mm/min were tried on the Instron 8500 but this provided very limited data and the shape of the trend line was very similar to the trend lines shown in Figure 4.5a. Therefore, the loading speeds from 2mm/min to 20 mm/min had to be enough to describe the mechanical properties of the EVOH nanofibre sheets on the tensile extension tests, using the Instron 8500.

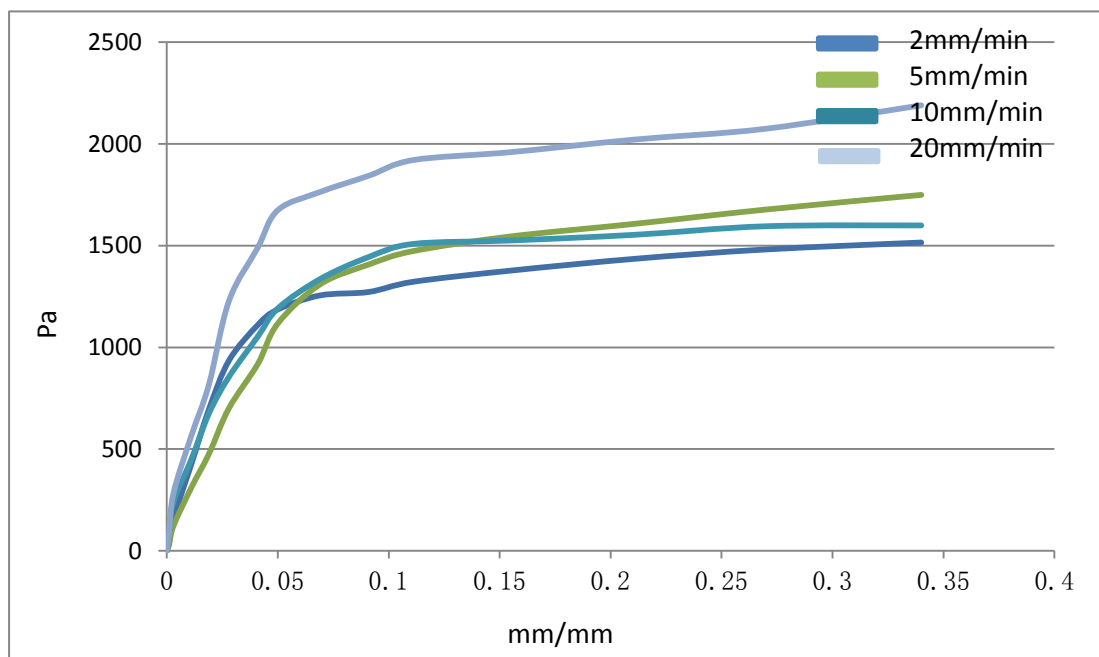


Figure 4.5b The average strain-stress curve of 10% EVOH nanofibre sheets in response to different loading speeds

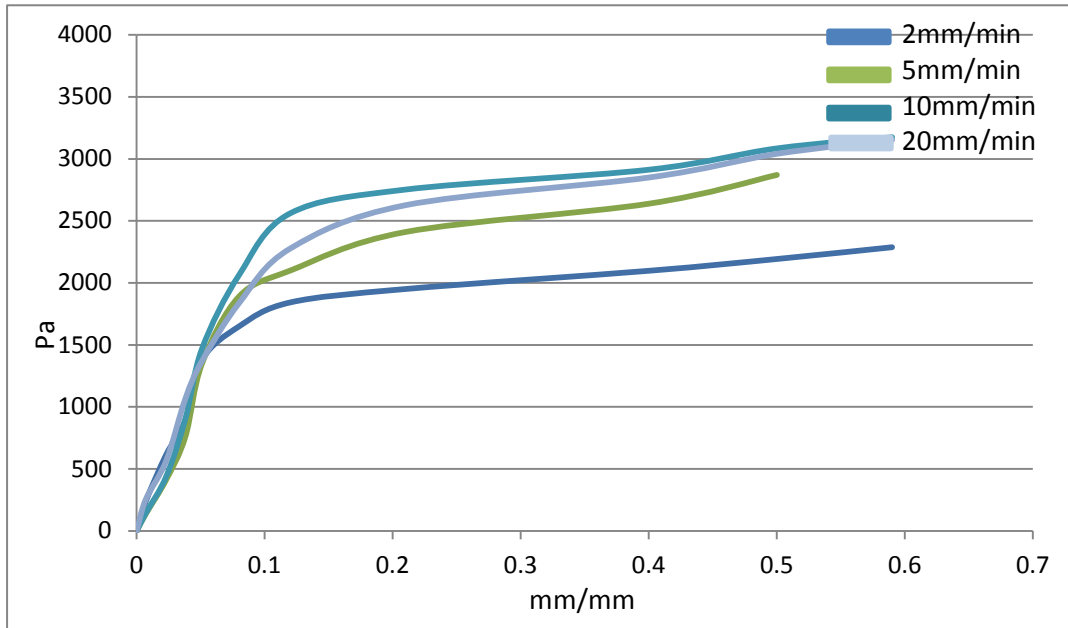


Figure 4.5c The average strain-stress curve of 12.5% EVOH nanofibre sheets in response to different loading speeds

Figures 4.5b and 4.5c show the strain-stress curves of 10% and 12.5% EVOH nanofibre sheets at loading speeds of 2 mm/min, 5 mm/min, 10 mm/min and 20 mm/min. As mentioned, the trend lines were all obtained by using 20 per moving average. Figures 4.5b and 4.5c clearly show that, even though the loading speed was changed, the trend lines were not obviously influenced by an increase in the loading speed. Moreover, the Young's modulus ( E ) and Yield stress are obviously very close.

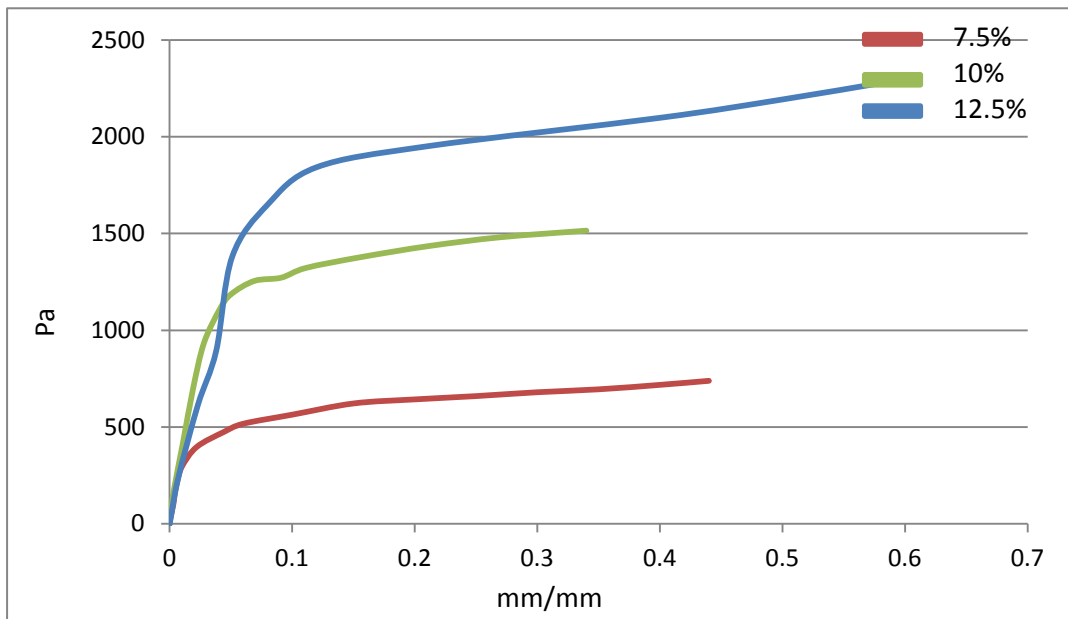


Figure 4.6a Average strain-stress curve of 3 different EVOH nanofibre sheets (7.5%, 10% and 12.5%) at 2mm/min loading speed

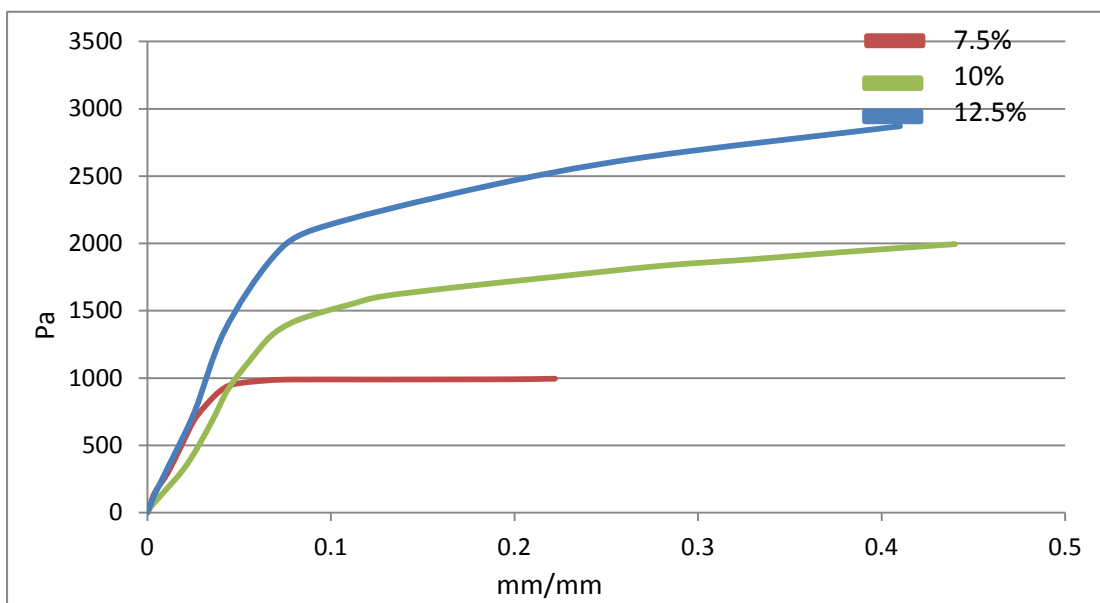


Figure 4.6b Average strain-stress curve of 3 different EVOH nanofibre sheets (7.5%, 10% and 12.5%) at 5mm/min loading speed

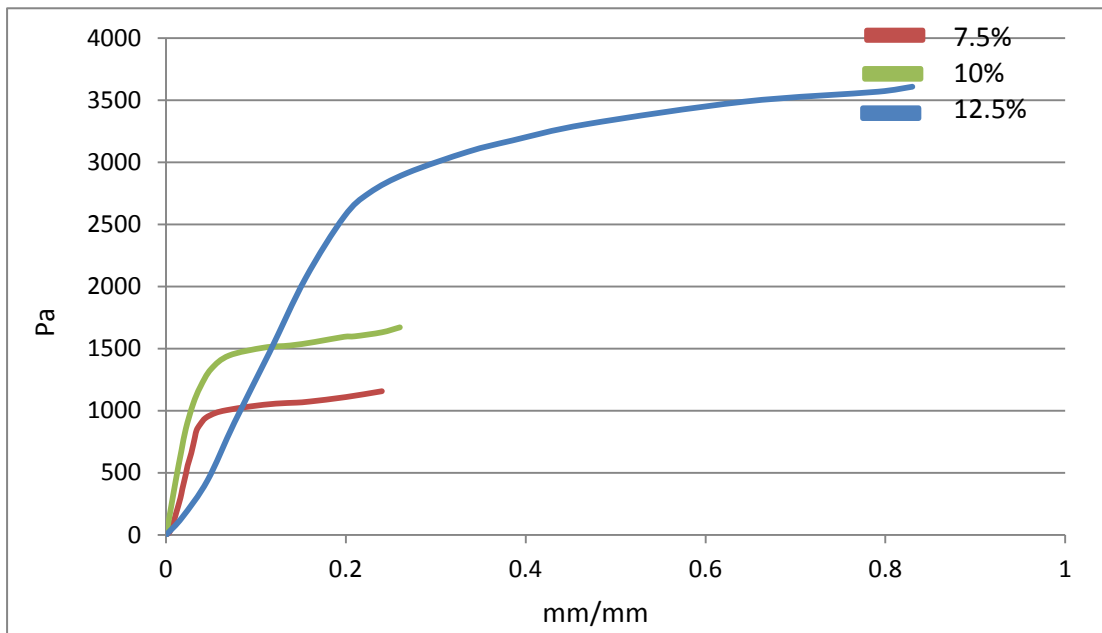


Figure 4.6c Average strain-stress curve of 3 different EVOH nanofibre sheets (7.5%, 10% and 12.5%) at 10mm/min loading speed

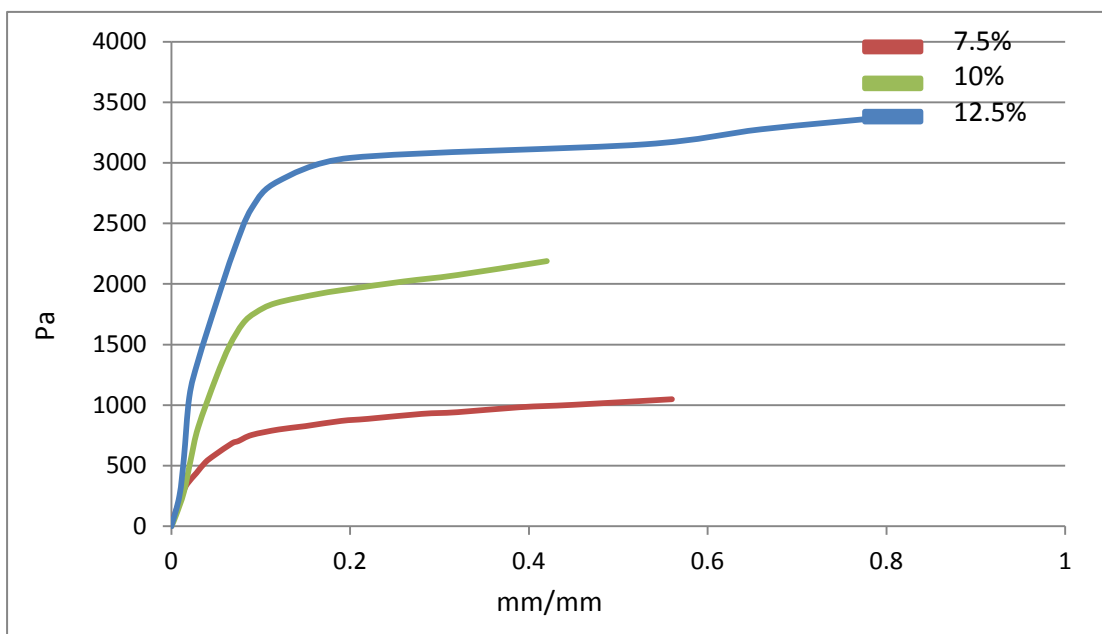


Figure 4.6d Average strain-stress curve of 3 different EVOH nanofibre sheets (7.5%, 10% and 12.5%) at 20mm/min loading speed

Figures 4.6a, 4.6b, 4.6c and 4.6d show the average strain-stress curves of 3 different EVOH nanofibre sheets (7.5%, 10% and 12.5%) at loading speeds of 2mm/min, 5mm/min, 10mm/min and 20mm/min. From the shapes of the trend

lines, the similarity is obvious, but the maximum load and yield stress were evidently increased by increasing the density of the EVOH polymer solution. As Table 5 and Table 6 suggest, as soon as the density of the EVOH polymer solution is increased, the diameter of the EVOH nanofibre and the thickness of the EVOH nanofibre sheet samples are both increased. So increasing the fibre diameter and sample thickness evidently caused the maximum load and yield stress to increase.

## **4.4 Unloading and reloading tests**

### **4.4.1 Purpose**

The nonlinear behaviour of the sample provides no clear indication of the yield point. Thus, unloading tests were conducted to identify the yield stress corresponding to 0.4 or 0.5% proof strain, as shown in Figure 4.8. The Young's modulus  $E$ , taking as the tangent from the origin, and the linear hardening modulus  $K_P$  as the tangent of the plastic range from the yield point were obtained. A straight line from the origin to the yield point was also drawn, giving the slope  $E_y$ .  $E_y$  is of a lower value than  $E$  and can be used as an approximate Young's modulus if the materials are not highly non-linear, as in the present case.

#### 4.4.2 Process of the unloading and reloading tests

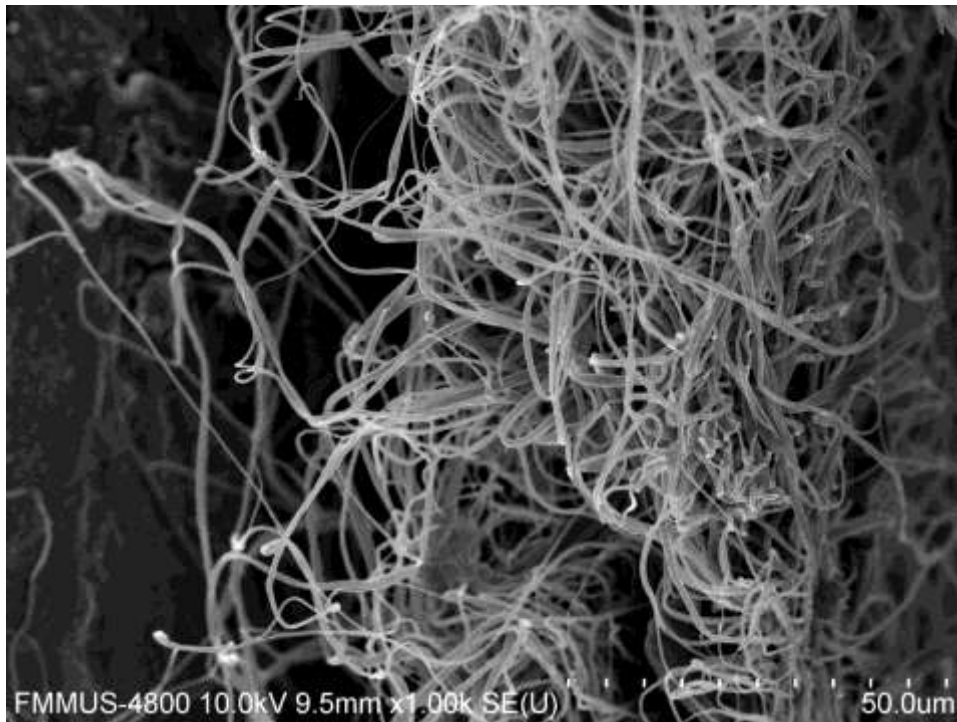


Figure 4.7 SEM image on the fractured edge of a 10% EVOH nanofibre after the tensile test

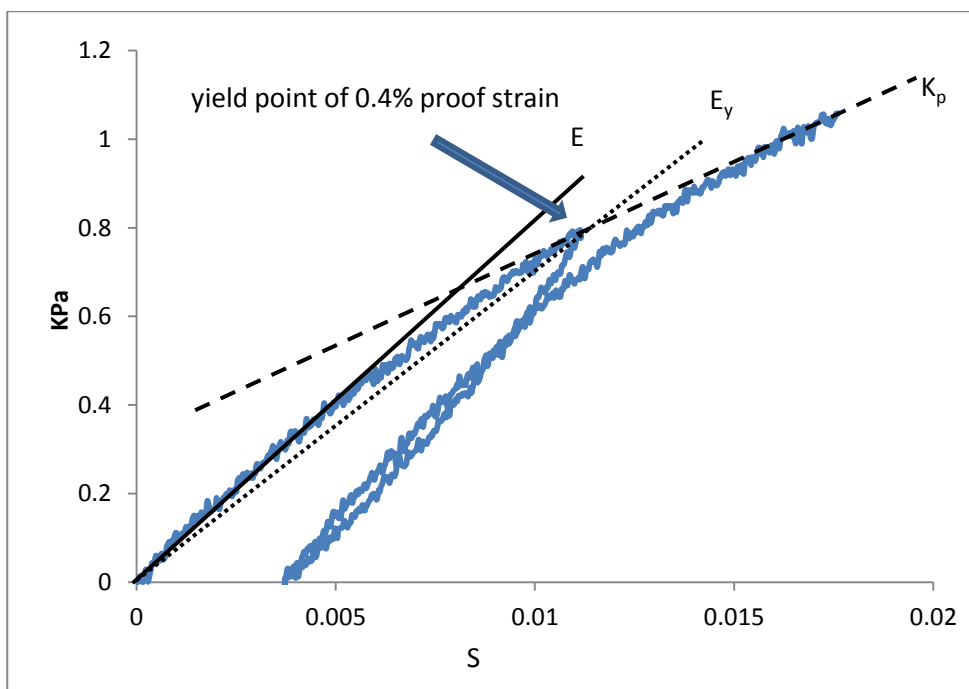


Figure 4.8 Yield stress at 0.4% proof strain and moduli

Figure 4.8 gives an image of a broken sample resulting from a 7.5% EVOH solution after the tensile test.

#### 4.4.3 Results and discussions

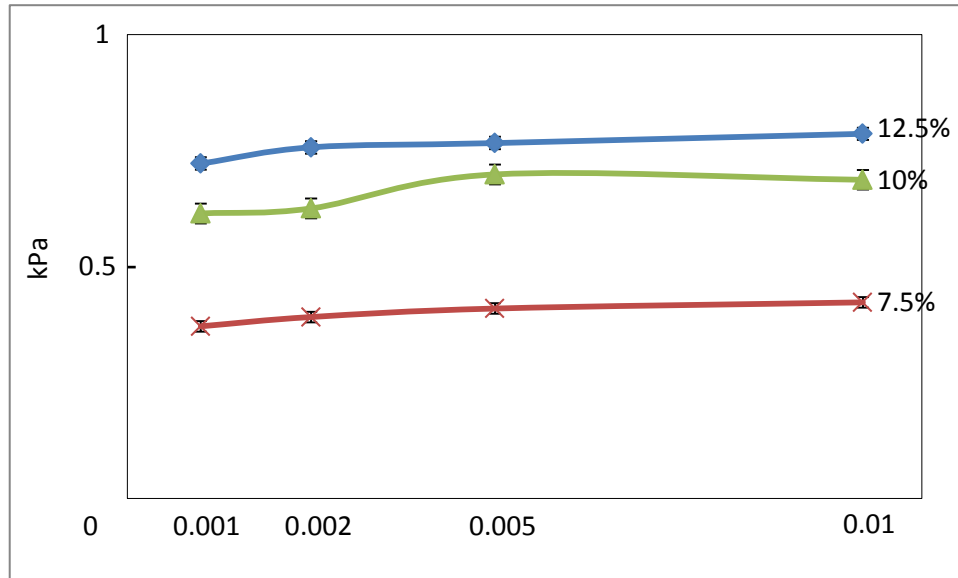


Figure 4.9 Yield stresses of the samples under different strain rates

The influence of the strain rate on the value of the yield stress is illustrated in Figure 4.9. It shows a negligible effect, indicating that none of the sample materials was sensitive to the strain rate. The EVOH content in the solution, however, has a clear influence, with higher content leading to stronger material.

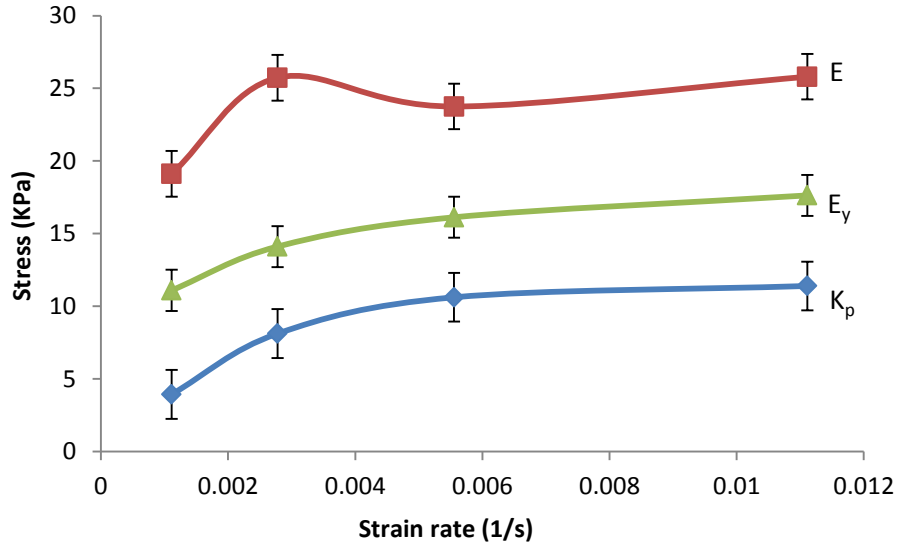


Figure 4.10a Moduli E,  $E_y$  and  $K_p$  vs strain rate. (a) Sample A

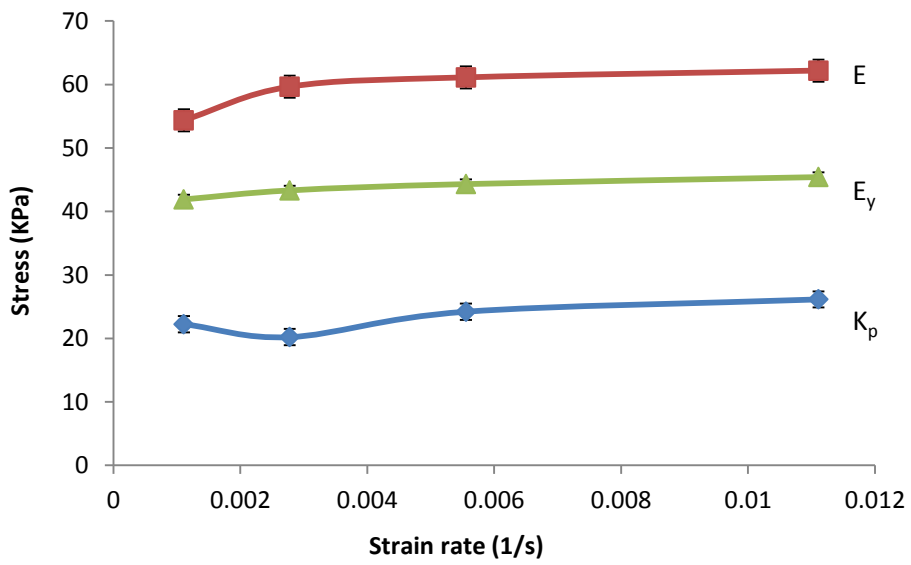


Figure 4.10b Moduli E,  $E_y$  and  $K_p$  vs strain rate. (b) Sample B

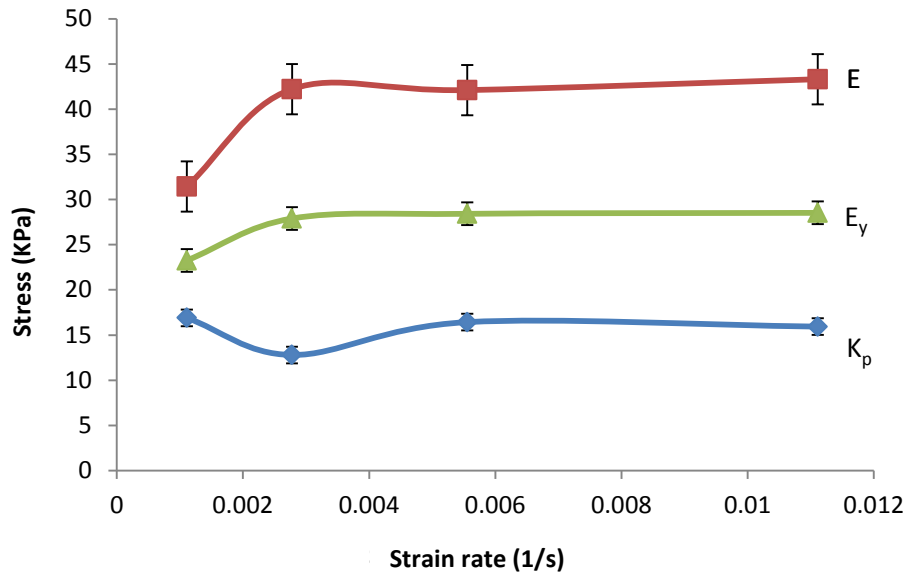


Figure 4.10c Moduli E,  $E_y$  and  $K_p$  vs. strain rate. (c) Sample C

Figures 4.10a, 4.10b and 4.10c show the trend lines of change in the three moduli defined in Figure 4.8. For each sample, E is of the highest value, followed by  $E_y$ , with  $K_p$  next. The strain rate effect on the moduli is weak, except at the low range.

Across all the samples, the EVOH content in the solutions clearly shows its influence. The higher the value of the content, the higher the corresponding moduli. The strain rate effect is also weakened by the increasing content in the solution.

#### 4.4.4 Repeated unloading and reloading for the Damage Parameter

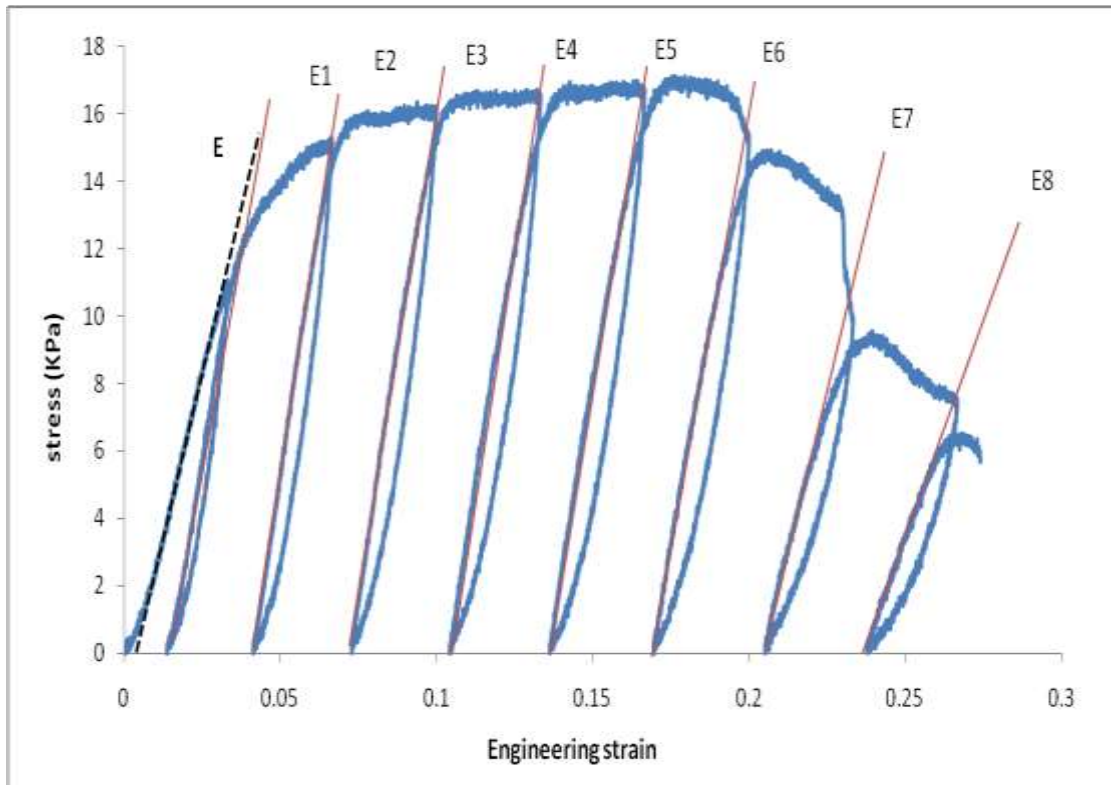


Figure 4.11 Repeated unloading and reloading test on Sample B at a strain rate of  $1.11 \times 10^{-3}$

Repeated unloading and reloading tests were carried out to see how damage might occur to the samples. A commonly used damage parameter is defined as

$$\text{Damage} = 1 - (E_{\text{reloading}}/E_0) \text{ (A. Pirondi, 2006)}$$

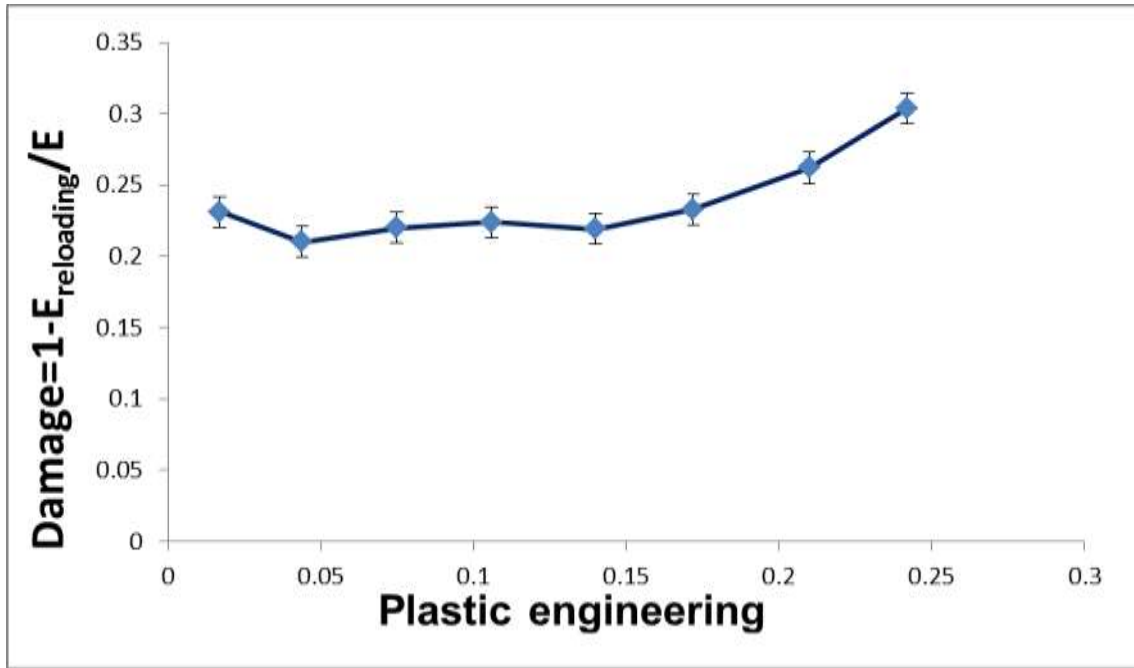


Figure 4.12 Damage parameter in terms of the plastic strain

It is a useful indication of the progress of deterioration that a test sample may undergo during repeated tensile loading. As shown in Figure 4.12 for Sample B, repeated unloading and reloading tests were carried out. Each time, the reloading modulus was measured. It is interesting to note that the initial modulus was actually lower than the modulus in the following reloading. This is likely to have been due to the alignment of the random fibres in the loading direction in the first loading. Once this alignment was made, the sample was “reinforced” with more fibres in the loading direction, thus showing a stronger response. This phenomenon continued into the plastic range until the ultimate tensile loading was reached. After this the material showed clear damage, probably through the fibre breaks yielding in the fracture of the sample. The reloading modulus reduced in value while the load bearing capacity diminished. Figure 4.12 shows the calculated damage value, based on the measurement of the modulus in Figure 4.11. Note that  $E_0$  was not used in the calculation but that  $E$  was used instead, because of the issue of alignment, as explained above. The first reloading modulus gives a better indication of the developing damage. It is clearly shown that the damage built up quickly when total strain went beyond 0.15.

## 4.5 Chapter summary

In this part, the mechanical properties of the 3 different EVOH nanofibre membrane samples (sample A, B and C) were tested. These 3 samples were all made by using 15 kV, 20 cm distance and 2.0 ml/hr flow rate for 5 minutes, the different parameter is the solution concentration, which was used 7.5% for sample A, 10% and 12.5% for sample B and C.

The first achievement in this chapter is that the strain-stress curve was found via typical tensile extension tests. Secondly, The nonlinear behaviour of the sample provides no clear indication of the yield point. Thus, unloading tests were conducted to identify the yield stress corresponding to 0.4 or 0.5% proof strain was presented. The Young's modulus  $E$ , taking as the tangent from the origin, and the linear hardening modulus  $K_p$  as the tangent of the plastic range from the yield point were obtained. A straight line from the origin to the yield point was also drawn, giving the slope  $E_y$ .  $E_y$  is of a lower value than  $E$  and can be used as an approximate Young's modulus if the materials are not highly non-linear, as in the present case. Thirdly, to qualify the damage parameter of the 3 different EVOH nanofibre sheet samples, the unloading and reloading tests were carried out to see how damage might occur to the samples. Finally, the viscos-elastic tests were presented in appendix.

## **5. Fabrication of Ag, iodine and gentamicin EVOH nanofibres and Ag degradation test**

### **5.1 Introduction**

The choice of dressing material plays a key role in the treatment and recovery of skin wounds, providing surface protection, tissue and cell restriction, moisture maintenance, air permeability, bacteriostatic controlling activities, drug delivery and other functions. The control of inflammation caused by bacteria is particularly critical for the large or widespread wounds often seen in injuries caused by fire and chemical burns. One would naturally hope that the dressing material contained some bacteria suppression functionality to improve treatment and cure.

Electro-spinning, also known as electrostatic spinning, is a popular method of fabricating nonwoven fibres of different shapes and sizes [He, J.H. et al., 2004]. It is currently the only method used to prepare the fabric of fibres which have a diameter of a few nanometers [Greiner, A. et al., 2007]. A number of methods are available for introducing drugs into the fibrous materials [Sill, T.J. et al., 2008] produced by the electro-spinning technology are good candidates in skin wound treatment. EVOH was selected for this study due to its good biocompatibility and proven use in the preparation of nanofibres by means of electro-spinning [Kenawy, E.R. et al., 2003].

In this study, we investigated the effectiveness of the bacteria control by nanofibres impregnated with three commonly used anti-bacterial agents, Ag, iodine and gentamicin. *Staphylococcus aureus*, one of the main pathogenic bacteria found on both animal and human wound surfaces [Xu. C. et al., 2011], was chosen to test the anti-bacterial capacity of the material. Degradation tests by both phosphate buffer solution and ultraviolet lamp were carried out, so that the degradation performance of the materials could be indicated both in a simulated body environment and a radiation accelerated environment.

## **5.2 Fabrication of Ag EVOH nanofibres**

### **5.2.1 Electro-spinning system and solutions**

The system used for electro-spinning is an improved platform based our previous study in chapter 3 which was made up of a high voltage power supply with a  $\mu\text{A}$  range low current output (Spellman CZE1000R, 0-30 kV), a peristaltic pump with a feeding capacity in the range of 1.0-15.0 ml h<sup>-1</sup> (Masterflex, 77120-52) and a tube with a fine metal needle.

All EVOH nanofibre samples with and without a bacterial agent were prepared from the solution with 7.5% (w/v) EVOH powders diluted in solvent containing 80% (v/v) propanol-2 and water. AgNO<sub>3</sub> powders, iodine and gentamicin were then added to the three EVOH solutions in turn, in different weight percentages. The solutions were injected at a speed 2.5 ml/h and spun under the charged needle and collector by 25 kV at a distance of 350 mm.

### **5.2.2 Ag and EVOH polymer solution**

EVOH was ordered in powdered form from Sigma-Aldrich (Batch number: 12822PE). AgNO<sub>3</sub> was purchased in powder form from Alfa Aesar (Alfa Aesar, 7761-88-8). Iodine was purchased from Tianli (Tianli, AR/250g) in powdered form. Finally, gentamicin of a clinical grade was ordered from JXYY in the specification of 2 ml: 80000 units (JXYY, 2 ml: 80000 units). Staphylococcus aureus were taken from the laboratory.

### **5.2.3 Electro-spinning process of producing Ag EVOH nanofibres, iodine and gentamicin EVOH nanofibre**

To produce Ag, iodine and gentamicin EVOH nanofibre, we used the same design of electro-spinning system as is described in Chapter 3. For making iodine and gentamicin EVOH nanofibre mat samples, the iodine and gentamicin were able to be added directly to the EVOH polymer solution before the electro-spinning process, due to the fact that the iodine and gentamicin had been obtained in liquid form, and there was therefore no need to process them further. In the electro-spinning parameters of making the iodine and gentamicin EVOH

nanofibre mat samples, a higher voltage and longer needle tip-to-collector distance (10% increase on the original parameters for making fine EVOH nanofibres) were required to keep the electro-spinning working properly and to obtain better EVOH fibre samples. Because there was water in the iodine and gentamicin, this caused the density of the EVOH polymer solution to be lower; as a result, more electrical power and distance were required.

Various concentrations of iodine and gentamicin were tried and it was found that there is a maximum concentration (0.1 ml iodine and 0.25 ml gentamicin) which can be used for electro-spinning fabrication. Any higher concentration of iodine and gentamicin would have caused the polymer solution to drip in droplets, rather than being jetted out in a spin, without which there could be no fibre formation. As will be discussed later in connection with the bacteria tests, due to the limited concentration of iodine and gentamicin achievable for nanofibre sheet fibres, a better performance can be obtained with mats containing Ag articles. This is the primary reason for not choosing to have iodine and gentamicin reinforced nanofibre mats. Various secondary reasons, such as potential allergic reaction by patients to iodine or gentamicin, the poor stability of iodine and gentamicin compared with that of Ag, resulting in an earlier expiry date and higher material cost, add to the arguments in support of the choice of Ag.

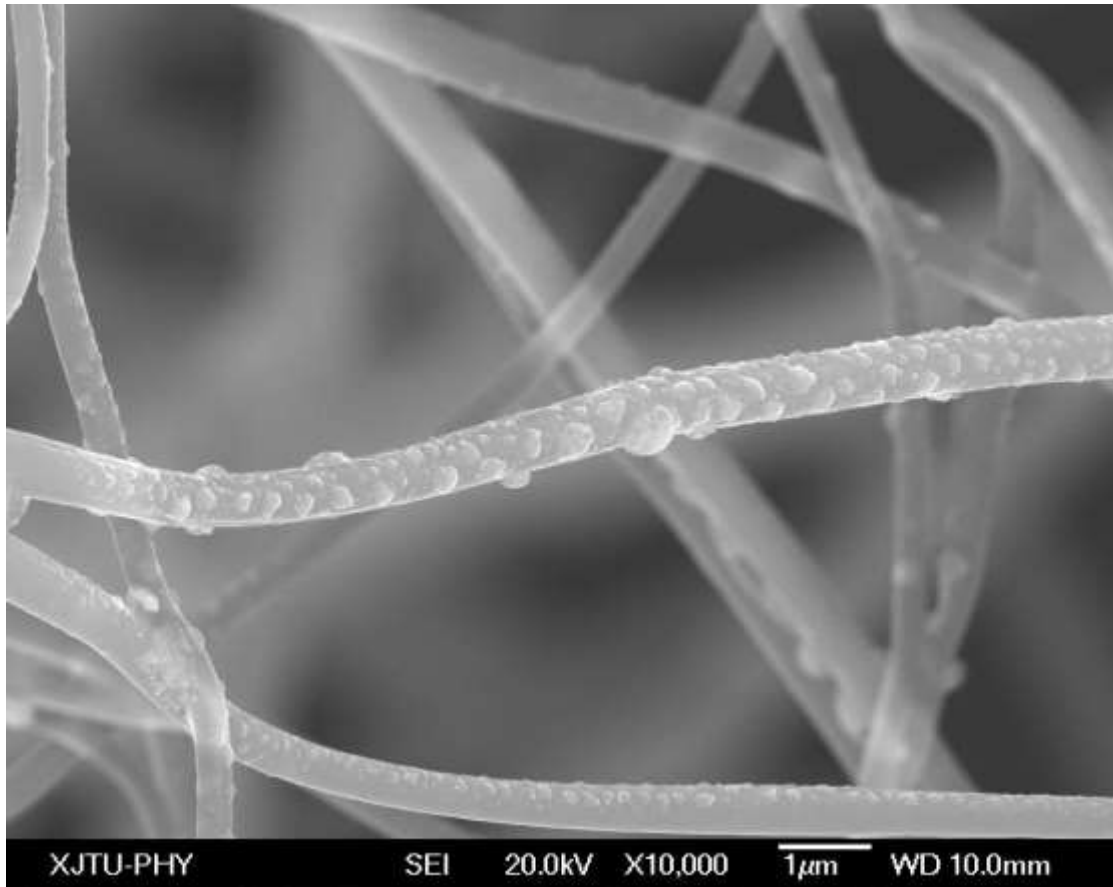


Figure 5.1 An SEM image of 7.5% Ag EVOH nanofibres (0.04g AgNO<sub>3</sub> added to 10 ml 7.5% EVOH polymer solution)

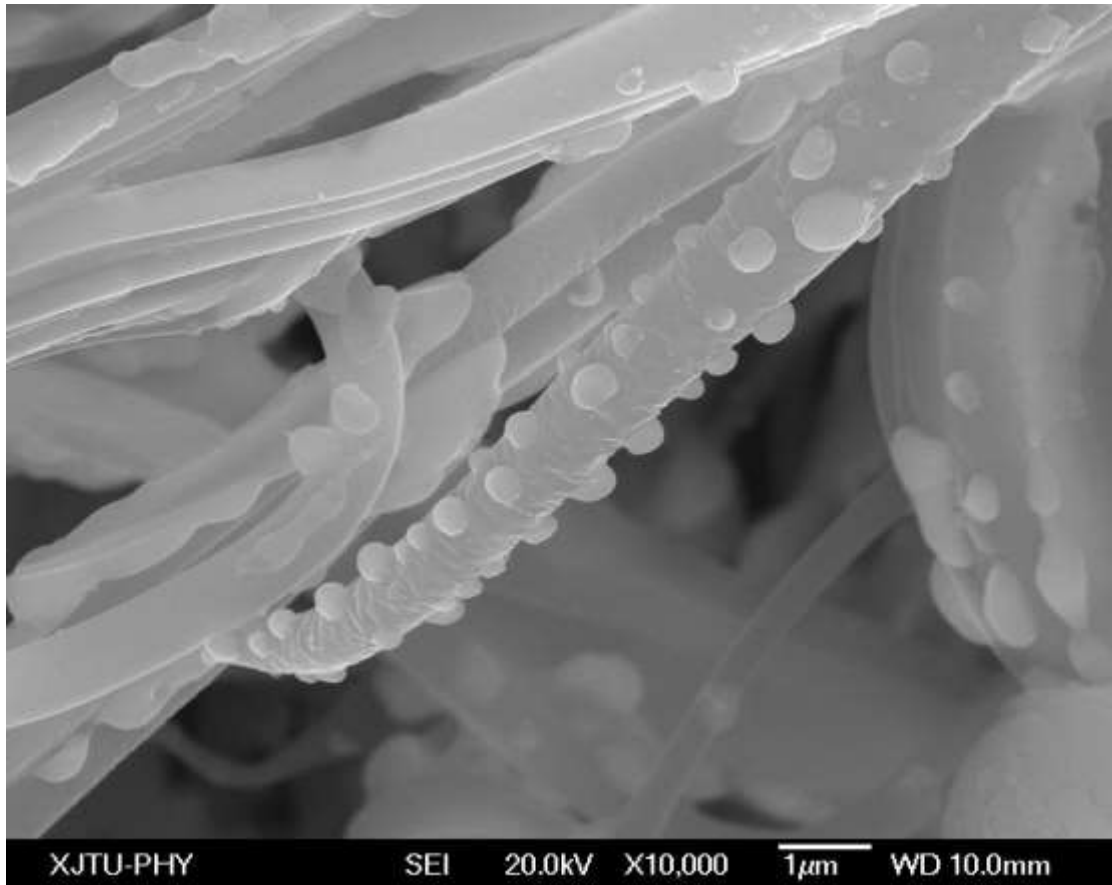
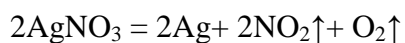


Figure 5.2 An SEM image of Ag particles attached to and imbedded in EVOH nanofibres (0.15g AgNO<sub>3</sub> was added to 10 ml 10% EVOH polymer solution)

Figures 5.1 and 5.2 show the microcosmic structures of Ag in EVOH nanofibres. Solid AgNO<sub>3</sub> was first dissolved in distilled water, then added to EVOH solution, which was kept on a magnetic stirrer for 10 minutes at 40°C. During the process of fibre formation, AgNO<sub>3</sub> decomposes under illumination, even in normal room light:



Nitrogen dioxide and oxygen gas will be released during the decomposition process and this leaves pure Ag (simple substance) inhering in the fibre. This decomposition process may continue after fabrication until all the Ag is encapsulated in the fibre.

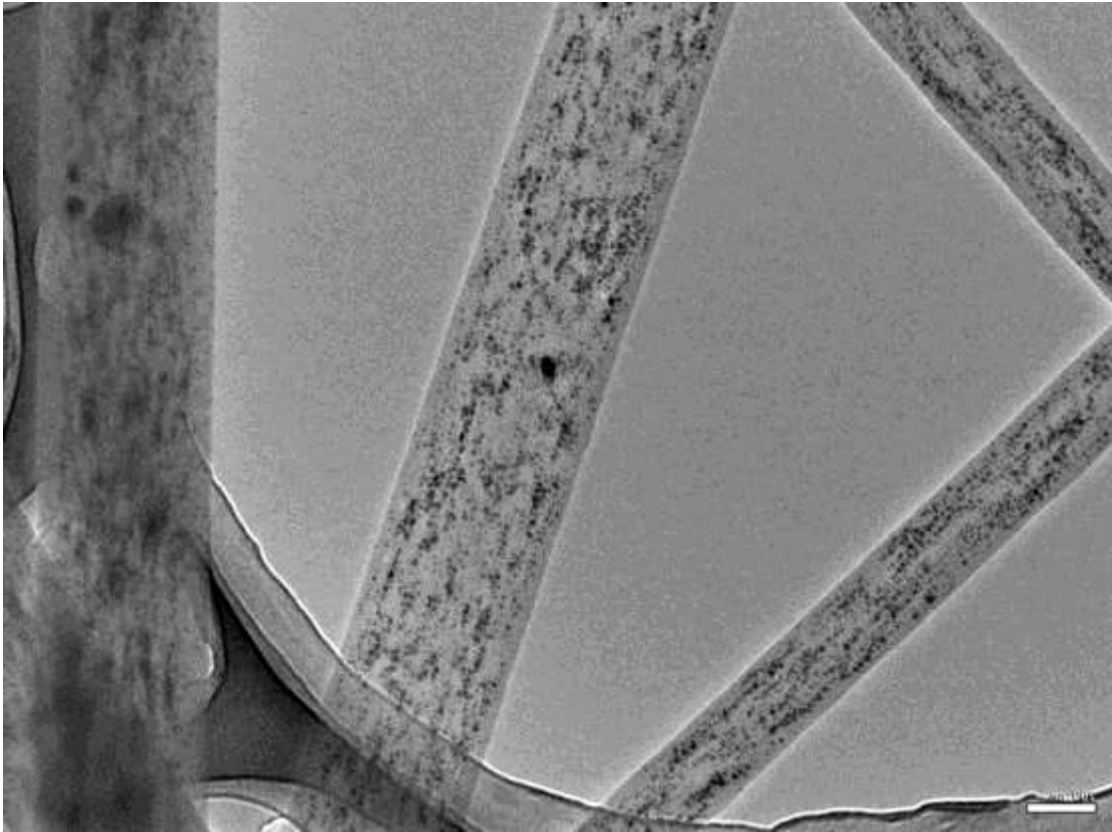


Figure 5.3 A TEM image of Ag EVOH nanofibre

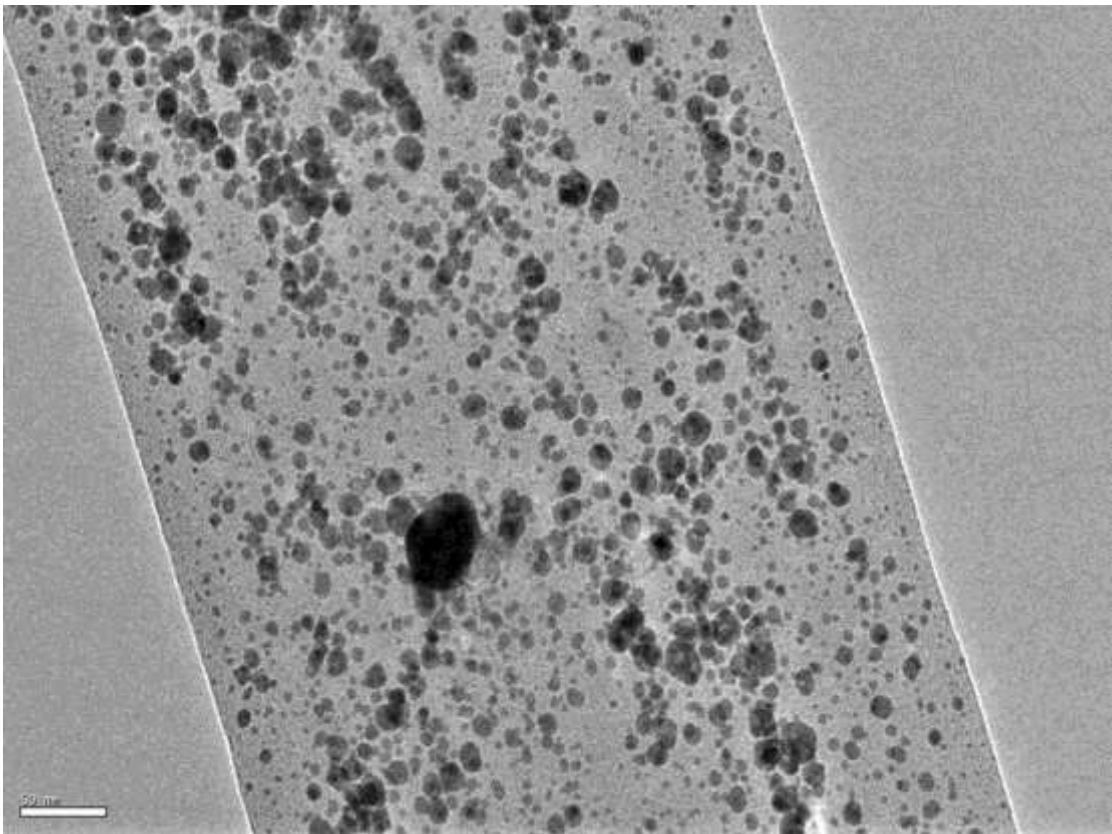


Figure 5.4 A TEM image of a single fibre of Ag EVOH nanofibre

Figure 5.3 and. Figure 5.4 show that the Ag nanoparticles are encapsulated inside the EVOH fibres. The distribution is reasonably evenly distributed with particles of various sizes. It is not clear whether the intensity of the illumination may be used to control the Ag particle sizes, though size is not an issue for the functionality of bacteria suppression.

#### 5.2.4 Energy spectrum check of encapsulated Ag particles

The suppressive effect of Ag on inflammation is related to the purity of the Ag (as a simple substance) encapsulated. To check the content of the Ag particles obtained, the energy spectrum function of the SEM was used. Figures 5.5 and 5.6 show the composition of the Ag particles and the image of the Ag particle in the fibres. It shows that the particles are made of simple substance Ag, where the elements C and O are from the EVOH polymer.

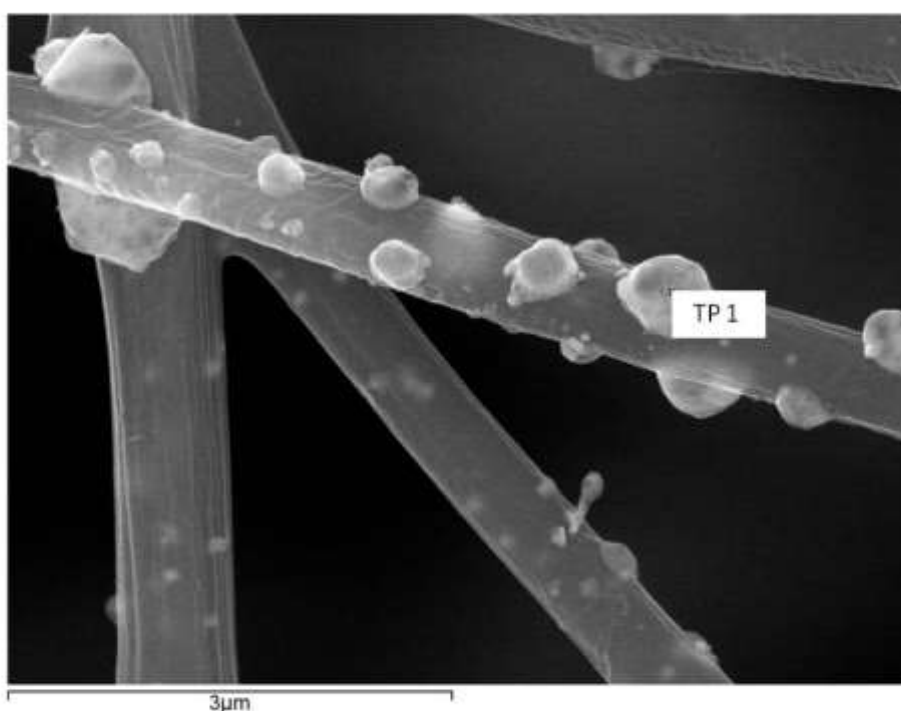


Figure 5.5 Energy spectrum using an SEM for the encapsulated Ag particles

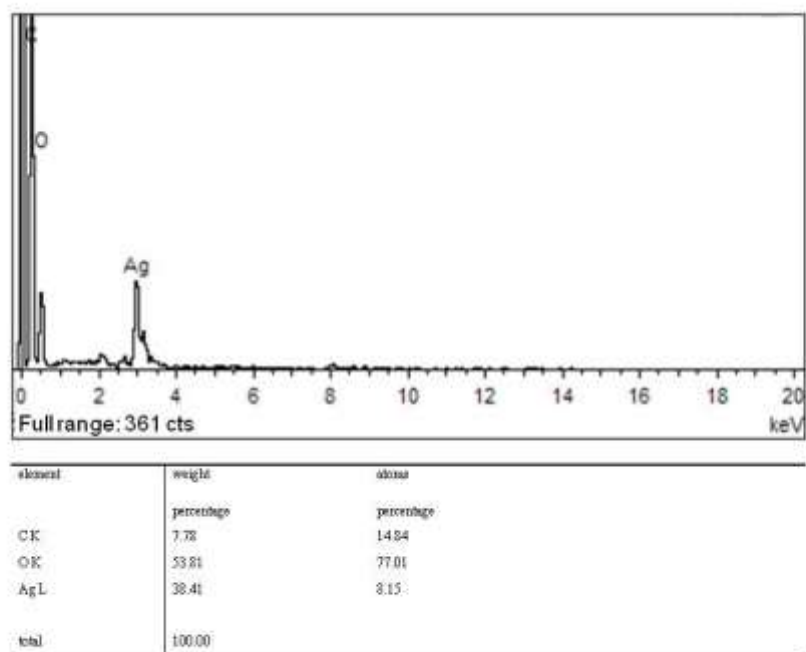


Figure 5.6 The results of the energy spectrum using an SEM for the encapsulated Ag particles

## 5.3 Fibre degradation and the release of Ag particles

### 5.3.1 Introduction

The EVOH nanofibres encapsulated with Ag as the anti-bacterial agent were obtained in this study from the electro-spinning process. Degradation tests indicated that the mechanical property of the materials is stable in vitro, indicating that it is a good candidate for wound dressing applications where the stable shielding of the wound area is a primary requirement.

### 5.3.2 Process of Ag release tests

A hydrolysis test and ultraviolet light exposures were carried out as the degradation tests. For the hydrolysis tests, nanofibre samples were submerged in phosphate buffer solution (PBS) of a pH value of 7.2 and kept at 37°C. The test

was aimed to evaluate the time-based integrity of the material in simulated *in vivo* conditions. The samples were weighed every 72 hours with a bio-electronic balance after being dried at 37°C.

The simulated sunlight and ultraviolet degradation tests were performed in a photochemical reaction machine. The irradiation strength of the light at a wavelength of 254 nm was  $3.23 \times 10^3 \mu\text{W cm}^{-2}$  measured with a UV radiometer at the point where the samples were placed. The samples were weighed and photographed after every 24 hours' exposure.

### 5.3.3 Water and PBS release tests

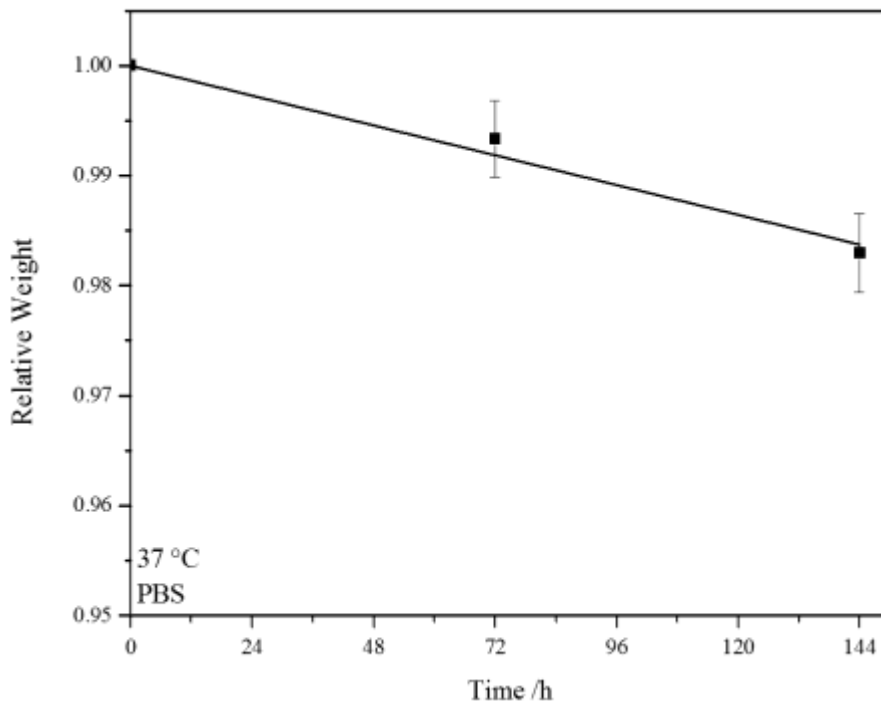


Figure 5.7 Degradation of the EVOH nanofibre in a PBS solution (note: three data points for a straight line is not enough; more data should be added.)

As shown in Figure 5.7, only a 2% change in the weight of the samples was noted over 7 days in a PBS solution. Little degradation indicates that the fibres preserve their integrity for long term use, which is an important consideration for dressing materials.

### 5.3.4 Simulated sunlight and UV light release tests

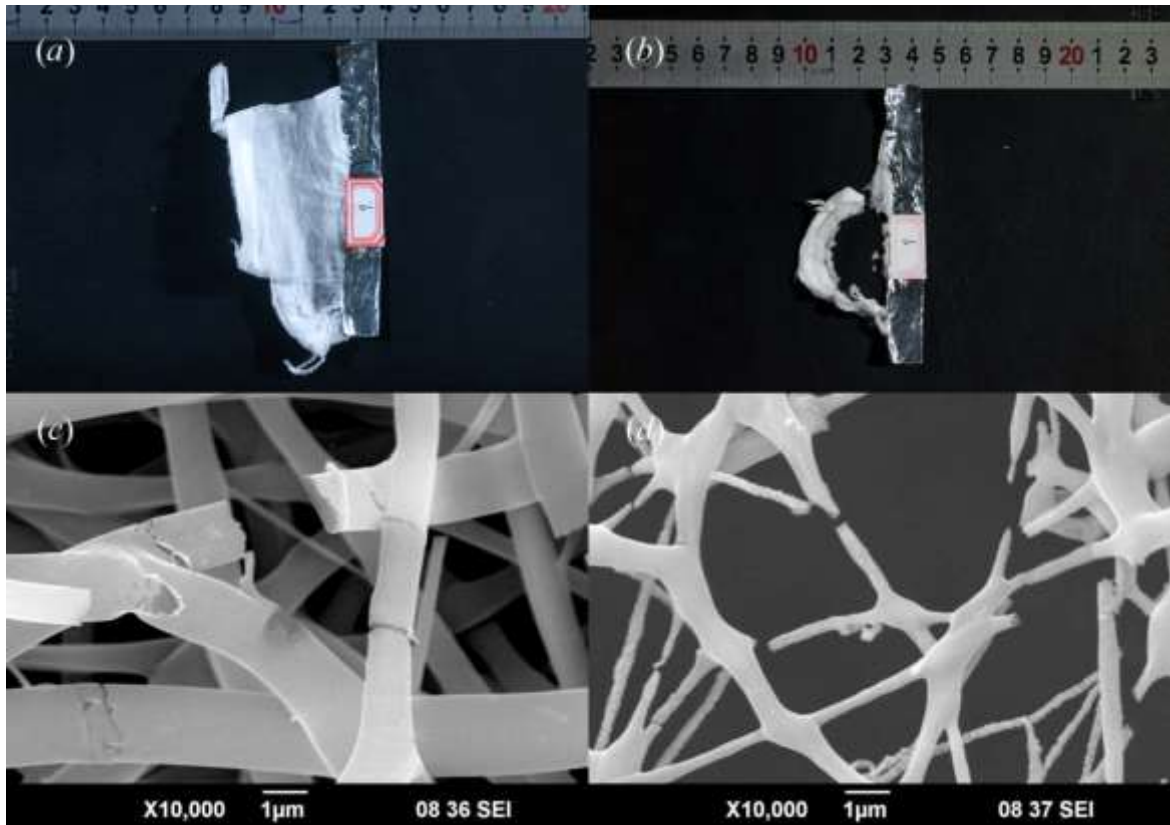


Figure 5.8 (a) Original fine fibre sample before exposure to UV light, (b) fibre sample after 72 h continuous exposure to UV light, (c) SEM image of EVOH fibre after 24 h UV degradation test, (d) SEM image of EVOH fibre after 72 h UV degradation test.

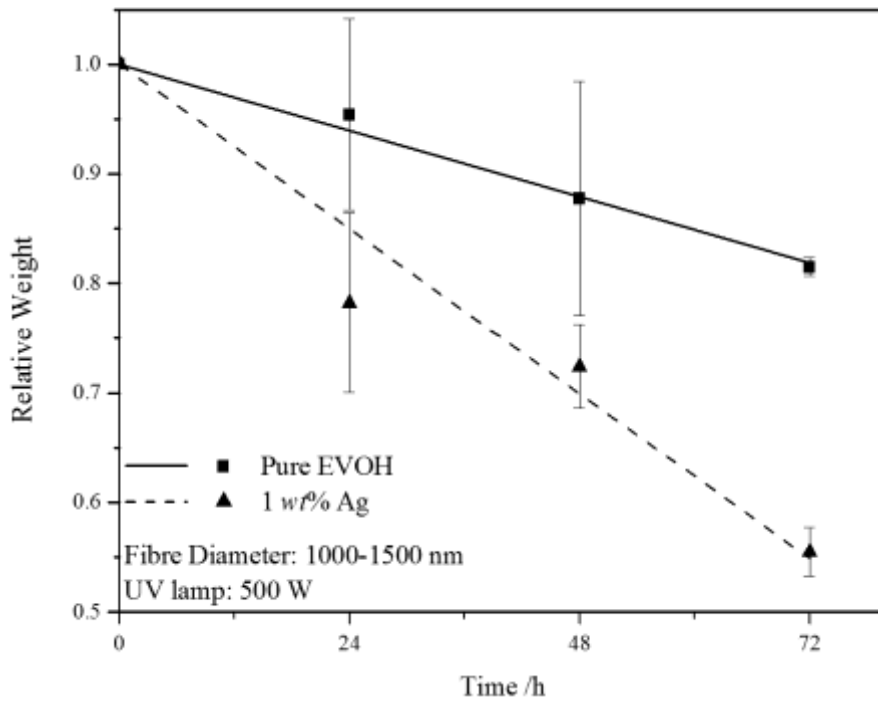


Figure 5.9 UV degradation test of nanofibres.

Figure 5.9 shows the weight variation of the nanofibres with and without Ag nanoparticles over the hours of exposure. It is seen that the nanofibres degrade approximately linearly, but those containing Ag nanoparticles degrade faster, with a reduction in weight of more than 40% compared with the 20% reduction of pure EVOH nanofibres over 72 hours of exposure.

### 5.3.5 Results of Ag particles release

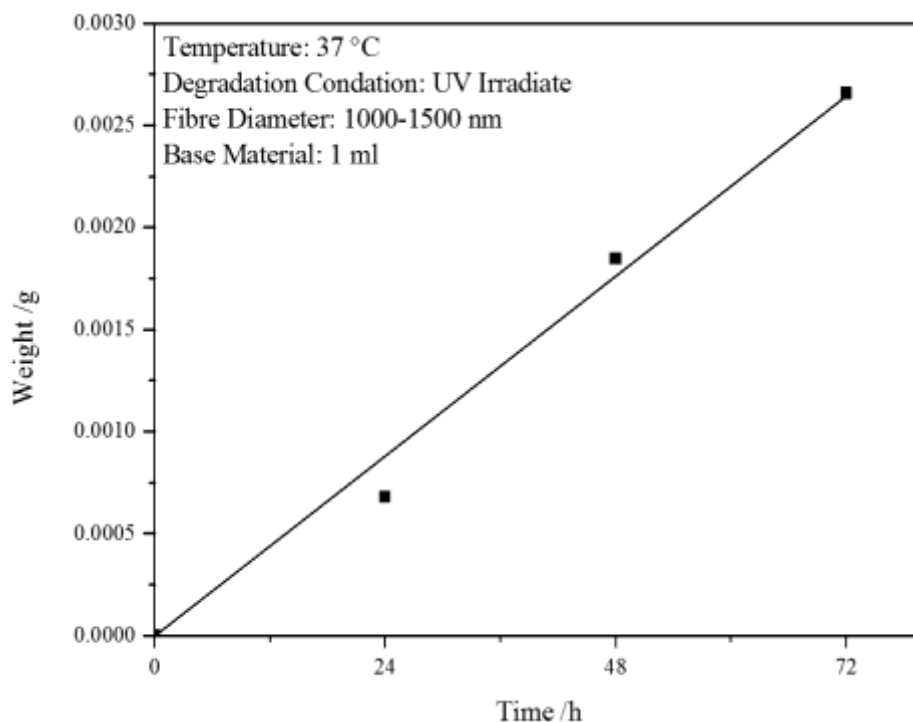


Figure 5.10 The release speed of Ag nanoparticles exposed to UV light

The release of Ag nanoparticles can be calculated on the basis of the total weight reduction, as shown in Figure 5.10. The high sensitivity shown by the EVOH nanofibre degradation under UV exposure leads to two interesting features. First, the UV light can be used to speed up the release of Ag nanoparticles and possibly that of other drugs if EVOH nanofibres are used as the carrier. Second, the rapid texture deterioration under UV light means that there could be repercussions from using the EVOH nanofibres as dressing or bandage for prolonged periods. In such cases, some UV shielding may be required.

## 5.4 Chapter summary

First of all, this part of this thesis presents the methods of producing functional EVOH nanofibres – iodine EVOH nanofibres, gentamicin EVOH nanofibres and Ag nanoparticle EVOH nanofibres, besides, the reason of choosing Ag particle EVOH nanofibre as the final functional dressing material was discussed.

Secondly, to qualify the release speed of Ag nanoparticles under different conditions, the degradation tests in different conditions (water, PBS and UV lights) were presented, besides, the results from degradation tests were also discussed. Considering the purpose of this study is to develop a new dressing material for skin wounds healing, the Ag nanoparticle EVOH nanofibres were slowly degraded in the PBS, in other words, this will proof it can be degraded very slowly on wounds surface, therefore, this is a suitable condition for producing a new dressing material by EVOH nanofibre sheets.

## 6. Anti-bacteria tests on and animal tests

The purpose of the anti-bacteria tests was to evaluate how far the nanofibre mats could suppress bacteria. As explained in Chapter 5, three anti-bacterial agents were introduced into the nanofibre mats, namely, Ag, iodine and gentamicin. These mats were tested *in vitro* and the *Staphylococcus aureus*, which is one of the most commonly seen pathogenic bacteria in human burn injuries, was the bacterium used. This study provides a comparison of the effectiveness of the bacteria suppression function of these three mats, underpinning the further development of this new dressing material.

### 6.1 Process of anti-bacteria tests

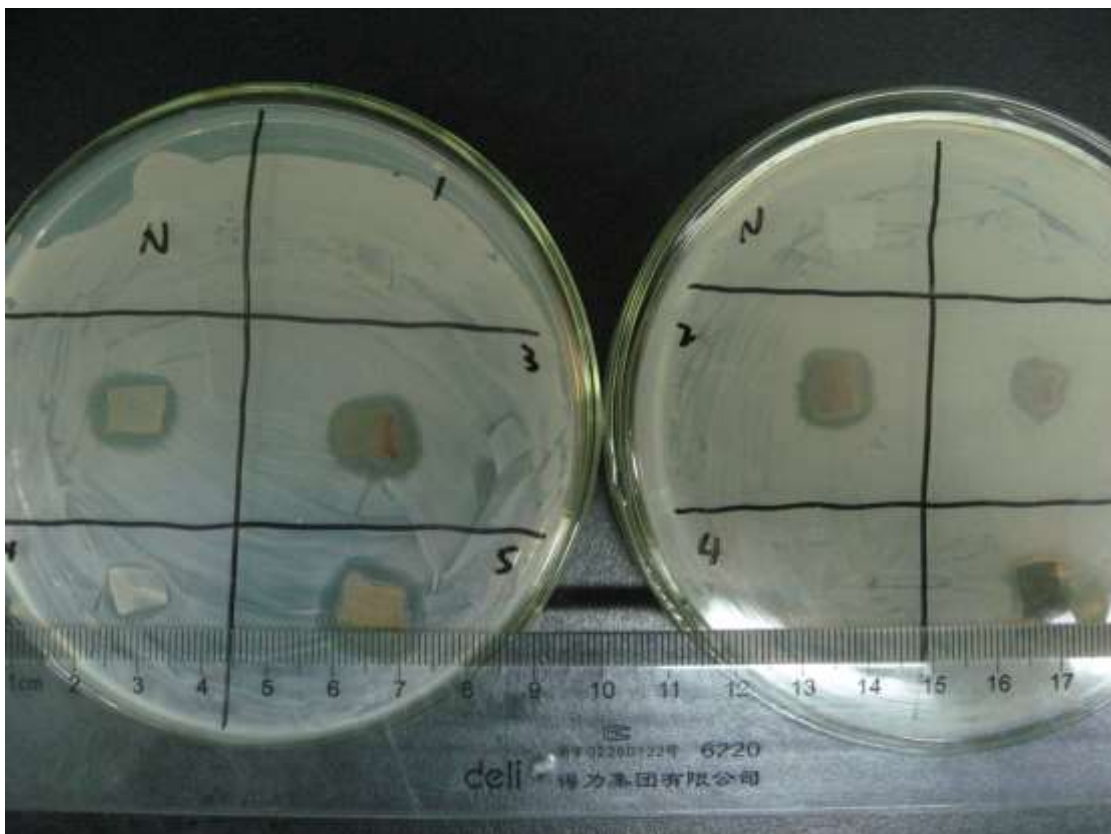


Figure 6.1 Anti-bacterial tests at 37°C with 10 mm x 10 mm square shaped EVOH nanofibre samples impregnated with Ag nanoparticles.

After the Ag, iodine and gentamicin EVOH nanofibre samples were produced, the samples were cut into 10 mm x 10 mm squares for the testing of

anti-bacterial abilities. The first few rounds of the anti-bacteria culture tests with 10 mm x 10 mm square samples proved that Ag, iodine and gentamicin EVOH nanofibre samples all had anti-bacterial abilities, but it was found difficult to measure the Bacteriostatic Loops were found. Because these samples were cut in squares measuring 10 mm x 10 mm, they caused the shapes of the bacteriostatic loops to become random; in other words, large errors in the values of the loop diameters were obtained.

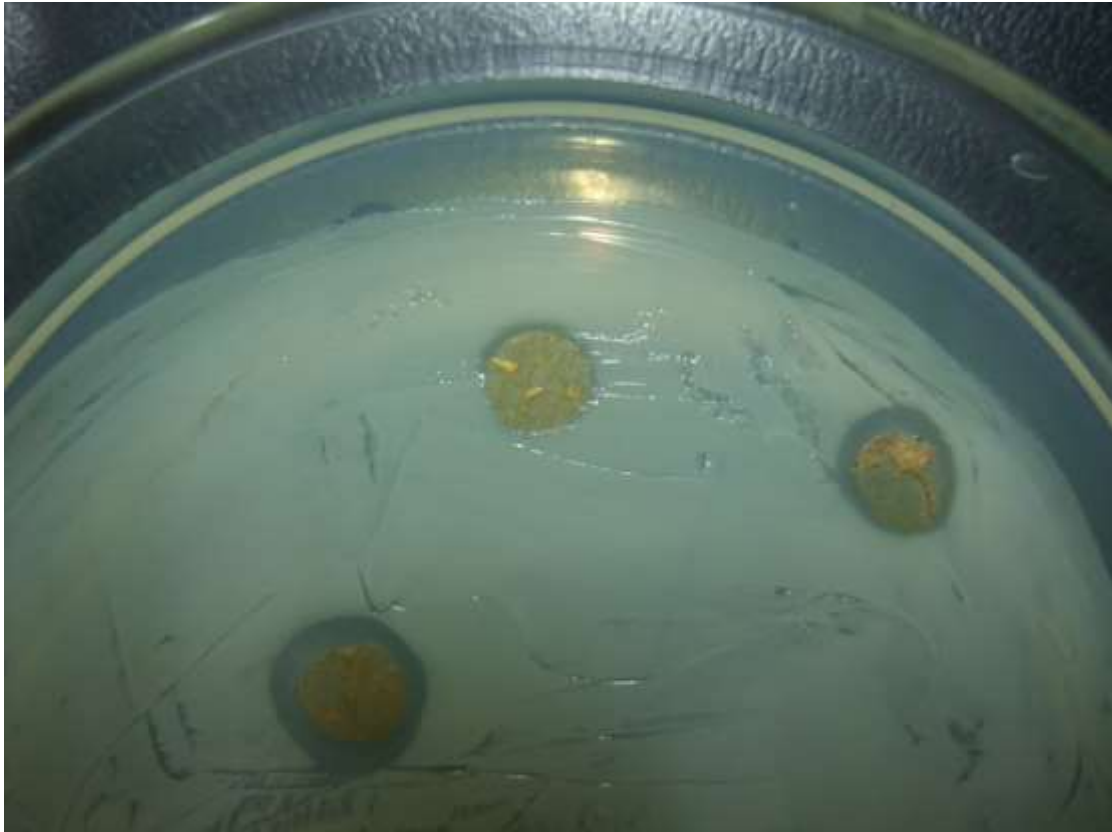


Figure 6.2 Anti-bacterial tests at 37°C with EVOH nanofibre samples impregnated with circular Ag nanoparticles of 10 mm diameter.

Nanofibre mats containing Ag, iodine and gentamicin were first covered by aluminium foil, then cut with a stopper borer into circular disks of 100 mm diameter. As Figure 6.1 shows, the circular samples provided a good boundary to form bacteriostatic loops where the bacteria were killed. The germ killing capacity of the samples is determined by measuring the size of the outer diameter or width

of the rings. Clearly, a good accurate roundness in the sample is important to allow the highest possible accuracy to be achieved in the measurement.

Once cut, the Ag, iodine and gentamicin EVOH nanofibre samples were tiled into plastic culture dishes with the *Staphylococcus aureus* pasted evenly on the base. The culture was then carried out in an incubator at a shaking speed of 50 r/min for 6 hours at 37°C. To quantify the effectiveness of the restraining pathogens, we measured the Bacteriostatic Loops 6 times at timed intervals of 6 hours using a digital camera and measuring the diameters with an electronic venire caliper.

## 6.2 The choice of the virus used

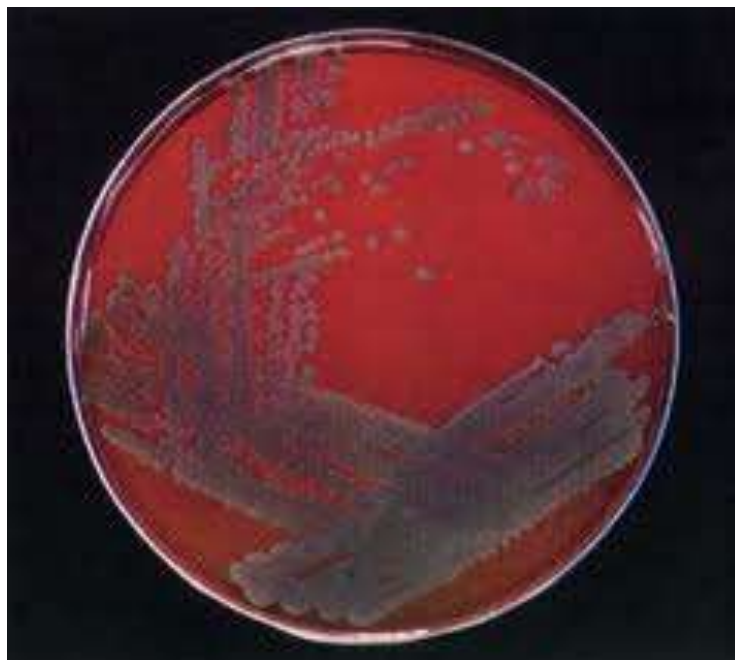


Figure 6.3 *Staphylococcus aureus*

[<http://www.picsearch.com/pictures/Science/Bacteri>, 2010]

The main pathogens on the surface of skin burns are generally *Staphylococcus aureus* (>80%) [Arthur, S. et al., 1998]. The *Staphylococcus aureus*, abbreviated to Staph aureus in the medical literature, was first identified in Aberdeen, Scotland (1880) by the surgeon Sir Alexander Ogston; it was found in pus from surgical abscesses [Ogston, A. 1984]. Bacteria of the genus

Staphylococcus are gram-positive cocci which can be seen under a microscope as individual organisms, in pairs and in irregular, grapelike clusters. The term Staphylococcus is derived from the Greek term staphyle, meaning "a bunch of grapes." Staphylococci are nonmotile, do not form spores and are catalase-positive bacteria. Their cell walls contain peptidoglycan and teichoic acid. The organisms are resistant to temperatures as high as 50°C, to high salt concentrations and to drying. Colonies are usually large (6-8 mm in diameter), smooth and translucent. The colonies of most strains are pigmented, ranging from cream-yellow to orange.

The ability to clot plasma continues to be the most widely used and generally accepted criterion for the identification of *Staphylococcus aureus*. One such factor, bound coagulase, also known as the clumping factor, reacts with fibrinogen to cause organisms to aggregate. Another factor, extracellular staphylocoagulase, reacts with prothrombin to form staphylothrombin, which can convert fibrinogen to fibrin. Approximately 97% of human *S. aureus* isolates possess both of these forms of coagulase.

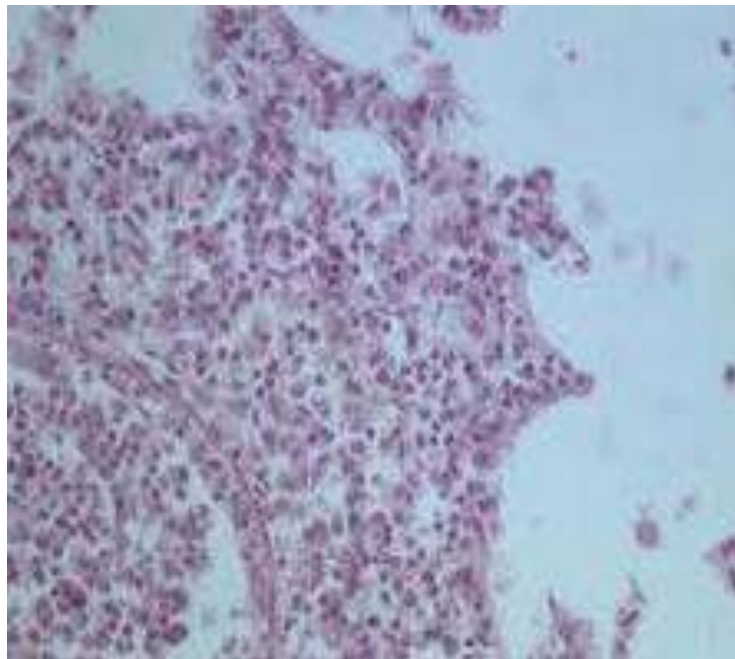


Figure 6.4 An image of *Staphylococcus aureus*  
[<http://www.picsearch.com/pictures/Science/Bacteri>, 2010]

*S. aureus* is ubiquitous and may be part of the human flora found in the axillae, the inguinal and perineal areas and the anterior nares. Von Eiff et al described 3 patterns of carriage: those who always carry a strain, those who carry the organism intermittently with changing strains and a minority of people who never carry *S. aureus* (Eiff, C. et al., 2001). Persistent carriage is more common in children than in adults. Nasal carriers may be divided into persistent carriers with high risk of infection and intermittent or noncarriers with a low risk of infection [Belkum, A et al., 2009]. *S. aureus* can cause a range of illnesses, from minor skin infections, such as pimples, impetigo, boils (furuncles), cellulitis folliculitis, carbuncles, scalded skin syndrome and abscesses, to life-threatening diseases such as pneumonia, meningitis, osteomyelitis, endocarditis, toxic shock syndrome (TSS), bacteremia and sepsis. Its incidence ranges from skin, soft tissue, respiratory, bone, joint and endovascular to wound infections. It is still one of the five most common causes of nosocomial infections and is often the cause of postsurgical wound infections. Each year, some 500,000 patients in American hospitals contract a staphylococcal infection [Bowersox, John, 1999].

In our study, the *Staphylococcus aureus* was diluted by LB culture fluid to an OD600 value of 1.1. The base of a culture dish was fully covered by 0.5 ml of the diluted fluid.

### 6.3 Anti-bacterial tests on Ag, gentamicin and iodine

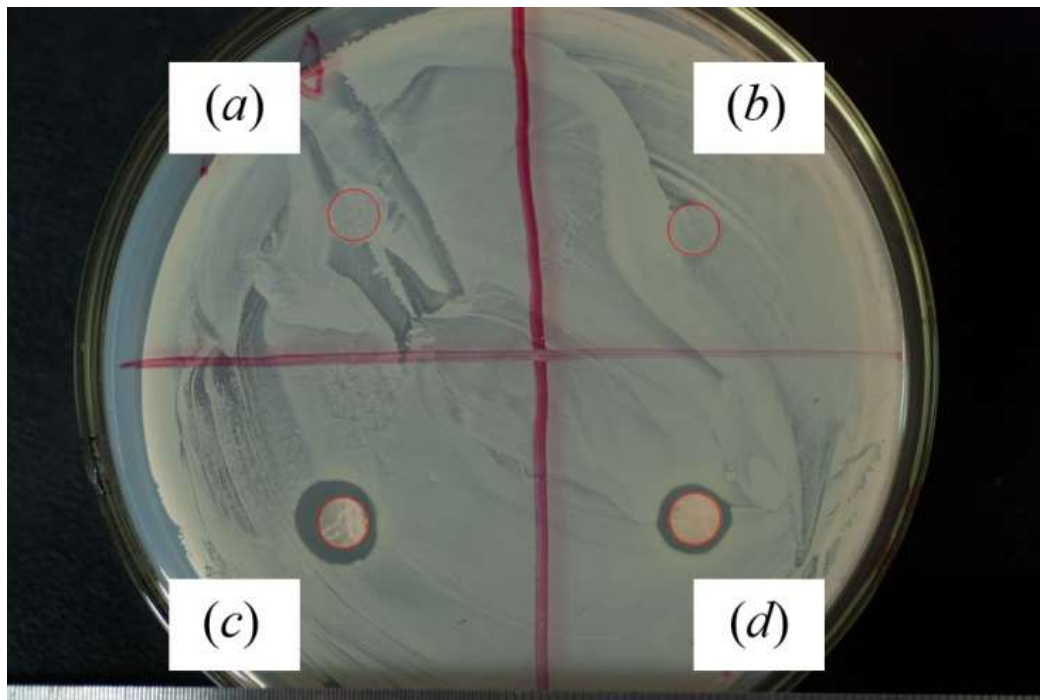


Figure 6.5 Bacteria test after 6 hours of incubation at 37°C, for EVOH nanofibres encapsulated with (a) no agent, (b) gentamicin, (c) Ag nanoparticle, (d) iodine.

Figure 6.5 shows culture dishes for samples containing different anti-bacterial agents after 6 hours of incubation at 37 °C. The dark shaded rings surrounding the samples (the 10 mm diameter pads are marked in Figure 6.5 with red circles) are the bacteriostatic loops where *Staphylococcus aureus* from which had been eliminated. The bigger the outer diameter of the rings (bacteriostatic loop diameter), the stronger was the anti-bacterial effectiveness.

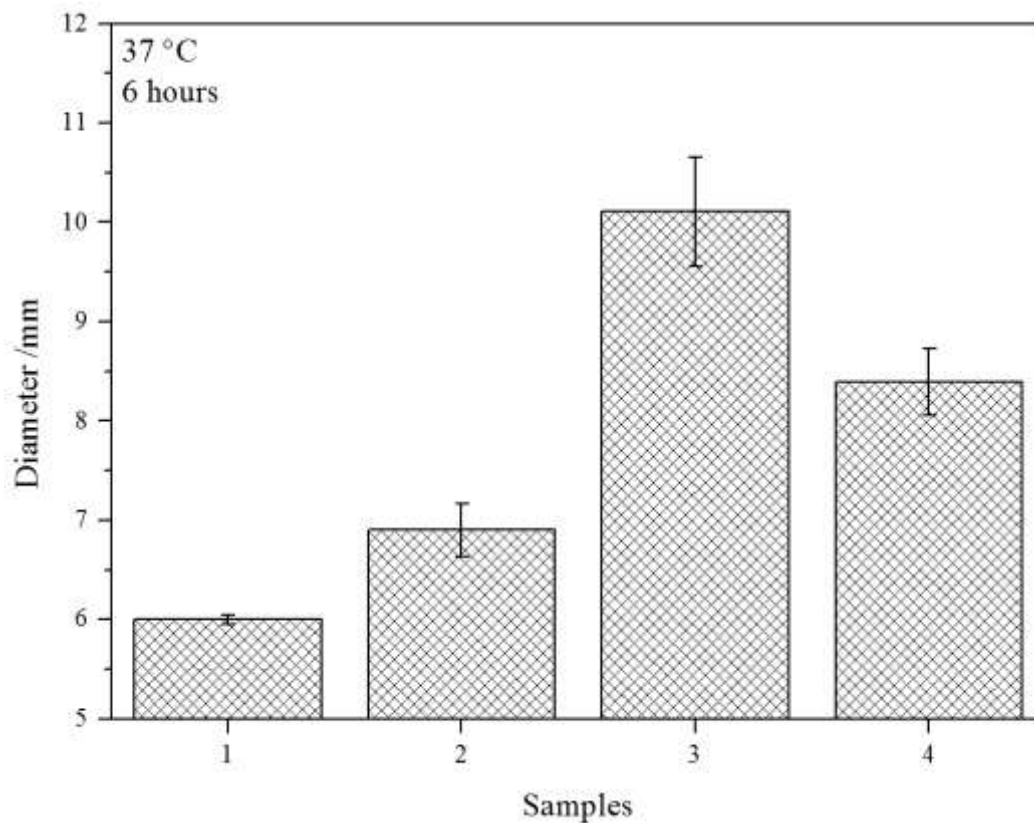


Figure 6.6 Average diameter of the bacterial loop for: EVOH nanofibre containing: 1) no agent; 2. Gentamicin; 3. Ag nanoparticles; and 4. iodine.

Figure 6.6 shows the measured diameters of the anti-bacteriostatic loops. Nanofibres containing Ag nanoparticles clearly demonstrate the highest germ killing capacity amongst all the samples with different anti-bacterial agents under the densities tested. Two reasons have been identified as contributing to reason that Ag performs better than iodine and gentamicin: 1. The electro-spinning process cannot work properly to produce good quality fibres when the concentration of iodine and gentamicin is increased to 0.1 ml and 0.25 ml per 10 ml EVOH solution. For this reason, the tests were limited to the concentration level where nanofibres could be produced; and 2. The anti-bacterial function of iodine and gentamicin may be damaged by the fabrication process, for example, by being subjected to high voltage and high temperatures (circa 50°C for a prolonged duration), though this was not quantified due to the difficulty of finding suitable equipment in the lab to pursue further study of this question. Furthermore, the stability of Ag is much greater than that of either iodine or gentamicin when it comes to the long term storage of the nanofibre dressing. Cost is a further reason:

as the consumption of iodine and gentamicin is much higher than that of  $\text{AgNO}_3$ , it makes Ag a much more attractive choice as the anti-bacterial agent for EVOH nanofibre mats. For these reasons, the research focused on nanofibre mats with Ag because of their performance in varied concentrations and their success in animal tests.

#### **6.4 Anti-bacterial tests on different concentrations of Ag particles**

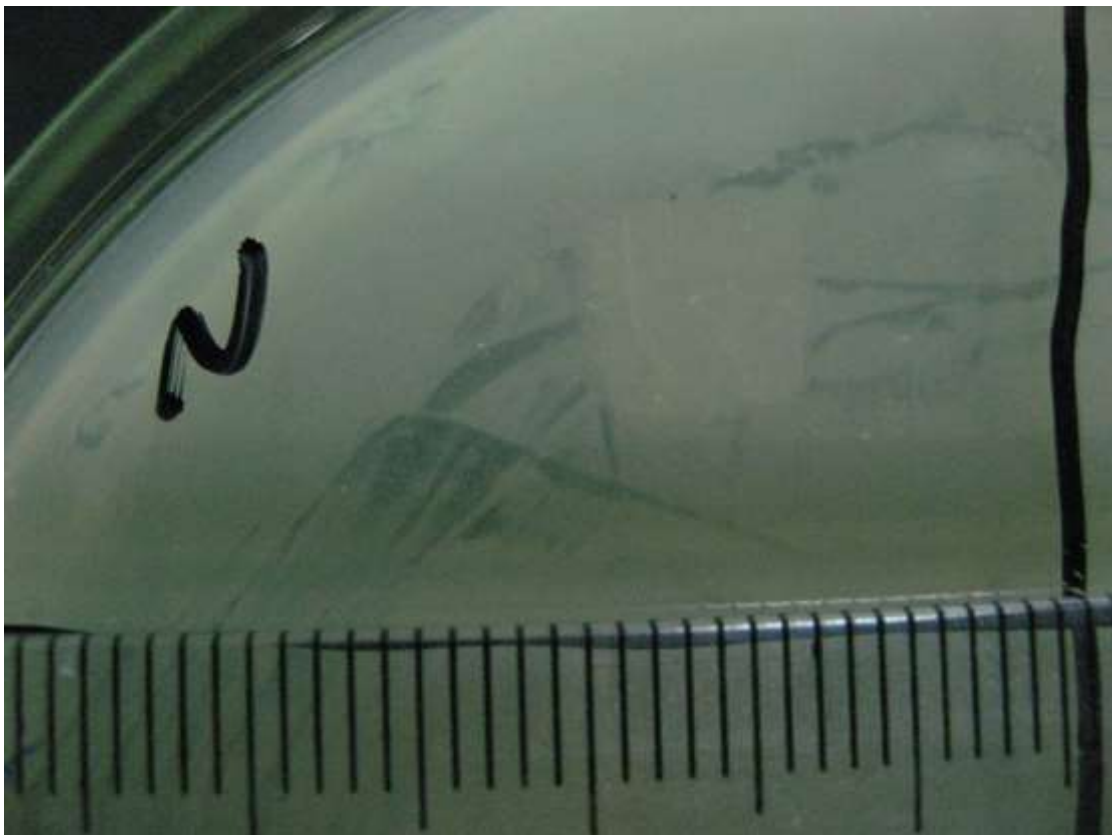


Figure 6.7 An image of EVOH fibre without Ag, iodine and gentamicin in the bacterial test



Figure 6.8 An image of one set of cultures in a test for Bacteriostatic Loop measurement

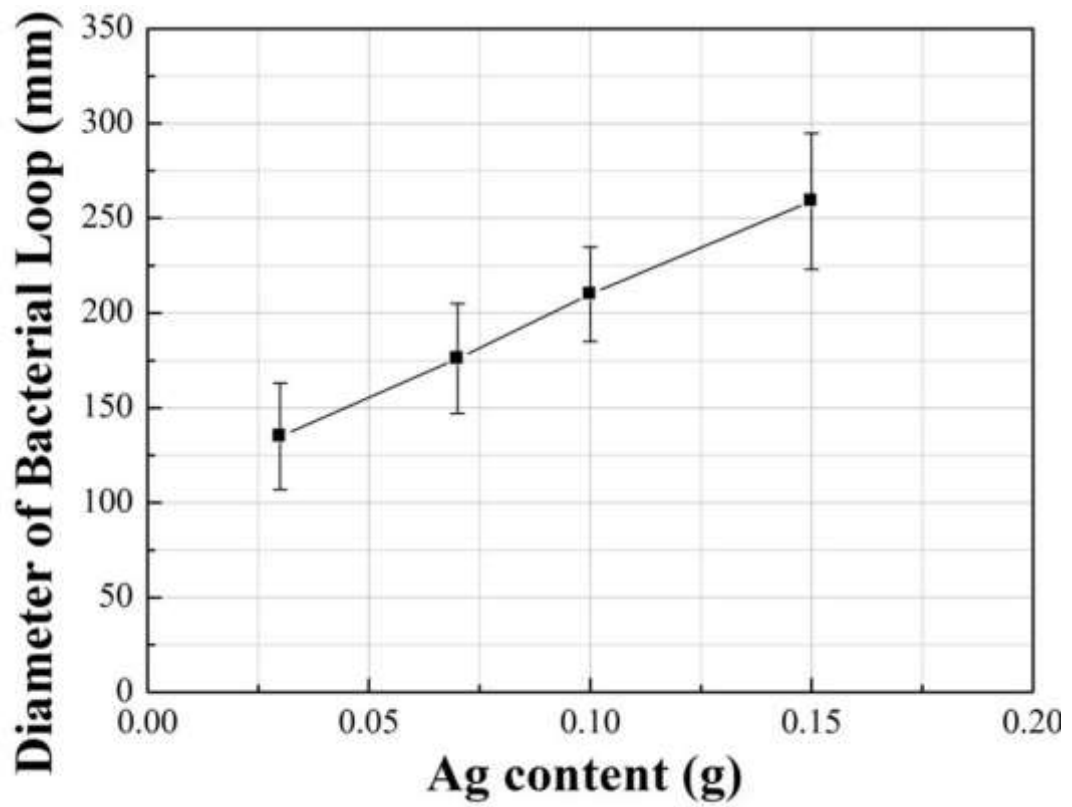


Figure 6.9 Averaged measurement of the Bacterial Loop diameter vs. Ag concentration (wt/10ml)

To assess the pathogen restraining ability of the Ag-encapsulating nanofibres, we performed bacterial tests on EVOH fibres with different Ag concentrations. We produced 4 samples with different Ag content, i.e., 0.03, 0.07, 0.1 and 0.15 grams of Ag, respectively, in 10 ml 7.5wt% 80%/20% 2-propanol/water solution, as shown in Figure 6.6 and EVOH fibres without Ag, shown in Figure 6.5. The results of the bacterial tests are based on the measurements of the Bacteriostatic Loop. The diameter of the various Bacteriostatic Loops [Zheng Qixing, et al., 2010] were measured after culture, as illustrated in Figure 6.7. A linear increase in their effectiveness is found in the four concentrations used, with the highest Ag concentration yielding the biggest loop for fibre patches of the same area, clearly indicating a stronger pathogen restraining effect. In contrast, no Bacteriostatic Loop was observed for pure EVOH fibres with Ag, indicating that there is no pathogen restraining ability for fibres without Ag (Figure 6.5).

In this study, no biodegradable tests were carried out on the nanofibres, though this feature of the EVOH is well known [El-Refaie Kenawya,2003]. Some challenges remain in the simulation of the temperature, moisture and, importantly, the PH value in the environment of a skin wound and variations of these features during the application of the fibres. This is a potentially important feature because it may determine the release speed of the Ag particles which are not on the surface of the fibre and of any drugs which can be contained in the fibre. This remains a key test to be conducted in any studies that follow.

## **6.5 Animal tests**

### **6.5.1 The license, site and protocol of the animal test**

The animal tests were completed in a cooperating university in China, which is called the Xi'an Jiaotong University. The whole testing process was held in the medical school of Xi'an Jiaotong University. The operation process was carried out by a medical group from the medical school in Xi'an Jiaotong University and the operations were complete finished under a full anaesthetic effect. This medical

school and the group responsible are fully licensed. The entire process for the animal tests were monitored by a lab supervisor.

### 6.5.2 The design, make and test of a burn machine



Figure 6.10a The burn machine

In order to carry out the animal tests for skin burn healing, the amount of heat applied on the animal skin or skin burn wounds needs to be quantified.



Figure 6.10b The touching point of a burn machine for making level 3 skin burn wounds

To achieve this, it was necessary to construct a burn machine (Figure 6.10a), because no such device existed. It was designed to have 3 main parts: a), a 2000 watt electric iron to provide controllable and continuous source of heat; b), a real-time temperature sensor to provide feed to the control system; and c), a control system to provide control for both temperature and time with by means of a display. Figure 7.10b shows the touching surface on which skin burn wounds could be made. It is made of a copper rod, which can produce temperatures of up to 300°C with a time control. The whole system was developed in house, including the design, construction and calibration. The working set-up is shown in Figure 7.10a.

### 6.5.3 The process of animal testing



Figure 6.11a The skin burn wounds were produced at a temperature of 150°C applied for 60 seconds.

To choose the testing animal for this study, pigs were obtained from the University animal test centre. Four piglets aged 6 months were used. The animals were quarantined for 10 days before the tests started. After the animal had been fully anesthetized, using pentobarbital sodium, the burn machine was applied to produce skin burn wounds at designated locations, as shown in Figure 6.11a The skin burn wounds were produced at a temperature of 150°C applied for 60 seconds, leading to an equivalent of a second degree burn in the clinical category.



Figure 6.11b The skin burn wound covered EVOH nanofibrescontaining Ag nanoparticles.

Staphylococcus aureus was then applied to the surface of the burn wounds. The Staphylococcus aureus was the same as had been used in the anti-bacterial tests. The purpose was to stimulate accelerated infection in order to test the bacteriostatic ability of theEVOH nanofibres containing Ag.

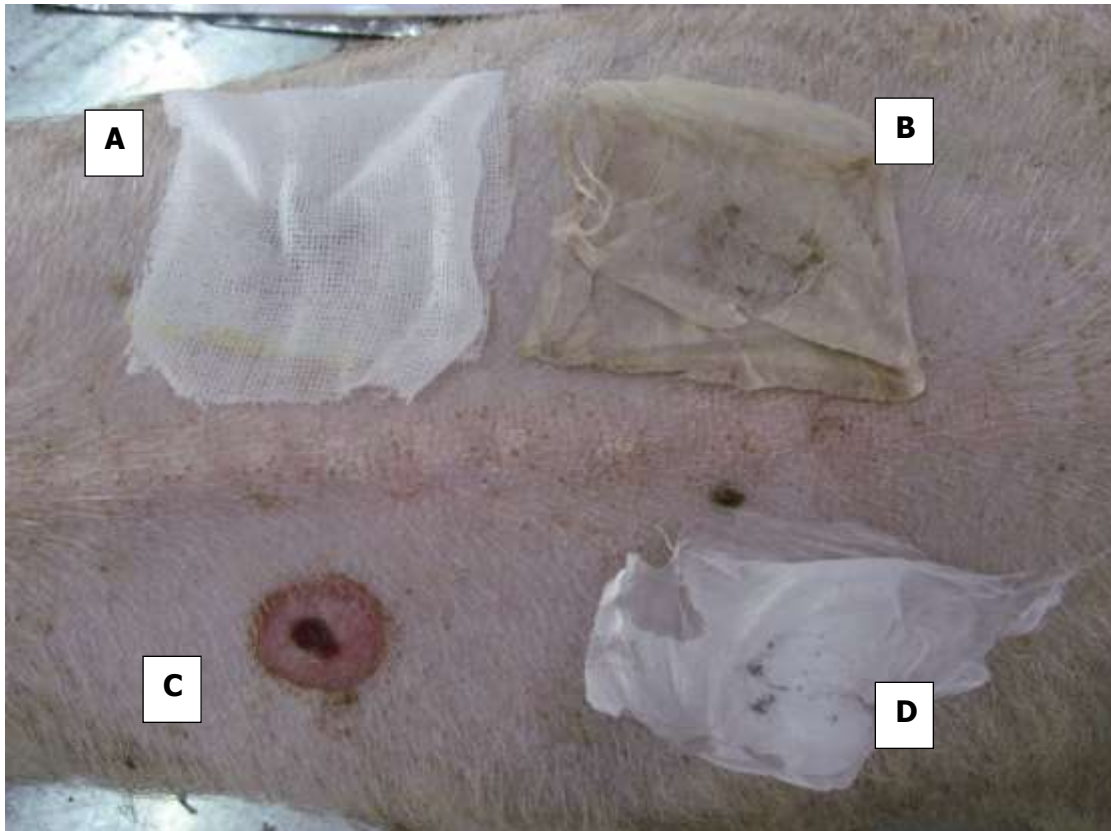


Figure 6.11c Skin burn wounds covered in different materials: A- Traditional cotton dressing with Vaseline; B- EVOH nanofibre with Ag; C- Normal bandage only; D- EVOH nanofibres without Ag.

Figure 6.11c shows the third step, which was to enswathe the burn wounds with different materials. The wounds were then covered with different dressings, including a traditional material, which is made from a cotton bandage covered with Vaseline as applied to location A in Fig. 7.11c. Location B was covered by EVOH nanofibres with Ag (the concentration is 0.07, as shown in Figure 6.7). Location C was covered directly with a normal bandage without anything else being applied. Location D was covered by EVOH nanofibres without Ag nanoparticles.



Figure 6.11d The burn wound areas were enswathed by normal bandage

Finally the wound areas were all protected with a normal bandage.

The burn areas were examined after the first 72 hours and then every 24 hours until they were fully healed.

#### 6.5.4 Results of the animal tests



Figure 6.12a A skin burn wound covered by EVOH nanofibres containing Ag nanoparticles after 72 hours

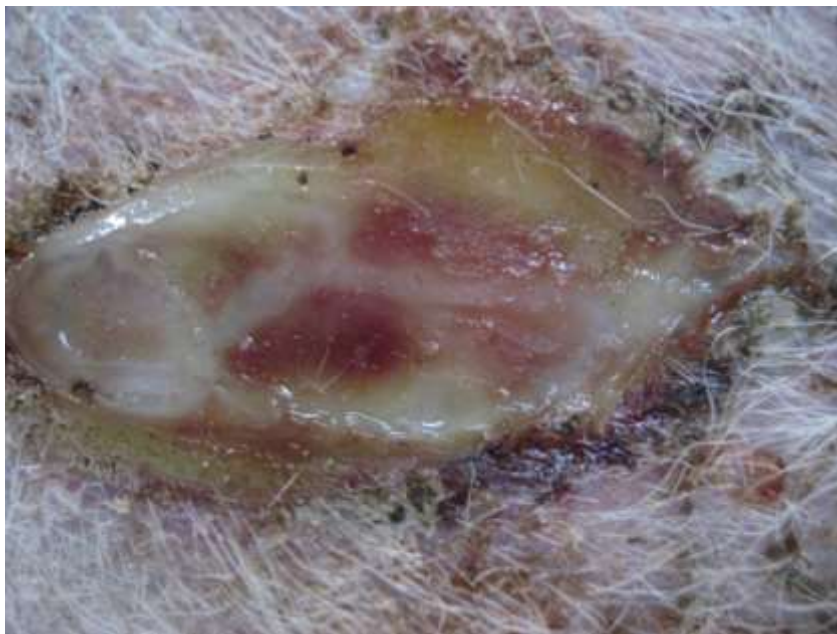


Figure 6.12b A skin burn wound covered by traditional material after 72 hours

Figure 6.12a and 6.12b show the skin burn in Locations B and C respectively after the first 72 hours. The wound in Figure 6.12a had been covered by EVOH nanofibres with Ag. It shows that the surface of the wounds was very dry and without infection, already in the process of recovering. The burn area in Figure

6.12b was covered by cotton roll; here the wound surface shows signs of full infection with *Staphylococcus aureus*. The white discharge is pyogenesis as the consequence of the infection. The other two wound locations were in the same situation, as seen in Figure 6.12b.

## **6.6 Chapter summary**

First of all, the reason of using the *Staphylococcus aureus* for the anti-bacteria tests was clearly discussed in this chapter.

Secondly, the methods and process of the anti-bacteria tests were clearly performed. The results show that the 80 °C solution and electro-spinning process both did not reduce the bacteriostatic ability of the Ag nanoparticle EVOH nanofibres. Besides, the bacteriostatic abilities have been qualified in this chapter.

Overall, the bacteriostatic ability of the Ag nanoparticle EVOH nanofibre was clearly observed in all the animal tests. However, the animal study was not fully completed due to time constraints; more tests could have been carried out. This study was also limited by its budget and the lack of medical knowledge in clinical aspects.

## **7. Conclusions and future work**

### **7.1 Conclusions**

One of the conclusions which have been reached is that nanotechnology is at an extraordinarily new and exciting phase and also that nanotechnology has the potential to play a major role soon in the future technological achievements of mankind, in the military field, the information technology field and, in its potential to benefit mankind, in the medical field in general.

The phenomena of electro-spinning have been known about since the sixteenth century, while the patent for electro-spinning was obtained in 1902. Although the technology of electro-spinning has been developing for a few hundred years and it is a very simple process, which requires nothing more than simple laboratory equipment to yield polymer fibres down to the nano scale, the science behind it is not simple at all. The electro-spinning process involves the understanding of electrostatics, fluid rheology and the properties of polymer solutions, such as the rate of solvent evaporation, the surface tension and the conductivity of the solution. These fundamental properties are constantly interacting and influencing each other during the electro-spinning process.

The versatility of electro-spinning also means that fibres of different morphology and made of different materials can be made directly or indirectly by electro-spinning. Therefore, different polymers, blends, mixtures or precursors can be used to make into fibres to suit specific applications. Understanding the basics behind the materials and the fundamentals which affect electro-spinning will open new avenues and applications for electro-spun fibres.

After the part of theoretical study and the electro-spinning system and laboratory set up, there are the main achievements in this study shown below:

First of all, the controlling parameters (the inter-relations between EVOH fibre diameters and applied voltage, distance and solution density etc.) in the electro-spinning process have been achieved due to controlling any electro-spinning process is very important to investigate the parameters which

influence it. Besides, this work is very useful, because it was not discovered before, this will provide useful information for the people working in this area. This is an art demanding trial and error methods. The complexity of the fabrication process is such that an analytical modeling to predict the fibre outcome is unlikely to be achievable, in particular in the unstable spinning which combines both the stretching and the drying out of a fine jet of liquid into fine fibres on a nano scale. But through trials to vary the controlling parameters, electro-spun fibres of different diameters, fibre surface porosity, beaded and non-beaded can be produced. Depending on the application, fibres with different morphology and structures can be produced by using specific parameters and setups. The type of fibre mesh produced can also be varied by using different electro-spinning setups. Tubular scaffolds and yarns, made of both aligned and random fibres can already be produced. Structures made of fibres arranged in specific patterns may also be produced through the electro-spinning process. All these are made possible by the manipulation of the external electrical field and by using different types of collector. With greater understanding of the electro-spinning process, we may be able to gain a greater control over the behaviour of the electro-spinning jet and its resultant fibres.

Secondly, EVOH was selected for this study due to its proven biocompatibility and good mechanical properties. This study had identified the working windows for the fabrication of EVOH nanofibres in a range of different diameters. Characterization was carried out by microscopy using both an SEM and TEM, also for measuring and calculating the EVOH fibre diameter. With the development of a new generation of dressing material in mind, in particularly in the case of burn injuries, the research proceeded to investigate the mechanical properties and germ killing functionality of the newly developed material.

Thirdly, as the dressing materials will mainly be used under tension, not only to produce a needed wrapping, but also to produce pre-tension, a pressure effect will be generated on the wound surface to reduce the blood flow and to produce a harder protective layer. Thus our tests were focused mainly on uniaxial tensile loading. The mats show a type response as a non-woven material with random fibre orientations. A linear response is shown at low strain values, followed by nonlinear elastic behaviour, then the yield and a long range of mild strain

hardening shows in large strains. The failure mechanism is a typical torn type with fibre breakage and pull-out. Unloading tests allows a 0.4% proof yield stress to be quantified and this is shown to be in the magnitude of kilo-Pasca (Kpa). The unloading tests were conducted to identify the yield stress corresponding to 0.4 or 0.5% proof strain was presented and achieved. The Young's modulus  $E$ , taking as the tangent from the origin, and the linear hardening modulus  $KP$  as the tangent of the plastic range from the yield point were obtained. A straight line from the origin to the yield point was also drawn, giving the slope  $E_y$ .  $E_y$  is of a lower value than  $E$  and can be used as an approximate Young's modulus if the materials are not highly non-linear, as in the present case. To qualify the damage parameter of the 3 different EVOH nanofibre sheet samples, the unloading and reloading tests were carried out to see how damage might occur to the samples.

Finally, three different bacterial agents (Ag, iodine and gentamicin) were added to the nanofibres and the issues encountered in the fabrication were achieved and discussed. Moreover, the degradation tests in the conditions of water, PBS and UV lights were completed, and the results show that the EVOH nanofibres can only be degraded quickly under the UV lights condition which perfectly fits the requirements of a dressing material. Tests both *in vitro* (the bacterial culture test) and *in vivo* (the animal test) confirm the superiority of nanofibre mats containing Ag nanoparticles as an effective dressing material which has a better bacteria suppressing function than other anti-bacterial agents tested at the same time. Degradation tests were also carried out to confirm that EVOH fibres are stable in simulated human body liquid at body temperature, but disintegrate rapidly in the illumination of x-rays, which could be used as a means to accelerate Ag particle release where appropriate.

## 7.2 Future work

Much work remains to be done in the future. Three key recommendations are listed below:

1. Based on the fabrication of the electro-spinning EVOH nanofibres, the mechanical property test of an EVOH nanofibre sheet presents a dressing material which can be subjected to stretching, tearing, cutting and other types of

mechanical loading for its potential use. This test was completed at a room temperature in the range 18°C- 26°C but future work should repeat and complete the tests at lower temperatures and higher temperatures by using both the Instron 8500 and the DMA.

2. The Ag nanoparticles release test and degradation test were completed at the temperature of the human body (37°C) under different conditions, for example, water, PBS solution, sunlight and UV light. The future work on this part should change the temperature and test conditions and should test such things as the release speed of Ag nanoparticles under infrared light at -20°C to -40°C etc.

3. The animal tests were completed and the result plainly shows the bacteriostatic ability of the EVOH nanofibres with Ag nanoparticles on the wounds surface. The future work on this part should focus on the qualifying data from the animal tests.

## Appendices

### Appendix A:

Dynamic Mechanical Analysis 8000 (DMA 8000) is widely used to characterize the bulk properties of materials such as modulus, compliance and damping (tan delta). It measures changes of rheological behavior under dynamic conditions as a function of temperature, time, frequency, stress, atmosphere or a combination of these parameters. Stress-strain, creep recovery or thermo mechanical measurements are only a few examples of the possible uses of DMA. The creep tests were set up similarly to the relaxation tests reported in Appendix A in the thesis, except that the static force was set as automatic in the “Creep” mode provided by the manufacture. The results shown in Figure 7.2a , 7.2b and 7.2c. A1-A3 clearly show that the “creep” effect in increased elongation of the sample and reduced reaction force in tension. However, this “duo” change causes difficulties in data analysis as the effects from both the time and temperature are lumped together. It is intended at the next stage of research to address this issue and identify separate time and temperature effect on the tensile properties of EVOH nanofibre mats, including low temperature from  $-50^{\circ}\text{C}$ .

The tension mode is very useful for the analysis of thin films and fibres or can be used for bar samples with no static force if information in their expansion is required.

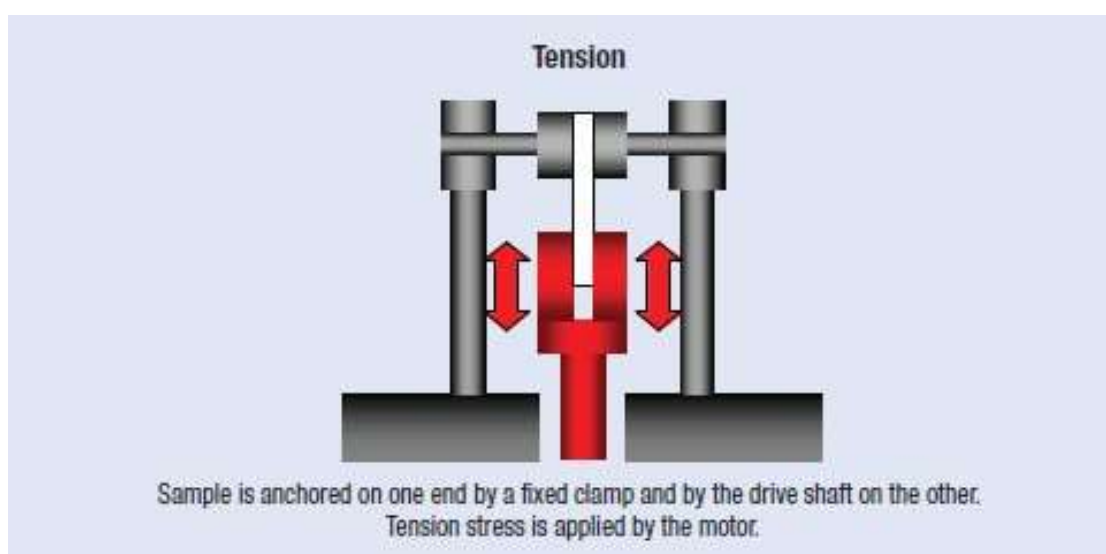


Figure 7.1 Sample holder for the Tension mode

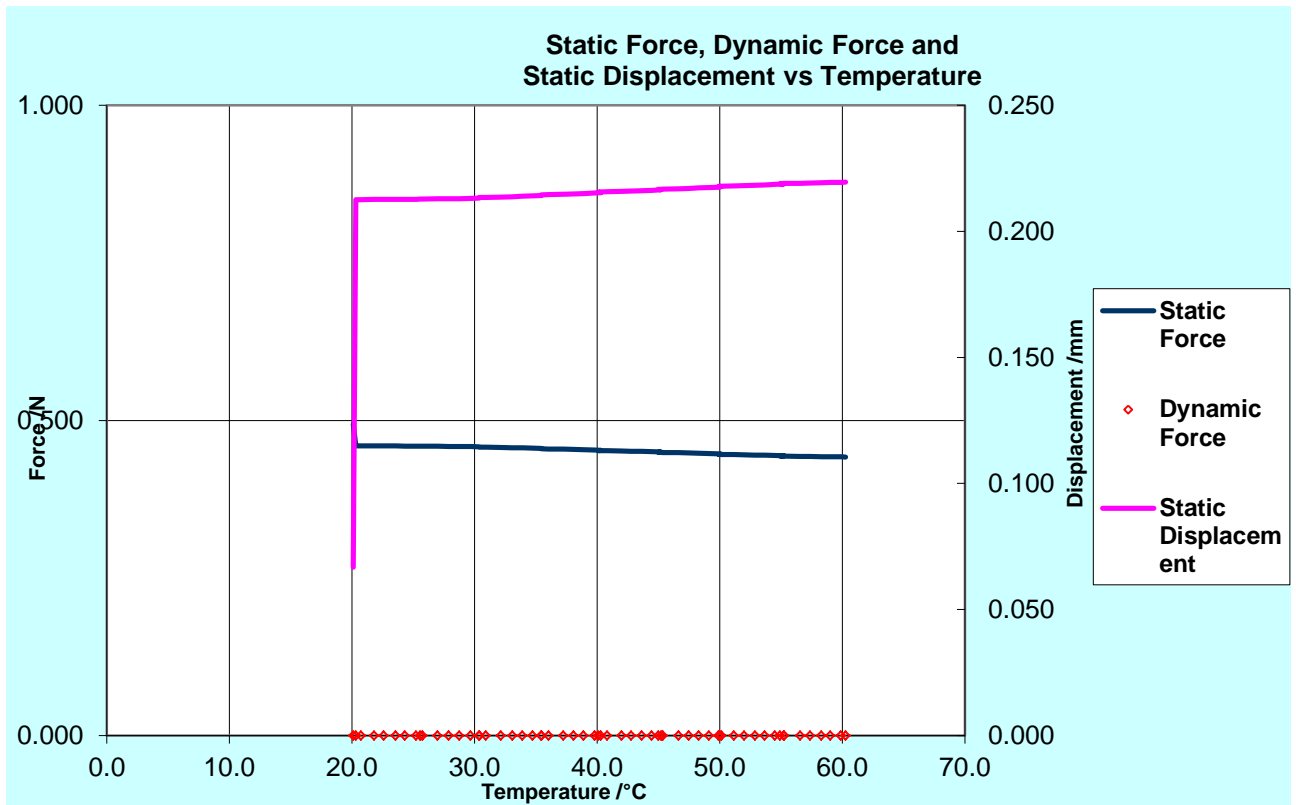


Figure 7.2a DMA creep test on 7.5% EVOH nanofibre sheets from 20 °C to 60 °C

Figure 7.2a shows the creep relaxation test of 7.5% EVOH nanofibre sheets on the DMA from room temperature to 60 °C. In this creep relaxation test, the dynamic force is zero. Because the purpose of this test is to check when the static force is applied on the EVOH nanofibre sheets, how the static displacement response by time and temperature increasing. Figure 7.2a shows when the static force was applied on the EVOH nanofibre sheets the static displacement was stable when the temperature increasing. In other words, the trend lines of the static force and the static displacement are performed as parallel lines.

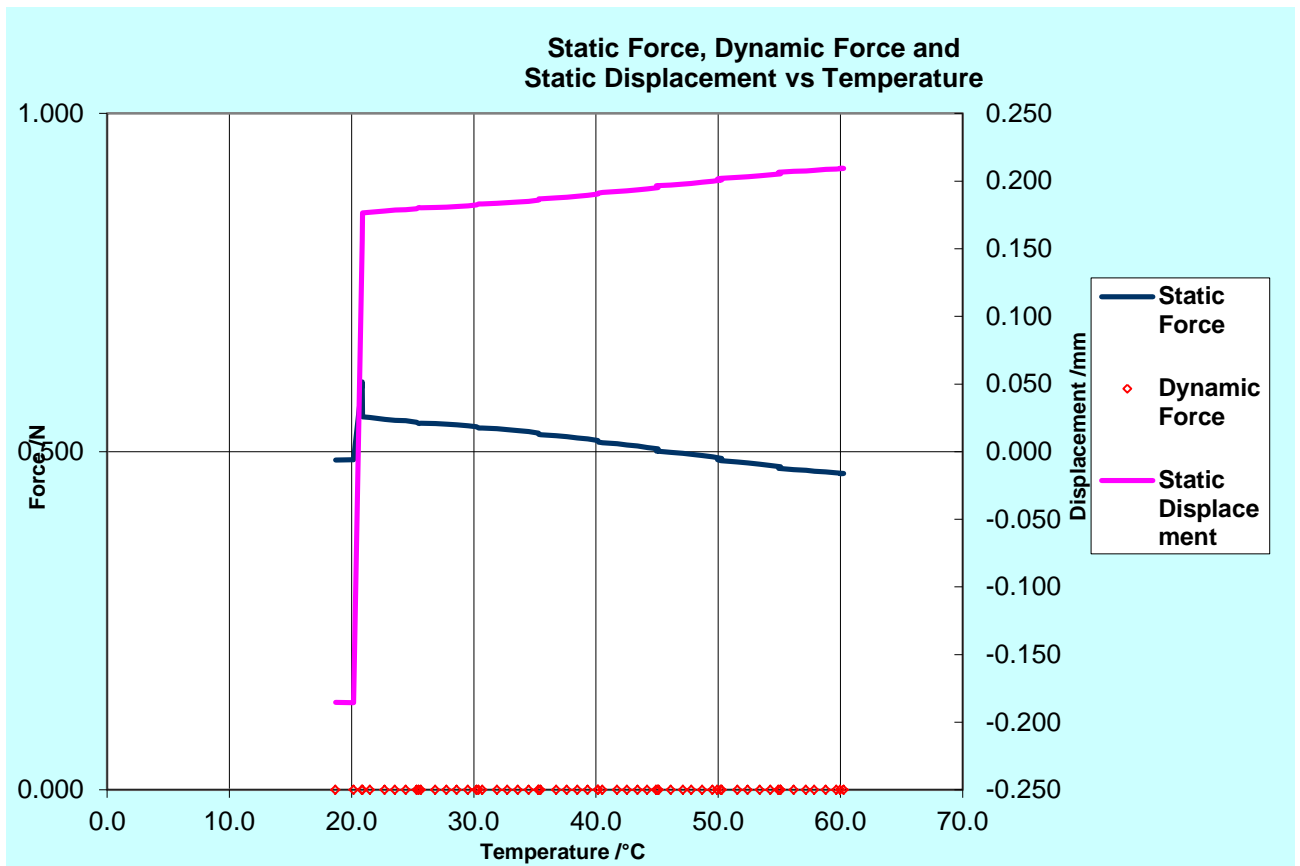


Figure 7.2b DMA creep test on 10% EVOH nanofibre sheets from 20 °C to 60 °C

However, in figure 7.2b, the trend lines of the static force and the static displacement for 10% EVOH nanofibre sheets started being unstable, which is not as parallel as figure 7.2a shown.

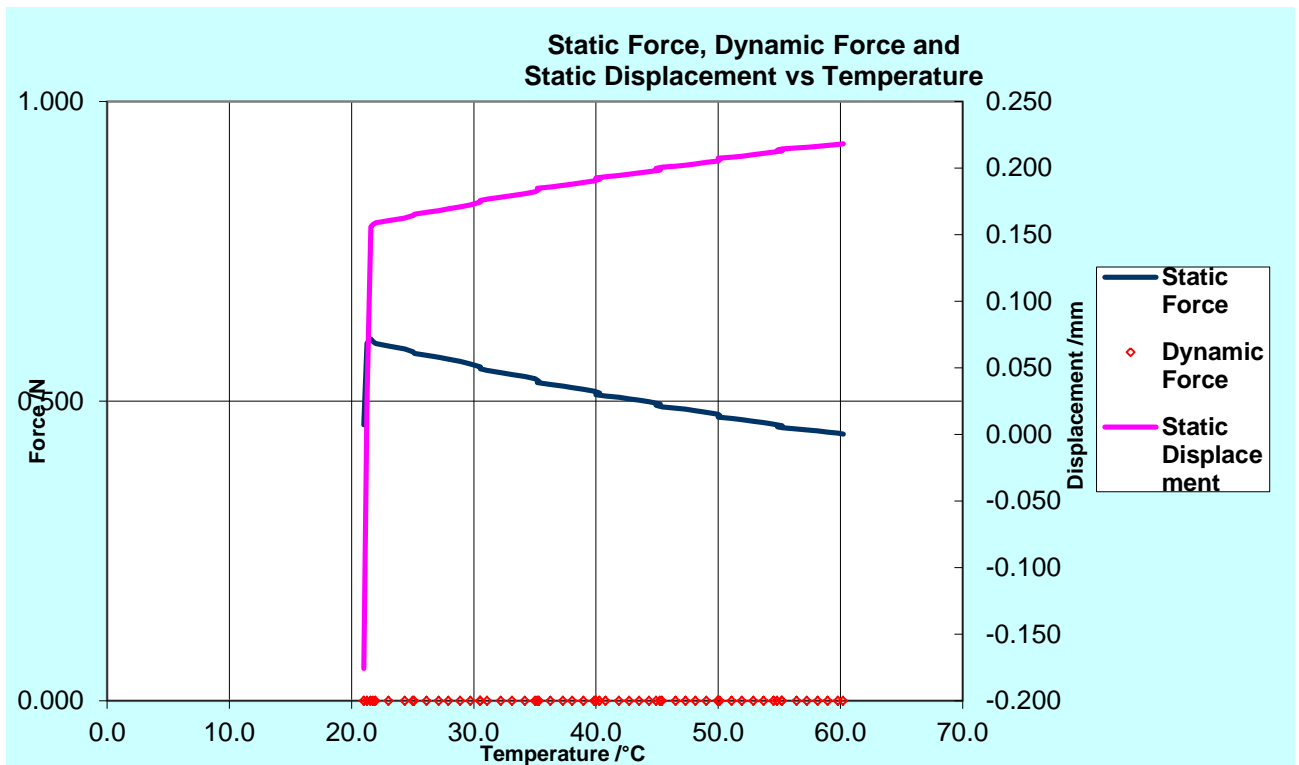


Figure 7.2c DMA creep test on 12.5% EVOH nanofibre sheets from 20 °C to 60 °C

In the figure 7.2c, the unstable situation of the 12.5% EVOH nanofibre sheets in the creep relaxation test when the temperature was increasing. The reason may be when the density of EVOH polymer solution is increased, the EVOH nanofibre diameter will be increased. Therefore, less space was left between the EVOH nanofibres. When surface volume was decreased which means the inter-connections between EVOH nanofibres have been dense, therefore, this can cause the static displacement become sensitive when the static force is applied.

We have also tested the 7.5%, 10% and 12.5% EVOH nanofibre sheet samples from -40 °C to 60 °C. All the 7.5%, 10% and 12.5% EVOH nanofibre sheet samples stay stable. From the macroscopical point of view, there was no change on the three EVOH nanofibre sheet samples comparing with the original samples before the creep tests.

### Viscoelastic tests

Polymer materials show viscous behavior under the temperature effect. For EVOH nanofibre mats, this behavior needs to be characterized under the

temperature range within which the material is to be used. This test was carried out for the three groups of samples from ambient temperature to the half melting temperature of EVOH where glass transition starts to occur. The melting temperature of EVOH is 129 °C, so the temperature range of the test was set from 30 to 60 °C. A special equipment DMA 8000 (Dynamic Mechanical Analysis 8000, PerkinElmer) for calibration of material's bulk properties was used.

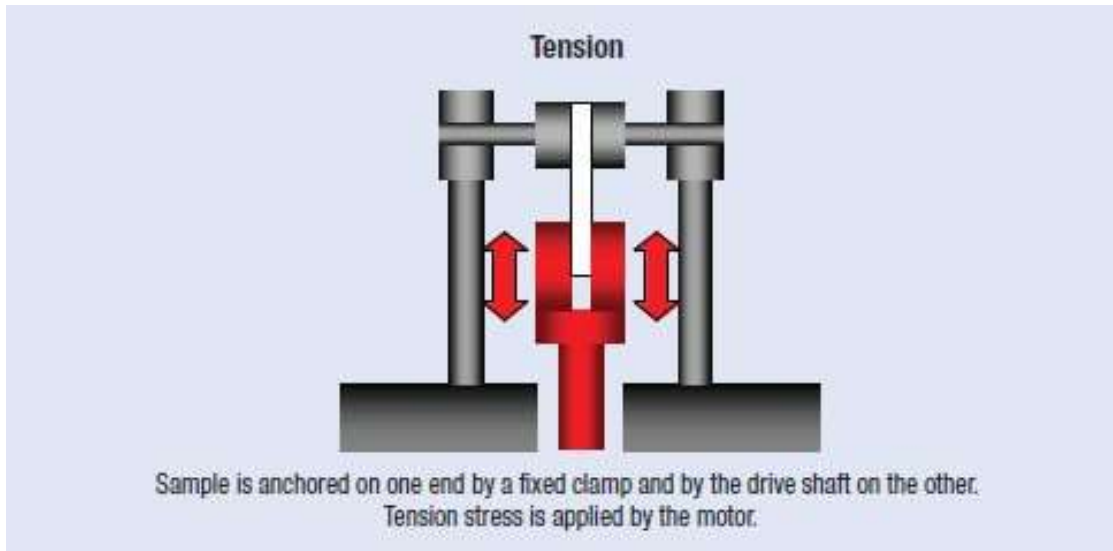


Figure 7.3 Sample holder for the Tension mode

Figure 7.3 shows the setup of the test mode where the sample (white colour) is pulled by the holder (red colour). Both dynamic and static forces can be applied. Samples of rectangular shape were cut into the size 10 mm by 8 mm, as required by DMA8000. This was done by clamping the sample sheet between glasses plates and cut by a sharp blade. Once mounted into the instrument, the crosshead distance is 10 mm. Test is fully program controlled. Once set, it is carried out automatically with live data display.

Figure 7.4 (a to c) shows the creep relaxation test of nanofibre sheets from around 30 (35) to 60 (55)°C. In this creep relaxation test, the dynamic force was set zero, and the static force was kept at 0.1N. The samples show a clear creep response in continuing displacement under a non-increasing tensile loading. The J-shape of the curve at the beginning of test indicates fibre alignment to the test direction and a range of linear behavior is exhibited. The alignment or rearrangement of fibres (involving inter-fibre actions such as friction etc.) shows

an increasingly stronger effect in samples of larger fibres as evidenced by the waving of the test curves. When the temperature increases towards the half-melting temperature, the increase in the displacement start to reduce.

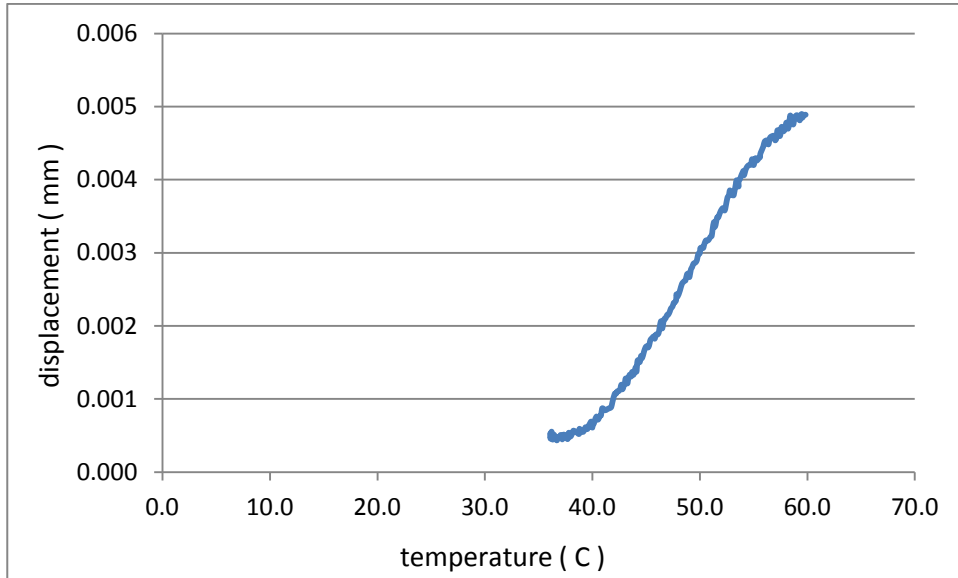


Figure 7.4a Displacement – temperature curve of 7.5% sample under 0.1N constant tensile load.

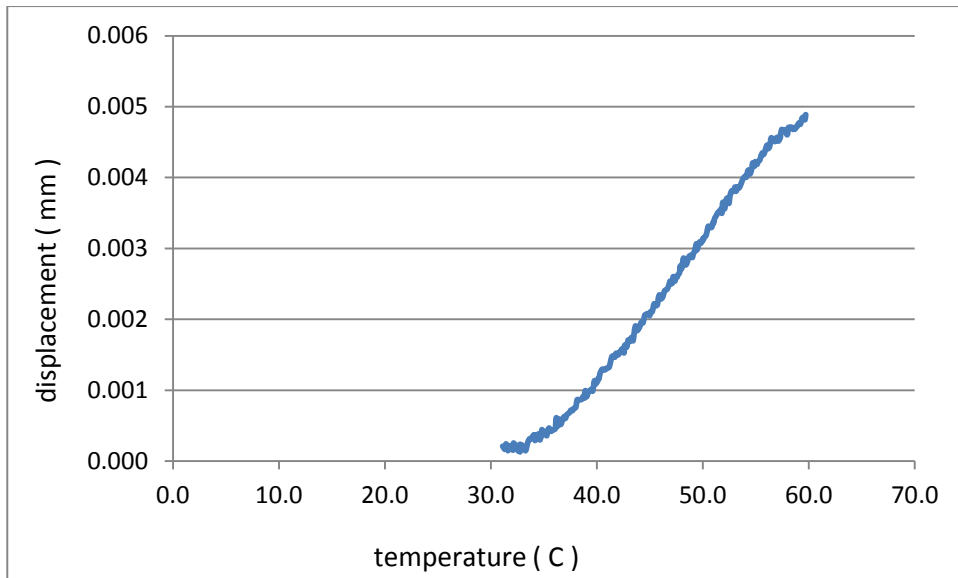


Figure 7.4b Displacement – temperature curve of 10% sample under 0.1N constant tensile load.

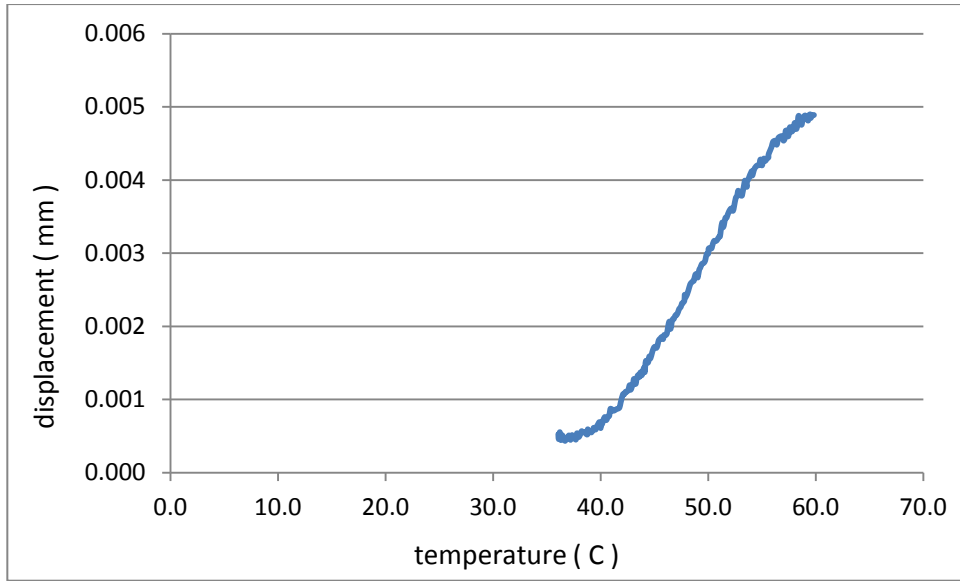


Figure 7.4c Displacement – temperature curve of 12.5% sample under 0.1N constant tensile load.

Due to the time constraint of this project and the need for calibration of the DMA device, the frequency/temperature dependent properties of EVOH have not been completed.

## Appendix B:

Quoted from A review on polymer nanofibers by electrospinning and their applications in nanocomposites.

No.	Polymer	Details	Solvent	Concentration	Perspective applications
1	Nylon6,6,PA-6,6		Formic acid	10 wt.%	Protective clothing
2	Polyurethanes, PU		Dimethyl formamide  Dimethyl formamide	10 wt.%  10 wt.%	Protective clothing  Electret filter
3	Polybenzimidazole, PBI		Dimethyl acetamide	10 wt.%	Protective clothing  nanofiber reinforced composites
4	Polycarbonate, PC	$M_w = 60,000$  $MI = 8-10g/10\text{ min}$	Dimethyl formamide: tetrahydrofuran (1:1)  Dichloromethane  Chloroform, tetrahydrofuran  Dimethyl formamide: tetrahydrofuran	10 wt.%  15 wt.%  14-15 wt.%  20 wt.%	Protective clothing  Sensor, filter  Electret filter

			(1:1) Dimethyl formamide: tetrahydrofuran (1:1)		
5	Polyacrylonitrile, PAN		Dimethyl formamide  Dimethyl formamide  Dimethyl formamide  Dimethyl formamide  Dimethyl formamide	600mgPAN/ 10-5m <sup>3</sup>  Dimethylformamide  15 wt.%	Carbon nanofiber
6	Polyvinil alcohol, PVA	M <sub>n</sub> = 65,000  M <sub>n</sub> = 150,000	Distilled water  Distilled water	8-16 wt.%  4-10 wt.%  1-10 wt.%	
7	Polylactic acid, PLA	Poly(D, L-lactic acid) M <sub>w</sub> =109,000  Poly(L-lactic acid) M <sub>w</sub> =100,000  Poly(L-lactic acid) M <sub>w</sub>	Dimethyl formamide  Methylene chloride and dimethyl formamide	5 wt.%  14 wt.%	Membrane for prevention of surfery induced-adhesion  Sama as above  Sensor, filter  Drug delivery

		=150,000g/mol  $M_w = 205$ kDa	Dichlormethane  Dichloromethane		system
8	Polyethylene-co-vinyl acetate, PEVA	$M_w = 60.4$ kDa		14 wt.%	Drug delivery system
9	PEVA/PLA	PEVA/PLA = 50/50		14 wt.%	Drug delivery system
10	Polymethacrylate (PMMA)/tetrahydroperfluorooctylacrylate (TAN)	0-10% TAN	Dimethyl formamide: toluene (1:9)		
11	Polyethylene oxide, PEO	2,000,000g/mol  $M_w = 400,000$  $M_w = 400,000$  $M_w = 9 \times 10^5$ g/mol  $M_w = 1,000,000$  $M_w = 300,000$  $M_n = 58,000$  $M_n = 100,000$  $M = 300K$  $M = 100K$ to 2	Distilled water  Distilled water  Distilled water  Distilled water and ethanol or NaCl  Distilled water, distilled water and chloroform,  distilled water and isopropanol  Distilled water: ethanol (3:2)	7-10 wt.%  7-10 wt.%  4-10 wt.%  1-4.3 wt.%  4 wt.%  4-10 wt.%  1-10 wt.%  1-10 wt.%  10 wt.%	Microelectronic wiring, interconnects    Electret filter

		M	Distilled water, chloroform, acetone, Ethanol  Isopropyle alcohol + water,  Isopropanol : water (6:1)  Isopropanol : water (6:1)  Chloroform	3-10 wt.%  0.5-30 wt.%	
12	Collagen-PEO	Purified collagen, nominal molecular  Weight 900 Kd  PEO: $M_n =$ 900,000	Hydrochloric acid  Hydrochloric acid (pH = 2.0)	1-2 wt.%  1 wt.%	Wound healing, tissue engineering, hemostatic agents  Wound healing, tissue engineering
13	Polyaniline (PANI)/PEO blend	Pan: $M_w =$ 120,000 Da, PEO: $M_w =$ 900,000Da, Pan/HCSA/PE O: 11-50 wt.%	Chloroform  Camphorsulfonic acid  Chloroform	2 wt.%  2-4 wt.%	Conductive fuber  Conductive fuber  Conductive fuber
14	Polyaniline (PANI)/ Polystyrene		Chloroform  Camphorsulfonic acid	2 wt.%	Conductive fuber  Conductive

					fuber
15	Silk-like polymer with fibronectin functionality		Formic acid	0.8-16.2 wt.%	Implantable device
16	Polyvinylcarbazole	$M_w = 1,100,000$ g/mol	Dichlormethane	7.5 wt.%	Sensor, filter
17	Polyethylene Terephthalate, PET	$M_w = 10,000-20,000$ g/mol	Dichlormethane and trifluoroacetic acid (1:1)	4 wt.%, 12-18 wt.%	
18	Polyacrylic acid-polypyrrene methanol, PAA-PM	$M_w = 50,000$ g/mol	Dimethyl formamide		Optical sensor
19	Polystyrene, PS	$M_w = 190,000$ $M = 200$ kDa $M = 280,000$ $M_w = 280,000$ $M_w = 280,000/$ $M_w = 28,000:$ 90/1  $M_w = 280,000/$ $M_w = 28,000:$ 50/50	Tetrahydrofuran, dimethylformamide,  CS <sub>2</sub> (carbon disulfide), toluene, Methylethylketone  Chloroform, dimethylformamide	18-35 wt.%, 8%, 2.5-10.7%, 25 wt.%,  30 wt.%, 15 wt.%, 15 wt.%	Enzymatic biotransformation  (Flat ribbons) Catalyst, filter Catalyst, filter Catalyst, filter Catalyst, filter

		$M_w = 280,000/$ $M_w = 2,430:$ 90/10	Tetrahydrofuran  Dimethyl formamide  Tetrahydrofuran  Tetrahydrofuran  Tetrahydrofuran  Tetrahydrofuran	15 wt.%  15 wt.%	
20	Polymethacrylate, PMMA	$M_w = 540,000$	Tetrahydrofuran, acetone, chloroform		
21	Polyamide, PA		Dimethylacetamide		Glass fiber filter media
22	Silk/PEO blend	$M_w$ (PEO) = 900,000 g/mol	Silk aqueous solutions	4.8-8.8 wt.%	Biomaterial scaffolds
23	Polyvinyl phenol, PVP	$M_w =$ 20,000,100,000	Tetrahydrofuran	20,60% (wt./vol.)	Antimicrobial agent
24	Polyvinylchloride, PVC		Tetrahydrofuran/ dimethylformamide = 100/0, 80/20, 60/40, 50/50, 40/60, 20/80, 0/100 (vol. %)	10-15 wt.%	
25	Cellulose acetate, CA		Acetone, acetic acid, dimethylacetamide	12.5-20%	Membrane

26	Mixture of PAA-PM (polyacrylic acid–poly(pyrene methanol)) and polyurethane		Dimethyl formamide	26 wt.%	Optical sensor
27	Polyvinil alcohol (PVA)/Silica.	PVA: $M_n = 86,000$ , silica content (wt.%): 0, 22, 34, 40, 49, 59 [132]	Distilled water		
28	Polyacrylamide, PAAm	$M_n = 5,000,000$		1-10 wt.%	
29	PLGA	PLGA (PLA/PGA) = (85/15)	Tetrahydrofuran: dimethyl formamide (1:1)	1 g/20 ml	Scaffold for tissue engineering
30	Collagen		Hexafluoro-2-propanol		Scaffold for tissue engineering
31	Polycaprolactone, PCL		Chloroform: methanol (3:1) toluene: methanol (1:1), and dichloromethane: methanol (3:1)		
32	Poly (2-hydroxyethyl)	$M = 200,000$	Ethanol: formic acid (1:1), ethanol	12, 20 wt.% / 8, 16, 20 wt.%	(Flat ribbons)

	methacrylate), HEMA				
33	Poly (vinylidene fluoride), PVDF	M = 107,000	Dimethyl formamide: dimethylacetami de (1/1)	20 wt.%	(Flat ribbons)
34	Polyether imide, PEI		Hexafluoro-2-pr opanol	10 wt.%	(Flat ribbons)
35	Polyethylene gricol, PEG	M = 10 K	Chloroform	0.5-30 wt.%	
36	Nylon-4,6, PA-4.6		Formic acid	10 wt.%	Transparent composite
37	Poly(ferroceny ldimethylsilan e), PFDMS	M <sub>w</sub> = 87,000 g/mol	Tetrahydrofuran: dimethyl formamide (9:1)	30 wt.%	
38	Nylon6 (PA-6) /montmorillon nite (Mt)	M <sub>t</sub> content = 7.5 wt.%	Hexa-fluoro-isop ropanol (HFIP).  HFIP/dimethyl formamide: 95/5 (wt.%)	10 wt.%	
39	Poly(ethylene- co-vinyl alcohol)	Vinyl alcohol repeat unit: 56-71 mol%	Isopropanol / water: 70/30 (%v/v)	2.5-20% w/v	Biomedical
40	Polyacrylnitril e (PAN) / TiO <sub>2</sub>				Photovoltaic and conductive polymers
41	Polycaprolacto ne (PCL) /	Metals: gold, ZnO,			ZnO: cosmetic use

	metal				
42	Polyvinyl pyrrolidone, PVP				
43	Polymetha-ph enylene isophthalamide				

## Bibliography

ALFREY, E. F. GURNEE & W. G. LLOYD (1966) Diffusion in Glassy Polymers. *J. Polym,Sci. : Part C*, 12, 249-261.

ALLEN DOUGLAS J., JOHNSON KIRK W. & NEVIN ROBERT S. (1994) Hydrophilic Polyurethane Membranes for Electrochemical Glucose Sensors. *Patent 5322063*.

A.L. YARIN, S. KOOMBHONGSE & D.H. RENEKER (2001) *J. Appl. Phys.*, 89, 3018.

ARTHUR S. COLSKY P., ROBERT S. KIRSNER & FRANCISCO A. KERDEL (1998) Analysis of Antibiotic Susceptibilities of Skin Wound Flora in Hospitalized Dermatology Patients. *Arch Dermatol*, p. 3.

BAJPAI A. K. & KANKANE S. (2008) Evaluation of Water Sorption Property and in Vitro Blood Compatibility of Poly(2-Hydroxyethyl Methacrylate) (Phema) Based Semi Interpenetrating Polymer Networks (Ipn). *J Mater Sci: Mater Med*, 19, 1921-1933.

BAUMGARTEN (1971) P.K.J. Colloid. *Interface Sci*, 36, 71.

BELKUM A, VERKAIK NJ, DE VOGEL CP, BOELENS HA, VERVEER J & NOUWEN JL (2009) Reclassification of Staphylococcus Aureus Nasal Carriage Types. *J Infect Dis*, 199(12): 1820-6.

BOWERSOX & JOHN (2007) Experimental Staph Vaccine Broadly Protective in Animal Studies. *NIH*.

BRIGHAM PA M. E. (1996) Burn Incidence and Medical Care Use in The United States: Estimate, Trends, and Data Sources. *J Burn Care Rehabil*, 17, p. 12.

BUCHKO CJ, CHEN LC, SHEN Y & MARTIN DC (1999) Processing and Microstructural Characterization of Porous Biocompatible Protein Polymer Thin Films. *Polymer*, 40: 26, 7397-7470.

CALIF I. (1997) U.S. Markets for Wound Management Products. *Medical Data International*.

CHABY G, SENET P, VANEAU M, MARTEL P, GUILLAUME JC, MEAUME S, TÉOT L, DEBURE C, DOMPMARTIN A, BACHELET H, CAR SIN H, MATZ V, RICHARD JL, ROCHET JM, SALES-AUSSIAS N, ZAGNOLI A, DENIS C, GUILLOT B & CHOSIDOW O (2007) Dressings for Acute and Chronic Wounds: A Systematic Review. *Arch Dermatol*, 143(10): 1297-304.

CHANG H, WIND S & KERSTEIN MD (1996) Moist Wound Healing. *Dermatol Nurs*, 8(3): 174-6, 204.

CHANG MC., KOA CC. & DOUGLASA WH. (2003) Conformational Change of Hydroxyapatite/Gelatin Nanocomposite by Glutaraldehyde. *Biomaterials*, 24, 3087-3094.

CHEN R., HUANG C., KEA Q., HE C., WANG H., & MO. X. (2010) Preparation and Characterization of Coaxial Electrospun Thermoplastic Polyurethane/Collagen Compound Nanofibers for Tissue Engineering Applications. *Colloids and Surfaces B: Biointerfaces*, 79, 315-325.

CHIU H. T., LIN J. M., CHENG T. H. 2 & CHOU S. Y. (2011) Fabrication of Electrospun Polyacrylonitrile Ion-Exchange Membranes for Application in Lysozym. *Express Polymer Letters*, 5, 4, 308-317.

CHOINIÈRE M., MELZACK R., GIRARD N., RONDEAU J. & PAQUIN M. J. (1990) Comparisons Between Patients' and Nurses' Assessment of Pain and Medication Efficacy in Severe Burn Injuries. *Pain*, 40 pp. 143-152.

CHONG E. J., PHAN T. T., LIM I. J., ZHANG Y. Z., BAY B. H., RAMAKRISHNA S. & LIM C. T. (2007) Evaluation of Electrospun Pcl/Gelatin

Nanofibrous Scaffold for Wound Healing and Layered Dermal Reconstitution, *Acta Biomaterialia*, 3, 3, 321-330.

CHRISTINE R. CARLISLE, C. C., MANOJ NAMBOOTHIRY, DAVID L. CARROLL, ROY R. HANTGAN & MARTIN GUTHOLD (2009) The Mechanical Properties of Individual, Electrospun Fibrinogen Fibers. *Biomaterials*, 30, p. 8.

CLAES L. E. (1992) Mechanical Characterization of Biodegradable Implants. *Clin Mater*, 10 (1-2), pp. 41-46.

COLSKY AS, KIRSNER RS & KERDEL FA (1998) Analysis of Antibiotic Susceptibilities of Skin Wound Flora in Hospitalized Dermatology Patients - The Crisis of Antibiotic Resistance Has come to The Surface. *Arch Dermatol*, 134: 1006-9.

COOLEY J. F. (1902) The Process of Electro-Spinning. *U. S. Patent, ed.USA*.

CORTESE B., GIGLI G. & RIEHLE M. (2009) Mechanical Gradient Cues for Guided Cell Motility and Control of Cell Behavior on Uniform Substrates. *Adv. Funct. Mater.* 2009;19: 2961-2968.

DEMIR M. M., YILGOR I., YILGOR E. & ERMAN B. (2002) Electrospinning of Polyurethane Fibers. *Polymer*, 43:33, 3-9.

DEMIR M. M. (2010) Investigation on Glassy Skin Formation of Porous Polystyrene Fibers Electrospun from DMF. *Express Polymer Letters*, 4: 1, 2-8.

DETTA N., ERRICO C., DINUCCI D., PUPPI D., CLARKE D. A., REILLY G. C. & CHIELLINI F. (2010) Novel Electrospun Polyurethane/Gelatin Composite Meshes for Vascular Grafts. *J Mater Sci: Mater Med*, 21: 1761-1769.

DÍAZ JE., FERNÁNDEZ-NIEVES A., BARRERO1 A., MÁRQUEZ M., & LOSCERTALES G. (2008) Fabrication of Structured Micro and Nanofibers by Coaxial Electrospinning. *Journal of Physics: 4th World Congress on Biomimetics, Artificial Muscles and Nanobio, Conference Series 127*, 012008.

DOMRES B., K. D. & RUTCZYNSKA J. (2007) Intermingled Skin Grafting: A Valid Transplantation Method at Low Cost. *Annals of Burns and Fire Disasters*, 10 (3).

DOTTI F., VARESANO A., MONTARSOLO A., ALUIGI A., TONIN C. & MAZZUCHETTI G. (2007) Electrospun Porous Mats for High Efficiency Filtration. *Journal of Industrial Textiles*, 37: 151-162.

DZENIS Y. (2004) Spinning Continuous Fibers for Nanotechnology. *Science*, 304 (5679), pp. 1917-1919.

EIFF C, BECKER K, MACHKA K, STAMMER H & PETERS G (2001) Nasal Carriage as A Source of Staphylococcus Aureus Bacteremia. *Study group. N engl j med*, 344(1): 11-6.

G.A. HOLZAPFEL (2000) Biomechanics of Soft Tissue. HANDBOOK OF MATERIAL BEHAVIOR-Nonlinear Models and Properties. 2000 Paper No.7 edited by Jean Lemaitre, LMT-Cachan, France

Geoffrey Taylor, F.R.S. (1969) Electrically driven jets. *Pr. Roy. Soc. Lond. A*. 313, 453-475

G.C. RUTLEDGE, Y. LI, S. FRIDRIKH, S.B. WANER, V.E. KALAYCI & P. PATRA (2001) *NTC Annual Report M01-D22*.

GREINER A & WENDORFF JH (2007) Electrospinning: A Fascinating Method for The Preparation of Ultrathin Fibres. *Angew Chem-Int Edit*, 46: 5670-703.

EL-REFAIE KENAWYA, J. M. L., JESSICA R. WATKINSA, GARY L. BOWLINB, JAMIL A. MATTHEWSB, DAVID G. SIMPSONC & GARY E. WNEKA (2003) Electrospinning of Poly(Ethylene-Co-Vinyl Alcohol) Fibers. *Biomaterials*, 24, p. 6, 907-913.

K. HERBERT, K TIMMANAGOUDAR (FROST & SULLIVAN) (2005) Nanotechnology: Growth Opportunities and Investment Overview.

<http://www.frost.com/prod/servlet/cpo/40230968>)

KO F., GOGOTSI Y., ALI A., NAGUIB N., ET AL. (2003) Electrospinning of Continuous Carbon Nanofiber Yarns. *Advanced Materials*, 15(14), 1161-1165.

HAN D., BOYCE S. T. & STECKL A. J. (2008) Versatile Core-Sheath Biofibers Using Coaxial Electrospinning Mater. Res. Soc. Symp. Proc., 1094-DD06-02.

HAN D. & STECKL A. (2009) Superhydrophobic and Oleophobic Fibers by Coaxial Electrospinning Langmuir. 25 (16), 9454-9462.

HARTMAN O., ZHANG C., ADAMS EL., FARACH-CARSON MC., PETRELLI NJ., CHASE BD. & RABOLT JF. (2009) Microfabricated Electrospun Collagen Membranes for 3-D Cancer Models and Drug Screening Applications. *Biomacromolecules*, 10, 2019-2032.

HE JH, Wan YQ & Yu JY (2004) Application of Vibration Technology to Polymer Electrospinning. *Int J Nonlinear Sci.*, 5: 253-62.

HINSEY & C. B. D. J. (2006) The Recovery of Diameter and Impulse Conduction in Regenerating Nerve Fibers. *Annals of The New York Academy of Sciences*, 47 (4).

HEYDARKHAN-HAGVALL S, SCHENKE-LAYLAND K, DHANASOPON AP, ROFAIL F, SMITH H & WU BM, ET AL. Three-Dimensional Electrospun Ecm-Based Hybrid Scaffolds for Cardiovascular Tissue Engineering. *Biomaterials*, 29: 2907-14.

HORNCastle J (1995) Wound Dressings. Past, Present, and Future. *Med Device Technol*, 6(1): 30-4, 36.

HSU C. M. & SHIVAKUMAR S.. N,N Dimethylformamide Additions to The Solution for The Electrospinning of Poly (E-Caprolactone) Nanofibers. *Macromol. Mater. Eng.* 289, 334-340.

HUANG Z. M., HE C. L., YANG A., ZHANG Y. Z., XU X., HAN X. J., YIN J. & WU Q. (2006) Encapsulating Drugs in Biodegradable Ultrafine Fibers Through

Co-Axial Electrospinning. *Journal of Biomedical Materials Research*, 77A, 1, 169-179.

HUANG Z. M., ZHANG Y. Z., KOTAKI M. & RAMAKRISHNA S. (2003) A Review on Polymer Nanofibers by Electrospinning and Their Applications in Nanocomposites. *Compos. Sci. Technol.*, 63, 2223-2253.

HUANG Z. M., ZHANG Y.Z. & RAMAKRISHNA S. (2005) Double-Layered Composite Nanofibers and Their Mechanical Performance. *Journal of Polymer Science: Part B: Polymer Physics*, 43, 2852-861.

IGNATIUS A. A. & CLAES L. E. (1996) In Vitro Biocompatibility of Bioresorbable Polymers: Poly(L, DL-Lactide) and Poly(L-Lactide-Co-Glycolide). *Biomaterials*, 17 (8), pp. 831-839.

JAMES N. R., PHILIP J. & YAKRISHNAN A. (2006) Polyurethanes with Radiopaque Properties. *Biomaterials*, 27 (2), 160-166.

J.H. Lee, T.G. Park, H.S. Park, D.S. Lee, Y.K. Lee, S.C. Yoon, J-D. Nam. (2003) *Biomaterials*, 24, 2773-2778.

JIANG Z., YUAN K.-J., LI S. F. & CHOW W. K. (2006) Study of Ftir Spectra and Thermal Analysis of Polyurethane. *Spectrosc. Spectr. Anal.*, 26, 624.

KENAWY ER, LAYMAN JM, WATKINS JR, BOWLIN GL, MATTHEWS JA & SIMPSON DG, ET AL. (2003) Electrospinning of Poly (Ethylene-Co-Vinyl Alcohol) Fibers. *Biomaterials*, 24: 907-13.

KEN HERBERT, KIRTITIMMANAGOUDAR (FROST & SULLIVAN) (2005) Nanotechnology: Growth Opportunities and Investment Overview .

KIM SE., HEO DN., LEE JB., KIM JR., PARK SH., JEON SH. & KWON IK. (2009) Electrospun Gelatin/Polyurethane Blended Nanofibers for Wound Healing Biomed. *Mater*, 4, 1-11.

KRISHNAN S, WEINMAN CJ & OBER CK (2008) Advances in Polymers for Anti-Biofouling Surfaces. *J Mater Chem*, 18(29):3405-13.

- LEE K. H., KIM H. Y., BANG H. J., JUNG Y. H. & LEE S. G. (2003) The Change of Bead Morphology Formed on Electrospun Polystyrene Fibers. *Polymer*, 44: 40, 29–4034
- LEE K. H., KIM H. Y., LA Y. M., LEE D. R. & SUNG N. H. (2002) Influence of A Mixing Solvent with Tetrahydrofuran and N, N- Dimethylformamide on Electrospun Poly (Vinyl Chloride) Nonwoven Mats. *Journal of Polymer Science: Part B: Polymer Physics*, 40: 2259-22.
- LEE J. S., CHOI K. H., GHIM H. D., KIM S. S., CHUN D. H., KIM H. Y. & LYOO W. S. (2004) Role of Molecular Weight of Atactic Poly (Vinyl Alcohol) (Pva) in The Structure and Properties of Pva Nanofabric Prepared by Electrospinning. *Journal of Applied Polymer Science*, 93:4, 1638-1646.
- LI D., FREY M. W. & JOO Y. L. (2006) Characterization of Nanofibrous Membranes with Capillary Flow Porometry. *Journal of Membrane Science*, 26, 104-114.
- LI D., WANG Y., XIA Y. (2003) Electrospinning of Polymeric and Ceramic Nanofibers as Uniaxially Aligned Arrays. *Nano Letter*, 3 (8), 1167-1171.
- LI L & HSIEH YL. (2005) Ph-Responsive Swelling Behavior of Poly(Vinyl Alcohol)/Poly(Acrylic Acid) Bi-Component Fibrous Hydrogel Membranes. *Polymer*, 46: 5133-5139.
- LO C-M, WANG H-B, DEMBO M & WANG Y-L (2000) Cell Movement is Guided by The Rigidity of The Substrate. *Biophysical Journal*, 79: 144-152.
- LO SF, CHANG CJ, HU WY, HAYTER M&CHANG YT (2009) The Effectiveness of Silver-Releasing Dressings in The Management of Non-Healing Chronic Wounds: A Meta-Analysis. *J Clin Nurs*, 18(5): 716-28.
- LUKE THOMPSON (2005) Preparation of Nano-Fibers Via Electro-Spinning Process. *NSC*, 93-2218-E-006-008.

- LUTOLF MP. & HUBBELL JA. (2005) Synthetic Biomaterials as Instructive Extracellular Microenvironments for Morphogenesis in Tissue Engineering. *Nature Biotechnology*, 23: 47-55.
- LU Y., JIANG H., TU K. & WANG L. (2009) Mild Immobilization of Diverse Macromolecular Bioactive Agents onto Multifunctional Fibrous Membranes Prepared by Coaxial Electrospinning. *Acta Biomaterialia*, 5, 1562-1574.
- MASARO L. & ZHU X. X. (1999) Physical Models of Diffusion for Polymer Solutions, Gels And Solids. *Prog. Polym. Sci.*, 24, 731-775.
- MEGELSKI S., STEPHENS JS., CHASE DB. & RABOLT JF. (2002) Micro- and Nanostructured Surface Morphology on Electrospun Polymer Fibers. *Macromolecules*, 35: 22, 8456-8466.
- MIT-UPPATHAM C., NITHITANAKUL M. & SUPAPHOL P. (2004) Ultrafine Electrospun Polyamide-6 Fibers: Effect of Solution Conditions on Morphology and Average Fiber Diameter. *Macromol. Chem.physic*, 205, 2327-2338.
- NGUYEN TH. & LEE BT. (2010) Fabrication and Characterization of Cross-Linked Gelatin Electro-Spun Nano-Fibers. *J. Biomedicl Science and Engineering*, 3, 1117-1124.
- OGSTON A (1984) On Abscesses Classics in Infectious Diseases. *Rev Infect Dis*, 6 (1): 122-28. PMID 6369479.
- OH BK, ROBBINS ME, NABLO BJ & SCHOENFISCH MH (2005) Miniaturized Glucose Biosensor Modified with A Nitric Oxide-Releasing Sol-Gel Microarray. *Biosens Bioelectron*, 21:749.
- PEDICINI A. & FARRIS, R. J. (2003) Mechanical Behavior of Electrospun Polyurethane. *Polymer*, 44(22), 6857-6862.
- PENG ZHANG S. P. & JOHANNA PUONTI-KAERLAS1 (2001) Improvement of Cassava Shoot Organogenesis by The Use of Silver Nitrate in Vitro. *Plant Cell, Tissue and Organ Culture*, 67, p. 7.

QUEEN D, ORSTED H, SANADA H & SUSSMAN G (2004) A Dressing History. *Int Wound J.*, 1: 59-77.

RAMAKRISHNA S., FUJIHARA K, TEO WE & LIM TC (2005) An Introduction to Electrospinning and Nanofibers. *World Scientific Publishing Co. Pte. Ltd.*, 106-113.

RAMAKRISHNA S. & SEERAM (2004) An Introduction to Electro-Spinning and Nanofibers. *Electro-Spinning Details*, Chapter 3, 133-160.

RAMAKRISHNA S. & SEERAM (2004) An Introduction to Electro-Spinning and Nanofibers. *Introduction*, Chapter 1, 45-93.

RENEKER D. H. & CHUN L. (1996) Nanometre Diameters of Polymer, Produced by Electrospinning. *Nanotechnology*, 7:216-23.

ROBERTZUFAN (2005) Electrospinning Nanofibres. *Conference Introduction*.

RUTLEDGE G. C., LI Y., FRIDRIKH S., WARNER S. B., KALAYCI V. E. & PATRA P. (2001) Electrostatic Spinning and Properties of Ultrafine Fibers, National Textile Center. Annual Report (M98-D01), National Textile Centre, 1-10.

SANDERS JE, CASSISI DV, NEUMANN T, GOLLEDGE SL, ZACHARIAH SG & RATNER BD, ET AL.(2003) Relative Influence of Polymer Fiber Diameter and Surface Charge on Fibrous Capsule Thickness and Vessel Density for Single-Fiber Implants. *J Biomed Mater Res.*, 65A (4): 462-7.

SARAF A., LOZIER G., HAESSLEIN A., KASPER FK., RAPHAEL RM., BAGGETT L. SCOTT & IKOS AG. (2009) Fabrication of Nonwoven Coaxial Fiber Meshes by Electrospinning. *Tissue Engineering: Part C*, 15, 3, 333-344.

S. B. WARNER, A. BUER, S. C. UGBOLUE, G. C. RUTLEDGE & Y. M. SHIN (1998) National Textile Center Annual Report , No. 83-90.

SHINAKO MASUDA, TATSUYA SHIMIZU, MASAYUKI YAMATO & TERUO OKANO (2008) Advanced Drug Delivery Reviews. 60(2), pp. 277-285.

SILL TJ & VON RECUM HA (2008) Electro Spinning: Applications in Drug Delivery and Tissue Engineering. *Biomaterials*, 29: 1989-2006.

SHERIDAN R. L. (2003) Burn Care: Results of Technical and Organizational Progress. *JAMA*, 290 (6), pp. 719-722.

SOLIMAN S., SANT S., NICHOL JW., KHABIRY M., TRAVERSA E. & KHADEMHOSEINI A. (2011) Controlling The Porosity of Fibrous Scaffolds by Modulating The Fibre Diameter and Packing Density. *Journal of Biomedical Materials Research*, 96A, 3, 566-574.

SRIVASTAVA Y., MARQUEZ M. & THORSEN T. (2007) Multijet Electrospinning of Conducting Nanofibers from Microfluidic Manifolds, *Journal of Applied Polymer Science*, 106: 3171-3178.

SZYCHER M., GRIFFIN J. C., WILLIAMS J. L., MCMENAMY J. P. & STAGG D. (1987) Blood ompatible Polyurethane Elastomers J Biomater Appl 2: 290-313.

TANG L, WU Y & TIMMONS RB. (1998) Fibrinogen Adsorption and Host Tissue Responses to Plasma Functionalized Surfaces. *J Biomed Mater Res*, 42(1):156-63.

TAYLOR G. (1969) Electrically Driven Jets. *Proceedings of the Royal Society of London: Mathematical, Physical & Engineering Sciences*, 313, 453-475

TAYLOR G. (1964) Disintegration of Water Drops in An Electric Field. *Proceedings of the Royal Society of LondonA: Mathematical, Physical & Engineering Sciences*, 280, 383-397.

TAYLOR G. (1965) The Force Exerted by An Electric Field on A Long Cylindrical Conductor. *Proceedings of the Royal Society of LondonA: Mathematical, Physical & Engineering Sciences*, 291, 145-158.

T. JAMES RUDD (2005) National Nanotechnology Initiative and Small Business Research Enterprises. *November*.

T.J RUDD (2005) National Nanotechnology Initiative and Small Business Research *Enterprises*. 1-37.

<http://www.ianano.org/Presentation-ICNT2005/Rudd-NSF-ICNT2005.pdf>)

T. SUBBIAN, G.S. BHAT, R.W. TOCK, S. PARAMESWARAN & S.S. RAMKUMAR. (2005) *Applied Polymer Science* 96 557-569.

WANG XF, UM IC, FANG DF, OKAMOTO A, HSIAO BS & CHU B. Formation of Water-Resistant Hyaluronic Acid Nanofibers by Blowing-Assisted Electro-Spinning and Non-Toxic Post Treatments. *Polymer*, 46: 4853-4867.

WAN Y.Q., GUO Q., PAN N. (2004) Thermo- Electro-Hydrodynamic Model for Electrospinning Process. *Int. J. Nonlinear Sci. Num. Simulation*, 5(1), 5-8.

WAN, Y.Q., ZHANG, J., HE, J.H., YU, J.Y. (2004) An Electrospinning Apparatus with Oscillating Polymer Solutions or Melts. *CHN Patent*. 200420020596.3.

W. HE, T. YONG, W.E. TEO, Z. MA & S. RAMAKRISHNA (2005) *Tissue Engineering*. 11 (9/10), 1574-1588.

WU L., LI H., LI S., LI X., YUAN X., LI X. & ZHANG Y. (2010) Composite Fibrous Membranes of Lga and Chitosan Prepared by Coelectrospinning and Coaxial Electrospinning. *J Iomed Mater Res*, 92A: 563-574.

X.H. ZONG, K. KIM, D.F. FANG, S.F. RAN, B.S. HSAIO & B.CHU. (2002) *Polymer*, 43, 4403.

XU C, XU F, WANG B & LU TJ (2011) Electrospinning of Poly(Ethylene-Co-Vinyl Alcohol) Nanofibres Encapsulated with Ag Nanoparticles for Skin Wound Healing. *J Nanomater*.

XU F. & LU T. J. (2009) Skin Biothermomechanics: Modeling and Experimental Characterization. *Advances in Applied Mechanics*, E. van der Giessen, and H. Aref, eds., pp. 147-248.

XU F., LU T. J., SEFFEN K. A. & NG E. Y. K. (2009) Bioheat Transfer of Skin Tissue. *Applied Mechanics Review*, 62 (5), pp. 050801, DOI:050810.051115/050801.3124646.

- XU F., WANG P. F., LIN M., NG E. Y. K., & LU T. J. (2010) Quantifying The Underlying Mechanism of Skin Thermal Damage: A Review. *Journal of Mechanics in Medicine and Biology*, 10 (3), pp. 373-400.
- YANG Q. B., LI Z. Y., HONG Y. L., ZHAO Y. Y., QIU S. L., WANG C. & WEI Y. (2004) Influence of Solvents on The Formation of Ultrathin Uniform Poly (Vinyl Pyrrolidone) Nanofibers with Electrospinning. *J Polym Sci Part B: Polym Phys*, 42: 3721-3726.
- YAO L, HAAS TW, GUISEPPI-ELIE A, BOWLIN GL, SIMPSON DG & WNEK GE. (2003) Electrospinning and Stabilization of Fully Hydrolyzed Poly(Vinyl Alcohol) Fibers. *Chem Mater*, 15: 1860-1864.
- Y.M. SHIN, M.M. HOHMAN, M.P. BRENNER & G.C. RUTLEDGE (2001) *Polymer*, 42, 9955.
- YU B.-H. & DIMSDALE J. E. (1999) Posttraumatic Stress Disorder in Patients with Burn Injuries. *Journal of Burn Care & Research*, 20 (5), pp. 426-433.
- YU B., MOUSSY Y. & MOUSSY F. (2005) Coil-Type Implantable Glucose Biosensor with Excess Enzyme Loading. *Frontiers in Bioscience*, 10, 512-520.
- YUE-SHENG HUANG & M. Z. (2010) Protective Effect Of Nitric Oxide Production On Myocardium in Severely Scalded Rats. *Chinese journal of burns*, p. 450.
- YU JH, FRIDRIKH SV & UTLEDGE GC. (2004) Production of Submicro-Meter Diameter Fibers by Two-Fluid Electrospinning. *AdvMater*, 16 (17) : 1562-1566.
- ZELNY J. (1914) The Electrical Discharge from Liquid Points, and A Hydrostatic Method of Measuring the Electric Intensity at their Surfaces. *Physical Review*, 3, 69-91.
- ZHANG C., YUAN X., WU L., HAN Y. & SHENG J. (2005) Study on Morphology of Electrospun Poly (Vinyl Alcohol) Mats. *Eur Polym J*, 41:423-32.
- ZHANG K., QIAN Y., WANG H., FAN L., HUANG C., YIN A. & MO X. (2010) Genipin-Crosslinked Silk Fibroin/Hydroxybutyl Chitosan Nanofibrous Scaffolds

for Tissue-Engineering Application. *Journal of Biomedical Materials Research*, 95A, 3, 870-881.

ZHANG Y. Z., HUANG Z. M., XU X., LIM C. T. & RAMAKRISHNA S. (2004) Preparation of Core-Shell Structured Pcl-R-Gelatin Bi-Component Nanofibers by Coaxial Electrospinning *Chem. Mater*, 16, 3406-3409.

ZHANG Y. Z., WANG X., FENG Y., LI J., LIM C. T. & RAMAKRISHNA S. (2006) Coaxial Electrospinning of (Fluorescein Isothiocyanate-Conjugated Bovine Serum Albumin) - Encapsulated Poly(Epsilon-Caprolactone) Nanofibers for Sustained Release. *Iomacromolecules*, 7, 1049-1057.

ZHANG Y. Z., VENUGOPAL J., HUANG Z.- M., LIM C. T. & RAMAKRISHNA (2005) Characterization of The Surface Biocompatibility of The Electrospun Pcl-Collagen Anofibers Using Fibroblasts. *Biomacromolecules*, 6, 2583-2589.

ZHAO P., JIANG H., PAN H., ZHU K., CHEN W. (2007) Biodegradable Fibrous Scaffolds Composed of Gelatin Coated Poly( $\epsilon$ -Caprolactone) Prepared by Coaxial Electrospinning. *Journal of Biomedical Materials Research Part A*, 83A, 2, 372-382.

ZHAO S, WU X, WANG L & HUANG Y, (2004) Electrospinning. Ethyl-Cyanoethyl Cellulose/Tetrahydrofuran Solutions. *Journal of Applied Polymer Science*, 91: 242-246.

ZHENG QIXING, W. H., DU JINGYUAN, LI SHIPU & YAN YUHUA (2010) The Bacterial Inhibitory Ability and in Vivo Drug Release Pattern of A New Drug Delivery System. *Journal of Huazhong University of Science and Technology, Medical Sciences*, 3, p. 4.

ZHOU L. (2008) Yegang Hu and Mei Zhang, Investigation on The Psychological Conditions of Face or Body Burned Patients (in Chinese). *Journal of North China Coal Medical College*, 10 (4), pp. 503-504.

ZHU XL, CUI WG, LI XH & JIN Y (2008) Electrospun Fibrous Mats with High Porosity as Potential Scaffolds for Skin Tissue Engineering. *Biomacromolecules*, 9, 1795-1801.

ZONG X. H., KIM K., FANG D. F., RAN S. F., HSIAO B. S. & CHU B. (2002) Structure and Process Relationship of Electrospun Bioabsorbable Nanofiber Membranes. *Polymer*, 43, 16, 4403-4412.

The process of electro-spinning was patented by J.F Cooley in February 1902 ([U.S. Patent 692,631](#)) and by W.J. Morton in July 1902 ([U.S. Patent 0,705,691](#).)